UNIVERSITY OF CALIFORNIA SAN DIEGO

Numerical methods for nonequilbrium impurity models

A dissertation submitted in partial satisfaction of the
requirements for the degree
Doctor of Philosophy

in

Physics

by

Feng Chen

Committee in charge:

Professor Michael Galperin, Chair
Professor Massimiliano Di Ventra, Co-Chair
Professor Michael Fogler
Professor Francesco Paesani
Professor John Wheare

2020

The dissertation of Feng Chen is approved, and it is acceptable in quality and form for publication on microfilm and electronically:

_____

_____

_____

_____
Co-Chair

_____
Chair

University of California San Diego

2020

DEDICATION

To my parents.

EPIGRAPH

The simulacrum is never that which conceals the truth—it is the truth which conceals that there is none. The simulacrum is true.

—Jean Baudrillard

TABLE OF CONTENTS

LIST OF FIGURES

ACKNOWLEDGEMENTS

First, I would like to thank my advisor Prof. Misha Galperin, who has given me strong economic and intellectual support during the past four years. Misha is very patient and he is always there to help. Without him, I would not have been able to finish all these projects.

Special thanks to all the wonderful teachers I've had in UCSD! Especially, I'm very thankful for the joyful and insightful classes taught by Prof. Daniel Arovas. His humour, passion for science and dedication to teaching have made him an example for me to follow.

I'm also indebted to my past officemates Dr. Kuniyuki Miwa and Gabriel Cabra for their companionship. Learning Japanese from Kuniyuki and teaching him Chinese in return were a lot of fun. And I'll never forget those discussions with Gabriel about morality and Christianity.

I'm grateful for all the brothers and sisters in my church. I appreciate your prayers during all the hard times in my life and all those happy moments spent with you. You guys are best!

Last but not least, I wouldn't have reached this stage at all without the spiritual support from my parents, who have been encouraging me to pursue higher and higher education although they themselves only finished elementary schools.

Chapter 2, in part, is a reprint of the material as it appears in 'F. Chen, E. Arrigoni, M. Galperin, New Journal of Physics 21, 123035 (2019)'. The dissertation author was the primary investigator and author of this paper.

Chapter 3, in part, is a reprint of the material as it appears in 'Feng Chen, Guy Cohen, Michael Galperin. Phys. Rev. Lett. 122, 186803 (2019)'. The dissertation author was the primary investigator and author of this paper.

Chapter 4, in part, is a reprint of the material as it appears in 'Feng Chen, Mikhail I. Katsnelson, Michael Galperin. arXiv:1912.08203(2019)'. The dissertation author was the primary investigator and author of this paper.

Chapter 5 is a preliminary draft, and will be coauthored with Michael Galperin. The dissertation author was the primary investigator and author of this draft.

VITA

2015 B. S. in Physics, University of Science and Technology of China.

2020 Ph. D. in Physics, University of California, San Diego

PUBLICATIONS

Feng Chen, Kuniyuki Miwa, Michael Galperin, "Current-induced forces for nonadiabatic molecular dynamics", *The Journal of Physical Chemistry A* 123, 693-701 (2018)

Feng Chen, Guy Cohen, Michael Galperin, "Auxiliary master equation for nonequilibrium dual-fermion approach", *Physical Review Letter* 122, 186803 (2019)

Feng Chen, Enrico Arrigoni, Michael Galperin, "Markovian treatment of non-Markovian dynamics of open Fermionic systems", *New Journal of Physics* 21, 123035 (2019)

Feng Chen, Mikhail Katsnelson, Michael Galperin, "Nonequilibrium dual-boson approach", *arXiv:1912.08230*

ABSTRACT OF THE DISSERTATION

Numerical methods for nonequilbrium impurity models

by

Feng Chen

Doctor of Philosophy in Physics

University of California San Diego, 2020

Professor Michael Galperin, Chair
Professor Massimiliano Di Ventra, Co-Chair

Theoretical studies of electron and energy transport in nanostructures usually involve nonequilibrium quantum impurity models, which feature a locally interacting quantum system (impurity) coupled to noninteracting bosonic and/or electronic baths each at its own equilibrium. In these models, the interplay of strong correlation, nonequilibrium effects and dissipation leads to rich and complex phenomena. As a nonequilibrium strongly correlated many-body problem, these models, except at some rare cases, have no exact analytical solution, and hence their treatment heavily relies upon numerical techniques. The goal of this thesis is to develop numerically accurate and relatively low-cost techniques for treatment of strongly correlated open

nonequilibirum quantum systems. Such impurity solvers are in high demand both as standalone methods for simulation of response in nanoscale junctions and as part of divide-and-conquer schemes such as dynamical mean field theory (DMFT).

For nonequilibirum open quantum systems, two characteristic energy scales governing the physics are intra-system interactions and strength of the system-baths couplings. Thus, systems strongly coupled to their baths with weak intra-system interactions or weakly coupled systems with strong local interactions can be treated within developed perturbation theory approaches. My research focuses on development of nonequilibirum dual techniques, which are capable to accurately treat situations where perturbative techniques are inapplicable due to absence of a small parameter in the system and which reduce to standard perturbative expansions in the limits of weak coupling or weak intra-system interaction.

Dual techniques rely on ability to solve exactly a simplified reference system. The latter includes exactly all intra-system interactions and accounts approximately for system-bath couplings. Dual techniques (described below) allow to account for deviation from the correct hybridization function in a organized and controlled manner of superperturbative expansion. Here, I use Markovian Lindbald quantum master equation (QME) as a solver for the reference system. In the thesis I discuss possibility of mapping between true non-Markov dynamics and simpler Markov Lindblad QME (mapping between physical and reference systems), numerical methods for the mapping and for solution of the resulting Lindblad QME, and application of the mapping in novel dual formulations: auxiliary-QME dual fermion and dual boson approaches.

First I analytically prove that the continuous fermionic baths that the impurity is coupled to can be mapped onto a set of dissipative auxiliary modes under Lindblad QME. Based on this mapping, complicated non-Markovian dynamics of the open fermionic system can be treated by a much simpler Markovian Lindblad QME. However, nice mapping generally requires many auxiliary modes, and numerically only a small number of modes can be exactly diagonalized due to exponential increase of the Hilbert space. To perturbatively treat the difference between the true

bath and the small-size auxiliary one, we introduce dual-fermion method. It can directly target the steady state and avoid long-time propagation. Besides current-voltage relation, it can also provide spectral functions, indicating itself as a potential impurity solver for DMFT. Furthermore, we generalize dual-fermion method to consider additionally the effects of bosonic environment; hence it is called dual-boson method. It can be used for studying electron-phonon interaction and light-matter interaction in nanojunctions. By comparing with numerically exact results we argue that both methods are very accurate and relatively cheap.

Finally, matrix product state representation of the Lindblad QME enables us to treat a large number of auxiliary modes, which provide an exponentially improved mapping. Adding counting field to the auxiliary QME, we can compute the generating function of time-dependent full-counting statistics of electron transport, which yields not only electronic current but also higher-order cumulants (e.g., zero-frequency noise).

Chapter 1

Nonequilibrium Impurity Models

1.1 Background

Open nonequilibirum systems are at the forefront of experimental and theoretical research due to the rich and complex physics they provide access to as well as their applicational prospects of building nanoscale devices for quantum based technologies and computations [1–3]. Theoretical investigation of these systems often starts from nonequilibrium impurity models, which feature an interacting few-body system coupled to noninteracting bosonic and/or electronic baths. These models show intriguing physics due to the interplay of strong correlation, dissipation and nonequilibrium effects. Despite their benevolent looking, these models, except in some rare cases, generally don't have exact analytic solutions, and hence one has to resort to numerical methods to understand the accompanying exotic phenomena.

1.2 Models

1.2.1 Anderson Impurity Model

For purely fermionic system, the paradigmatic example is Anderson impurity model(AIM). AIM characterizes a local spinful level (impurity) coupled to electronic leads. The leads are composed of free electrons but there is Coulomb repulsion U between electrons with different spins on the impurity. The Hamiltonian is

$$\hat{H} = \sum_{\sigma\in\{\uparrow,\downarrow\}} \varepsilon_0 \hat{d}^\dagger_\sigma \hat{d}_\sigma + U\hat{n}_\uparrow\hat{n}_\downarrow + \sum_{k\in L,R}\sum_{\sigma\in\{\uparrow,\downarrow\}} \left(\varepsilon_k \hat{c}^\dagger_{k\sigma}\hat{c}_{k\sigma} + V_k \hat{d}^\dagger_\sigma \hat{c}_{k\sigma} + V_k^* \hat{c}^\dagger_{k\sigma}\hat{d}_\sigma\right) \tag{1.1}$$

This model was originally proposed to study magnetic impurities in metal host [4], and harbors a many-body phenomena—Kondo effect [5]. In recent years, it has gained renewed interests due to the experimental advances in characterization of open nanoscale quantum systems such as quantum dots (QDs) and molecular junctions. Besides, AIM and its multi-orbital generalization are also the backbone of all calculations within DMFT [6, 7].

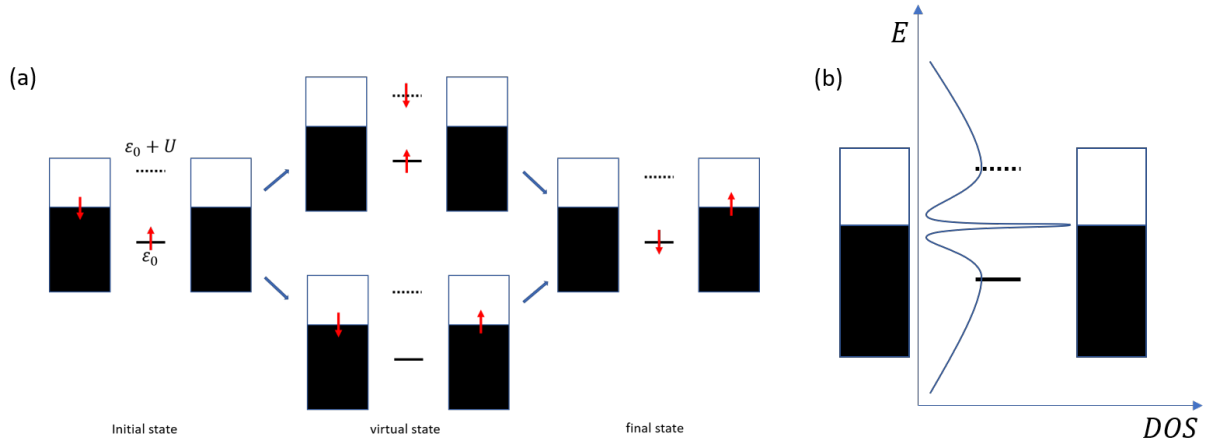

Figure 1.1: Kondo effect in quantum dots (a) two examples of the spin-flip conduction process via intermediate virtual states (b) Kondo resonance at Fermi energy

Kondo Effect in Quantum Dots: Kondo effect in electronic transport experiment through QDs happens when the QDs have net magnetic moments. In AIM, this is the case when the

impurity has one unpaired electron. Adding the second electron requires additional energy $\varepsilon_0 + U$; hence when the Fermi levels lie between ε_0 and $\varepsilon_0 + U$, the first-order tunneling process is prohibited. However, the electron conduction can be realized through spin-flip processes via virtual state such as illustrated in Figure 1.1(a). Many such spin-flip events together coherently give rise to a peak fixed at the Fermi level in the density of states (DOS) of the impurity (Figure 1.1(b)). The appearance of this peak can be most easily understood by the so-called Friedel sum rule [5], which is a consequence of the Fermi liquid properties of AIM. This peak, called Kondo resonance, gives rise to enhanced conductance because it provides a resonant channel for otherwises Couloumb blockade regime.

It is interesting to note that at finite source-drain voltage, there is no single chemical potential, and as a result, Kondo resonance splits into two peaks, which are roughly located at the chemical potential of source and drain respectively [31].

1.2.2 Single-level Holstein Model

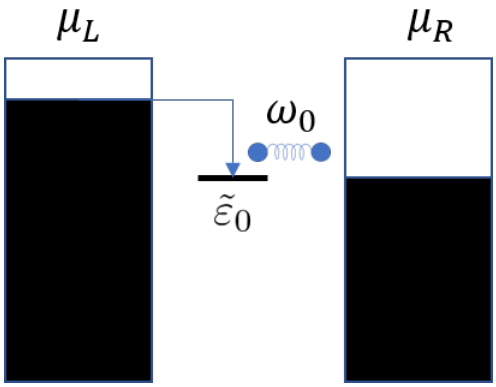

Figure 1.2: Inelastic electron tunneling accompanied by phonon emission.

Another well-know impurity model is single-level Holstein model, which consists of one spinless level coupled to free electron reservoirs and a localized phonon mode. Its Hamiltonian is

$$\hat{H} = \varepsilon_0 \hat{d}^\dagger \hat{d} + \omega_0 \hat{a}^\dagger \hat{a} + \lambda(\hat{a}^\dagger + \hat{a})\hat{d}^\dagger \hat{d} + \sum_{k \in L,R} \left(\varepsilon_k \hat{c}_k^\dagger \hat{c}_k + V_k \hat{d}^\dagger \hat{c}_k + V_k^* \hat{c}_k^\dagger \hat{d} \right) \tag{1.2}$$

where ω_0 is the frequency of the phonon mode and λ is the electron-phonon coupling strength. This model is used for studying inelastic transport due to the emission/absorption of phonon. Fixing the chemical potential of drain lead μ_d, when the chemical potential of source lead μ_s reaches thresholds $\mu_s - \tilde{\varepsilon}_0 = n\hbar\omega_0$, electrons from the source lead have enough energy to excite n phonons and become resonant with the impurity level. This gives rise to steps in the current-voltage relation [9]. Here $\tilde{\varepsilon}_0 = \varepsilon_0 - \lambda^2/\omega_0$ represents the renormalization of the energy level due to its coupling with the local phonon.

1.3 Nonequilibrium Green's Function

The theoretical tool used in this thesis for studying nonequilibrium impurity problems is nonequilibrium Green's function (NEGF). It has the advantage of calculating local observables such as occupation, density of states and current without diagonalizing the whole infinite system. Here we brief introduce this technique for fermions and readers can refer to [39, 99] for more details.

The difference between NEGF and equilibrium Green's function is that the adiabatic theorem doesn't hold when the system is driven out of equilibrium. As a result, the state at $t = +\infty$ is no longer the same as the state at $t = -\infty$ (up to a phase factor). A way to deal with this difficulty is to work on the Keldysh contour with both forward and backward propagation so that all quantities are evaluated with respect to the state at the infinite past, which is known. Particularly, in this thesis, the leads and impurity are initially decoupled and each is assumed to be in its own thermal equilibrium. At $t = -\infty$ the couplings are turned on, and the whole system evolves eventually to its steady state.

NEGF is defined as the correlator of two operators on the Keldysh contour, $G(\tau, \tau') \equiv$

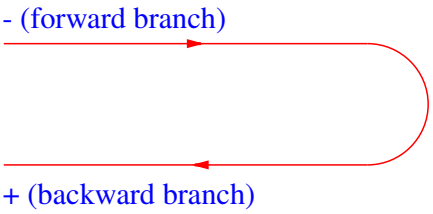

Figure 1.3: The Keldysh contour.

$-i\langle T_c\hat{\psi}(\tau)\hat{\psi}^\dagger(\tau')\rangle = -i\mathrm{Tr}\big(T_c\hat{\psi}(\tau)\hat{\psi}^\dagger(\tau')\hat{\rho}(-\infty)\big)$, where $\hat{\rho}(-\infty)$ is the initial state, τ and τ' are time variables on the contour, and T_c is the contour order operator which moves the operator later on the contour to the left. After projection of τ and τ' onto real time t and t' of particular branchs, one ends up with a 2×2 matrix structure for NEGF

$$\underline{\mathbf{G}} = \begin{pmatrix} G^{--} & G^{-+} \\ G^{+-} & G^{++} \end{pmatrix} \equiv \begin{pmatrix} G^T & G^< \\ G^> & G^{\tilde{T}} \end{pmatrix} \tag{1.3}$$

where $G^T \equiv -i\langle T\hat{\psi}(t)\hat{\psi}^\dagger(t')\rangle$ is the time-ordered Green's function; $G^< \equiv i\langle\hat{\psi}^\dagger(t')\hat{\psi}(t)\rangle$ the lesser Green's function; $G^> \equiv -i\langle\hat{\psi}(t)\hat{\psi}^\dagger(t')\rangle$ the greater Green's function; and $G^{\tilde{T}} \equiv -i\langle\tilde{T}\hat{\psi}(t)\hat{\psi}^\dagger(t')\rangle$ the anti-time-ordered Green's function. These four are not independent, and we can choose lesser and greater components as the independent functions. Another common choice is the retarded and Keldysh components, which are defined as:

$$\begin{aligned} G^R(t,t') &= -i\theta(t-t')\langle\{\hat{\psi}(t),\hat{\psi}^\dagger(t')\}\rangle \\ G^K(t,t') &= -i\langle[\hat{\psi}(t),\hat{\psi}^\dagger(t')]\rangle \end{aligned} \tag{1.4}$$

where $\{,\}$ and $[,]$ are anticommutator and commutator respectively. These satisfy

$$\begin{aligned} (G^R)^\dagger &= G^A \\ G^R - G^A &= G^> - G^< \\ G^K &= G^> + G^< \end{aligned} \tag{1.5}$$

where $G^A = i\theta(t'-t)\langle\{\hat{\psi}(t),\hat{\psi}^\dagger(t')\}\rangle$ is the advanced Green's function.

1.4 Hybridization Function

As far as the impurity is concered, the effects of baths can be fully characterized by the so-called "hybridization function" (here we'll focus on electronic bath, but bosonic bath will be similar):

$$\Delta(\tau,\tau') = \sum_\alpha \Delta_\alpha(\tau,\tau') = \sum_\alpha \sum_k |V_{\alpha k}|^2 g_{\alpha k}(\tau,\tau') \tag{1.6}$$

Here $g_{\alpha k}(\tau,\tau') = -i\langle \hat{c}_{\alpha k}(t)\hat{c}^\dagger_{\alpha k}(\tau')\rangle$ is the bare Green's function of the free electron at state k of bath α at equilibrium with density matrix $\hat{\rho}_\alpha = \frac{e^{-\beta(\hat{H}_\alpha-\mu_\alpha\hat{N}_\alpha)}}{\mathrm{Tr}e^{-\beta(\hat{H}_\alpha-\mu_\alpha\hat{N}_\alpha)}}$. Since each bath is at equilibrium, hybridization function only depends on the time difference $t-t'$, and it's convenient to transform it into frequency domain. Explicitly, retarded component is

$$\Delta^R_\alpha(\omega) = \sum_k \frac{|V_{\alpha k}|^2}{\omega - \varepsilon_{\alpha k} + i\eta} \tag{1.7}$$

its imaginary part $-\mathrm{Im}\Delta^R_\alpha(\omega) = \pi\sum_k |V_{\alpha k}|^2\delta(\omega-\varepsilon_{\alpha k})$ is usually denoted as $\Gamma_\alpha(\omega)$, and its real part can be deduced from the imaginary part by the Kramers-Kronig relation. For each bath, different components of the hybridization function are connected by fluctuation-dissipation theorem

$$\begin{aligned}
\Delta^K_\alpha(\omega) &= -2i[1-2f(\omega,\mu_\alpha,T_\alpha)]\Gamma(\omega)\\
\Delta^>_\alpha(\omega) &= -2i[1-f(\omega,\mu_\alpha,T_\alpha)]\Gamma(\omega)\\
\Delta^<_\alpha(\omega) &= 2if(\omega,\mu_\alpha,T_\alpha)\Gamma(\omega)
\end{aligned} \tag{1.8}$$

where $f(\omega,\mu,T)$ is the Fermi distribution function.

Chapter 2

Markovian Mapping for Fermionic Baths

2.1 Motivation

In DMFT, a many-body lattice problem is self-consistently mapped into an impurity model, which can be solved by a variety of impurity solvers. Among these impurity solvers are numerical renormalization group in the basis of scattering states [10, 11], flow equations [12, 13], time-dependent density matrix renormalization group [14, 15], multilayer multiconfiguration time-dependent Hartree (ML-MCTDH) [16, 17], and continuous time quantum Monte Carlo [18–20] approaches. These numerically exact techniques are very demanding and so far are mostly applicable to simple models only. At the same time, accurate numerically inexpensive impurity solvers are in great demand both as standalone techniques to be applied in simulation of, e.g., nanoscale junctions and as a part of DMFT calculations.

In this respect ability to map complicated non-Markovian dynamics of a system onto much simpler Markov consideration is an important step towards creating new computational techniques applicable in realistic simulations. In particular, such mapping was used in auxiliary master equation approach (AMEA) [8,21] introducing numerically inexpensive and pretty accurate solver for the nonequilibrium DMFT. Within AMEA the original unitary evolution is substituted with a

Lindblad-type quantum master equation consideration of an expanded system (system plus a set of auxiliary modes).We note that similar mapping ideas are employed also in the reaction coordinate formalism [23–25]. While the mappings appear to be very useful and accurate, in most cases only semi-quantitative arguments to justify the mapping were presented with main supporting evidence being benchmarking vs. numerically exact computational techniques. In particular, a justification for the mapping was put forward in Refs. [26–28] based upon the singular coupling derivation of the Lindblad equation.

Recently, a rigorous proof of non-Markov to Markov mapping for open Bose quantum systems was presented in the literature [29]. It was shown that the evolution of reduced density matrix in non-Markov system with unitary system-environment evolution can be equivalently obtained by a Markov evolution of an extended system (system plus modes of environment) under Lindblad-type evolution. In the following, we extend the consideration of Ref. [29] to fermionic open quantum systems and to multi-time correlation functions.

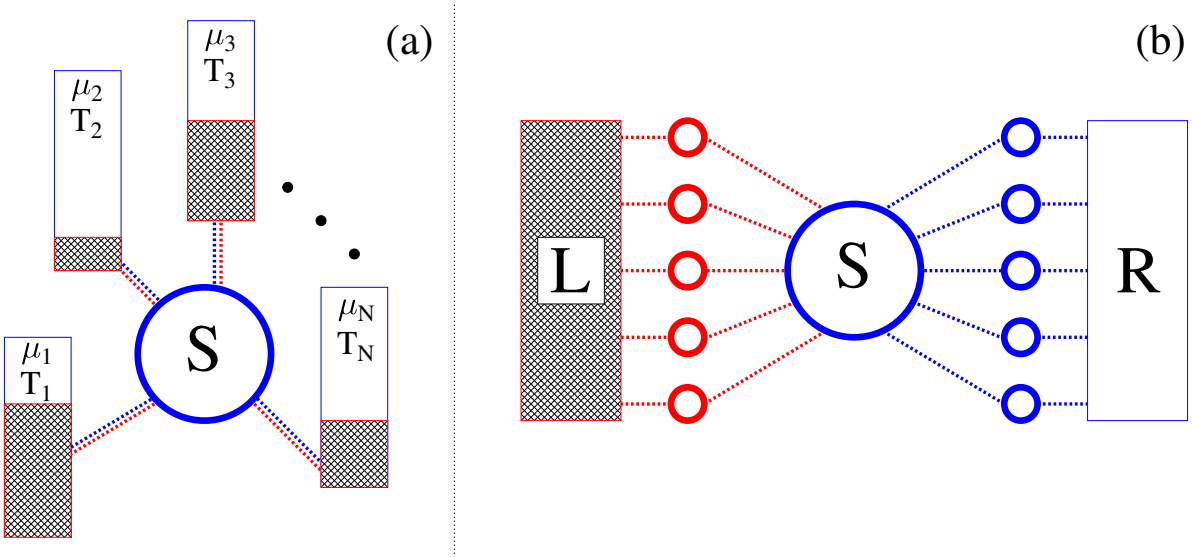

Figure 2.1: Sketch of an open fermionic system S. Shown are (a) physical system coupled to N baths and (b) illustration for an auxiliary system with coupling to full (left) and empty (right) baths.

2.2 Models

We consider an open fermionic system S coupled to an arbitrary number N of external baths, initially each at its own thermodynamic equilibrium, i.e. characterized by its own electrochemical potential and temperature (see Figure 2.1a). The Hamiltonian of the model is

$$\hat{H}^{phys}(t) = \hat{H}_S(t) + \sum_{B=1}^{N} \left(\hat{H}_B + \hat{V}_{SB} \right) \tag{2.1}$$

Here $\hat{H}_S(t)$ and $\hat{H}_B$ ($B \in \{1,\ldots,N\}$) are Hamiltonians of the system and baths. $\hat{V}_{SB}$ introduces coupling of the system to bath B. While the Hamiltonian of the system is general and may be time-dependent, we follow the usual paradigm by assuming bi-linear coupling in constructing fermionic junction models.

$$\hat{H}_B = \sum_{k \in B} \varepsilon_{Bk} \hat{c}^{\dagger}_{Bk} \hat{c}_{Bk} \tag{2.2}$$

$$\hat{V}_{SB} = \sum_{k \in B} \sum_{i \in S} \left(V_{i,Bk} \hat{d}^{\dagger}_i \hat{c}_{Bk} + H.c. \right) \tag{2.3}$$

where $\hat{d}^{\dagger}_i$ ($\hat{d}_i$) and $\hat{c}^{\dagger}_{Bk}$ ($\hat{c}_{Bk}$) create (annihilate) electron in level i of the system S and level k of bath B. In the model, dynamics of the system-plus-baths evolution is unitary. Below we call this model *phys* (physical). We note in passing that extension of the consideration to other types of system-baths couplings is straightforward, as long as baths are quadratic in the Fermi operators.

The other configuration we'll consider is a model we shall call *aux* (auxiliary; see Figure 2.1b). Here, the same system S is coupled to a number of auxiliary modes A, which in their turn are coupled to two baths. There are two Fermi baths in the configuration: one (L) is completely full ($\mu_L \to +\infty$), the other (R) is completely empty ($\mu_R \to -\infty$). The Hamiltonian of the total system is

$$\hat{H}^{aux}(t) = \hat{H}_S(t) + \hat{V}_{SA} + \hat{H}_A + \sum_{C=L,R} \left(\hat{H}_C + \hat{V}_{AC} \right) \tag{2.4}$$

where $\hat{H}_S$ is the same as in (2.1), $\hat{H}_A$ represents set of modes

$$\hat{H}_A = \sum_{m_1,m_2 \in A} H^A_{m_1 m_2} \hat{a}^\dagger_{m_1} \hat{a}_{m_2} \tag{2.5}$$

and $\hat{V}_{SA}$ their interaction with the system

$$\hat{V}_{SA} = \sum_{i \in S} \sum_{m \in A} \left(V^{SA}_{im} \hat{d}^\dagger_i \hat{a}_m + H.c. \right) \tag{2.6}$$

Here $\hat{a}^\dagger_m$ ($\hat{a}_m$) creates (annihilates) electron in the auxiliary mode m in A.

$\hat{H}_C$ represents continuum of states in contact C

$$\hat{H}_C = \sum_{k \in C} \varepsilon_{Ck} \hat{c}^\dagger_{Ck} \hat{c}_{Ck} \tag{2.7}$$

with constant density of states

$$N_C(E) \equiv \sum_{k \in C} \delta(E - \varepsilon_{Ck}) = const \tag{2.8}$$

and $\hat{V}_{AC}$ couples auxiliary modes A to bath C (L or R)

$$\hat{V}_{AC} = \sum_{k \in C} \sum_{m \in A} \left(t^C_m \hat{a}^\dagger_m \hat{c}_{Ck} + H.c. \right) \tag{2.9}$$

Dynamics of the whole configuration is unitary.

In the next section we show that the reduced time evolution of S in models *phys* and *aux* is the same (subject to certain conditions) and that the reduced dynamics of $S+A$ in model *aux* satisfies an appropriate Lindblad Markov evolution. This establishes procedure for Markovian Lindblad-type treatment of $S+A$ in *aux* exactly representing overall (i.e. system plus baths) unitary non-Markov dynamics of S in *phys* by tracing out A degrees of freedom.

2.3 Non-Markovian to Markovian Mapping

Consideration of the mapping consists of three levels of description: 1. overall (S plus baths) unitary dynamics of the physical system (*phys*); 2. overall ($S+A$ plus baths) unitary dynamics of the auxiliary system (*aux*); 3. Markovian Lindblad-type dynamics of $S+A$ in the auxiliary system (*aux*). Below we first discuss equivalence of the unitary dynamics of S in *phys* and *aux* systems, then we prove equivalence of unitary and Lindblad-type evolutions in the *aux* system.

First, we are going to prove that with an appropriate choice of parameters of *aux* the dynamics of S can be equivalently represented in the original model *phys* and auxiliary model *aux*. Because non-interacting baths are fully characterized by their two-time correlation functions, equivalence of system-bath(s) hybridizations (i.e. correlation functions of the bath(s) dressed with system-bath(s) interactions) for the two models indicates equivalence of the reduced system dynamics in the two cases. For example, hybridization function is the only information about baths in numerically exact simulations of strongly correlated systems [19]. Nonequilibrium character of the system requires fitting two projections of the hybridization function (also called self-energy in the literature). In particular, these may be retarded and Keldysh projections. Let $\Delta^r_B(E)$ and $\Delta^K_B(E)$ be matrices introducing the corresponding hybridization functions for bath B of the physical problem (Figure 2.1a). Retarded projection carries information on bath's spectral function and strength of system-bath coupling yielding dissipation rates for the system due to coupling to the bath. Keldysh projection yields information on bath's population which by Pauli principle defines possibility of electron exchange between system and bath.

$$\left(\Delta^r_B(E)\right)_{ij} = \sum_{k\in B} V_{i,Bk}\, g^r_{Bk}(E)\, V_{Bk,j} \tag{2.10}$$

$$\left(\Delta^K_B(E)\right)_{ij} = \sum_{k\in B} V_{i,Bk}\, g^K_{Bk}(E)\, V_{Bk,j} \tag{2.11}$$

where $g^{r(K)}_{Bk}(E)$ are the Fourier transforms of retarded (Keldysh) projections of the decoupled ($\hat{V}_{SB}=0$) electron Green's function $g_{Bk}(\tau,\tau')=-i\langle T_c\,\hat{c}_{Bk}(\tau)\,\hat{c}^{\dagger}_{Bk}(\tau')\rangle$ in contact B. The parameters of the auxiliary model should then be chosen such that the total hybridization functions for the system

$$\begin{aligned}\Delta^r(E) =&\sum_{B=1}^{N}\Delta^r_B(E)\\ \Delta^K(E) =&2\,i\sum_{B=1}^{N}\Big(1-2f_B(E)\Big)\,\mathrm{Im}\,\Delta^r_B(E)\end{aligned} \tag{2.12}$$

are as close as possible to the corresponding hybridization functions, $\tilde{\Delta}^r(E)$ and $\tilde{\Delta}^K(E)$, of S in the auxiliary model (Figure 2.1b) [8, 21, 27]. The latter have contribution from full (L) and empty (R) baths, and from auxiliary modes (A)

$$\begin{aligned}\tilde{\Delta}^r(E) =&\tilde{\Delta}^r_L(E)+\tilde{\Delta}^r_R(E)\\ \tilde{\Delta}^K(E) =&2\,i\,\mathrm{Im}\Big(\tilde{\Delta}^r_R(E)-\tilde{\Delta}^r_L(E)\Big)\end{aligned} \tag{2.13}$$

where we assume modes A initially in equilibrium with its contact (full or empty). In both Eq.(2.12) and Eq.(2.13), we used fluctuation-dissipation theorem for each equilibrium bath.

Requirement of equivalence can be expressed as

$$\begin{aligned}\mathrm{Im}\,\tilde{\Delta}^r_L(E) =&\frac{2\,i\,\mathrm{Im}\Delta^r(E)+\Delta^K(E)}{4\,i}\\ \mathrm{Im}\,\tilde{\Delta}^r_R(E) =&\frac{2\,i\,\mathrm{Im}\Delta^r(E)-\Delta^K(E)}{4\,i}\end{aligned} \tag{2.14}$$

where we used Kramers-Kronig relation. Thus, the problem reduces to fitting known functions on the right side of the expression with multiple contributions from auxiliary modes to the hybridization functions on the left side. We note that the knowledge of total (sum of contributions from all baths) hybridization function (retarded and Keldysh components) allows to fully determine interacting correlation functions in the S subspace of *phys*. That is, no information on

contribution from each separate bath is required. Thus, any number of baths B in physical system can be represented by only two baths (one full and one empty) in the auxiliary system. The exact mapping we prove below allows to evaluate correlation functions (and in particular, single particle Green's functions) in the S subspace of the physical system by considering Lindblad-type evolution in the *aux* system. After the correlation functions has been evaluated fluxes between the system S and baths B can be evaluated utilizing the well-known exact Jauho-Meir-Wingreen and similar expressions.

In principle fitting (2.14) can be done in many different ways [27]. For example, possibility of exact fitting of an arbitrary function with set of Lorentzians was discussed in Ref. [30]. In auxiliary systems such fitting corresponds to a construction where each auxiliary mode is coupled to its own bath. Note that in practical simulations accuracy of the results can be improved by increasing number of auxiliary modes or by considering more general (nondiagonal) level-bath geometries in the auxiliary system, as is implemented in, e.g, AMEA [31].

Having established the equivalence of reduced system (S) dynamics in *phys* and *aux*, we now turn to consideration of evolution of the *aux* model. We will show that reduced $S+A$ dynamics derived from unitary evolution of the *aux* model can be exactly represented by a suitable Markovian Lindblad-type evolution. Following Ref. [29] we consider the reduced density operator of $S+A$ in *aux*, $\hat{\rho}_{SA}$, which is defined by integrating out the baths degrees of freedom from the total density operator $\hat{\rho}^{aux}(t)$

$$\hat{\rho}_{SA}(t) \equiv \mathrm{Tr}_{LR}\left[\hat{\rho}^{aux}(t)\right] \tag{2.15}$$

$\hat{\rho}^{aux}$ follows an unitary evolution with initial condition given by $S+A$ decoupled from the baths

$$\hat{\rho}^{aux}(0) = \hat{\rho}_L \otimes \hat{\rho}_{SA}(0) \otimes \hat{\rho}_R \tag{2.16}$$

where $\hat{\rho}_L = |full\rangle\langle full|$, $\hat{\rho}_R = |empty\rangle\langle empty|$, and $\hat{\rho}_{SA}(0)$ can be arbitrary.

In Appendix A we prove that $\hat{\rho}_{SA}(t)$ satisfies the following Markov Lindblad-type equation

of motion

$$\begin{aligned}\frac{d}{dt}\hat{\rho}_{SA}(t) &= -i\left[\hat{H}_{SA}(t),\hat{\rho}_{SA}(t)\right] \\ &+ \sum_{m_1,m_2\in A}\left[\Gamma^{R}_{m_1m_2}\left(2\hat{a}_{m_2}\hat{\rho}_{SA}(t)\hat{a}^{\dagger}_{m_1} - \left\{\hat{\rho}_{SA}(t),\hat{a}^{\dagger}_{m_1}\hat{a}_{m_2}\right\}\right)\right. \\ &\qquad \left.+\Gamma^{L}_{m_1m_2}\left(2\hat{a}^{\dagger}_{m_1}\hat{\rho}_{SA}(t)\hat{a}_{m_2} - \left\{\hat{\rho}_{SA}(t),\hat{a}_{m_2}\hat{a}^{\dagger}_{m_1}\right\}\right)\right] \\ &\equiv \mathcal{L}_{SA}(t)|\rho_{SA}(t)\rangle\rangle\end{aligned} \tag{2.17}$$

where

$$\hat{H}_{SA}(t) \equiv \hat{H}_S(t) + \hat{V}_{SA} + \hat{H}_A, \tag{2.18}$$

$\mathcal{L}_{SA}$ is the Liouvillian superoperator defined on the $S+A$ subspace of the *aux* model and

$$\Gamma^{C}_{m_1m_2} \equiv \pi t^{C}_{m_1}(t^{C}_{m_2})^{*}N_C \qquad (C=L,R) \tag{2.19}$$

is the dissipation matrix due to the coupling to contact C.

Next we turn to multi-time correlation functions of operators in the $S+A$ subspace of the *aux* model. Following Ref. [29] we start consideration from two-time correlation function on real time axis. For arbitrary operators $\hat{O}_1$ and $\hat{O}_2$ in $S+A$ we define two-time ($t_1 \geq t_2 \geq 0$) correlation function as

$$\langle\hat{O}_1(t_1)\hat{O}_2(t_2)\rangle \equiv \mathrm{Tr}\left[\hat{O}_1\,\hat{U}^{aux}(t_1,t_2)\,\hat{O}_2\,\hat{U}^{aux}(t_2,0)\,\hat{\rho}^{aux}(0)\,\hat{U}^{aux\dagger}(t_1,0)\right] \tag{2.20}$$

Here $\hat{U}^{aux}$ is the evolution operator in the *aux* system

$$\hat{U}^{aux}(t,t') \equiv T\exp\left[-i\int_{t'}^{t} ds\,\hat{H}^{aux}(s)\right] \tag{2.21}$$

and T is the time-ordering operator. In Appendix B.1 we show that (2.20) can be equivalently

obtained from reduced Linblad-type evolution in the $S+A$ subspace

$$\langle \hat{O}_1(t_1)\hat{O}_2(t_2)\rangle = \langle\langle I| O_1^- \, \mathcal{U}_{SA}(t_1,t_2)\, O_2^- \, \mathcal{U}_{SA}(t_2,0)\, |\rho_{SA}(0)\rangle\rangle \tag{2.22}$$

Here $\langle\langle I|$ is Liouville space bra representation of the Hilbert space identity operator, $|\rho_{SA}(0)\rangle\rangle$ is Liouville space ket representation of the Hilbert space operator $\hat{\rho}_{SA}(0)$, O_i is the Liouville space superoperator corresponding to the Hilbert space operator $\hat{O}_i$ (see Figure 1.3)

$$O_i|\rho\rangle\rangle = \begin{cases} O_i^-|\rho\rangle\rangle \equiv \hat{O}_i\,\hat{\rho} & \text{forward branch} \\ O_i^+|\rho\rangle\rangle \equiv \hat{\rho}\,\hat{O}_i & \text{backward branch} \end{cases} \tag{2.23}$$

and $\mathcal{U}_{SA}$ is the Liouville space evolution superoperator

$$\mathcal{U}_{SA}(t,t') \equiv T \exp\left[\int_{t'}^{t} ds\, \mathcal{L}_{SA}(s)\right] \tag{2.24}$$

Finally, we extend consideration to multi-time correlation functions of arbitrary operators $\hat{O}_i$ ($i \in \{1,\ldots,N\}$) defined on the Keldysh contour (see Figure 1.3) as

$$\langle T_c\, \hat{O}_1(\tau_1)\, \hat{O}_2(\tau_2) \ldots \hat{O}_N(\tau_N)\rangle \equiv \mathrm{Tr}\left[T_c\, \hat{O}_1\, \hat{O}_2 \ldots \hat{O}_N\, \hat{U}_c\, \hat{\rho}^{aux}(0)\right] \tag{2.25}$$

where τ_i are the contour variables, T_c is the contour ordering operator, and

$$\hat{U}_c = T_c \exp\left[-i\int_c d\tau\, \hat{H}^{aux}(\tau)\right] \tag{2.26}$$

is the contour evolution operator. Note subscripts of operators O_i in the right side of (2.25) indicate operators on either side of the contour. In Appendix B.2 we prove that multi-time correlation functions (2.25) can be evaluated solely from Markov Lindblad-type evolution in

$S+A$ subspace of the *aux* model

$$\langle T_c \hat{O}_1(\tau_1)\hat{O}_2(\tau_2)\ldots\hat{O}_N(\tau_N)\rangle = \tag{2.27}$$
$$(-1)^P\langle\langle I|O_{\theta_1}\,\mathcal{U}_{SA}(t_{\theta_1},t_{\theta_2})\,O_{\theta_2}\,\mathcal{U}_{SA}(t_{\theta_2},t_{\theta_3})\ldots O_{\theta_N}\,\mathcal{U}_{SA}(t_{\theta_N},0)|\rho_{SA}(0)\rangle\rangle$$

Here P is number of Fermi interchanges in the permutation of operators $\hat{O}_i$ by T_c, θ_i are indices of operators $\hat{O}_i$ rearranged is such a way that $t_{\theta_1} > t_{\theta_2} > \ldots > t_{\theta_N}$ (t_{θ_i} is real time corresponding to contour variable τ_{θ_i}), O_{θ_i} are the superoperators defined in (2.23), and $\mathcal{U}_{SA}$ is the Liouville space evolution superoperator defined in (2.24).

Equivalence of S dynamics derived from unitary evolution of models *phys* and *aux* together with (2.17) and (2.27) completes the proof of the possibility of Markov treatment for non-Markovian dynamics in open quantum Fermi systems.

2.4 Numerical Illustration

Application of the mapping in realistic simulations relies on ability to fit hybridization function of the *phys* system with a set of auxiliary modes in the *aux* system. In general, to fit arbitrary function one needs infinite number of auxiliary modes, while in realistic calculations one can account for only finite number of modes. Thus, when applying the mapping one is looking for a trade-off between accuracy and efficiency: the more auxiliary modes are considered the better is the fit and the more involved is procedure to solve the auxiliary QME. For example, in Ref. [31] high accuracy of fitting with 16 auxiliary modes was demonstrated for the Anderson impurity model. However, for *aux* system of this size application of the matrix product states (MPS) was necessary to solve the QME.

Here we present a numerical simulation illustrating the equivalence of original unitary and Lindblad-type Markov treatment for the open quantum Fermi system. We note that the example

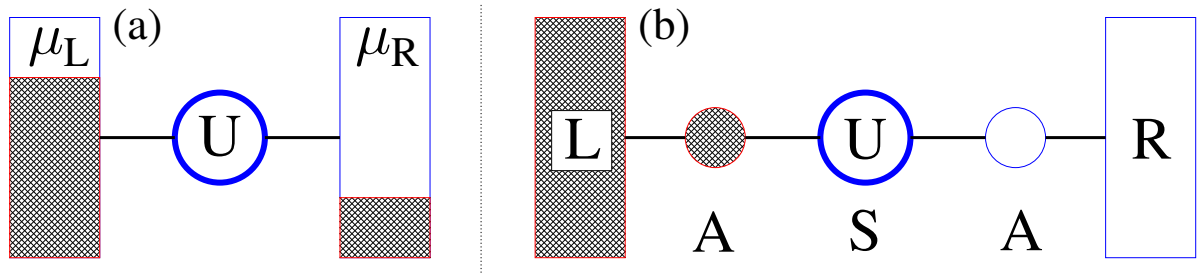

Figure 2.2: Original Anderson impurity (a) and corresponding auxiliary (b) models.

is a simple illustration only and that realistic simulations will require more than two auxiliary modes.

We consider the Anderson impurity model (Figure 2.2a)

$$\hat{H} = \sum_{\sigma\in\{\uparrow,\downarrow\}} \varepsilon_0 \hat{d}^\dagger_\sigma \hat{d}_\sigma + U\hat{n}_\uparrow\hat{n}_\downarrow + \sum_{k\in L,R}\sum_{\sigma\in\{\uparrow,\downarrow\}} \left(\varepsilon_k \hat{c}^\dagger_{k\sigma}\hat{c}_{k\sigma} + V_k \hat{d}^\dagger_\sigma \hat{c}_{k\sigma} + V_k^* \hat{c}^\dagger_{k\sigma}\hat{d}_\sigma\right) \tag{2.28}$$

where $\hat{n}_\sigma = \hat{d}^\dagger_\sigma \hat{d}_\sigma$. We calculate the system evolution after connecting initially empty site to baths at time $t = 0$. Parameters of the simulations are (numbers are in arbitrary units of energy E_0): $\varepsilon_0 = 0$ and $U = 1$. We assume

$$\Gamma_K(E) = \gamma_K \frac{t_K^2}{(E-\varepsilon_K)^2 + (\gamma_K/2)^2} \tag{2.29}$$

where $\Gamma_K(E) \equiv \pi\sum_{k\in K}|V_k|^2\delta(E-\varepsilon_k)$ is the electron escape rate into contact K ($K = L, R$), $\varepsilon_L = \varepsilon_R = 0$, $\gamma_L = \gamma_R = 0.1$, and $t_L = t_R = 1$.

For simplicity, we consider infinite bias, so that auxiliary model with only two sites (Figure 2.2b) is sufficient to reproduce dynamics in the physical system. After mapping, ε_L and ε_R become on-site energies of the auxiliary sites and γ_L and γ_R are taken as dissipation rates due to coupling to the L and R baths, respectively. In the auxiliary model we compare unitary evolution calculated within numerically exact td-DMRG [14, 15, 33, 34] with Lindblad QME results. Time is shown in units of $t_0 = \hbar/E_0$, currents in units of $I_0 = E_0/\hbar$, and $\hbar$ is assumed to

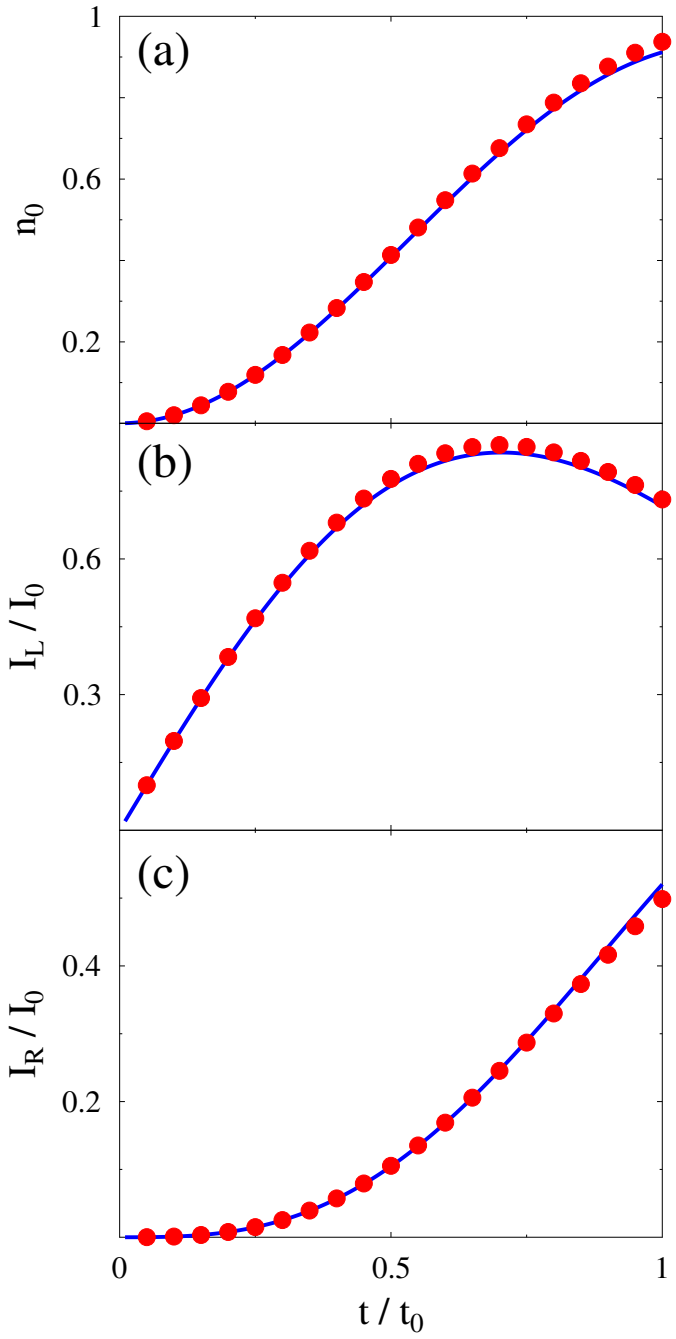

Figure 2.3: Unitary (filled circles, red) and Lindblad-type (solid line, blue) evolution in auxiliary model of Figure 2.2b after connecting initially empty central site to filled *L* and empty *R* baths. Shown are population of the level (a) and left (b) and right (c) currents. See text for parameters.

be 1. Figure 2.3 shows level population, $n_0 = \langle \hat{n}_\sigma \rangle$, as well as left, I_L, and right, I_R, currents in the system after quench. Close correspondence between the two numerical results is an illustration for exact analytical derivations presented in Section 2.3.

2.5 Conclusions

We consider an open quantum Fermi system S coupled to a number of external Fermi baths each at its own equilibrium (each bath has its own electrochemical potential μ_i and temperature T_i). The evolution of the model (system plus baths) is unitary. We show that reduced dynamics of the system S in the original unitary non-Markov model can be exactly reproduced by Markov Lindblad-type evolution of an auxiliary system, which consists of the system S coupled to a number of auxiliary modes A which in turn are coupled to two Fermi baths L and R: one full ($\mu_L \to +\infty$) and one empty ($\mu_R \to -\infty$). The proof is performed in two steps: first we show that reduced S dynamics in the physical model is equivalent to reduced dynamics of S in the auxiliary model, when A degrees of freedom and the two baths are traced out; second, we show that reduced dynamics of S+A in the auxiliary model with unitary evolution of the model can be exactly reproduced by the Lindblad-type Markov evolution of S+A. The correspondence is shown to hold for reduced density matrix and for multi-time correlation functions defined on the Keldysh contour. Our study extends a recent work about Bose systems [29] to open Fermi systems and beyond only reduced density matrix consideration. Establishing the possibility of exact mapping of reduced unitary non-Markov dynamics to much simpler non-unitary Markov Lindbald-type treatment sets firm basis for auxiliary quantum master equations (QME) methods employed in AMEA [21]. We note that in practical implementations improving the quality of mapping can be based on increasing number of A modes, as is done in advanced AMEA implementations [31]. Another way is to consider perturbatively the discrepancy between physical and auxiliary hybridization functions, as is done in the dual fermion formulation [32], and this will be the topic of next

chapter.

This chapter, in part, is a reprint of the material as it appears in 'F. Chen, E. Arrigoni, M. Galperin, New Journal of Physics 21, 123035 (2019)'. The dissertation author was the primary investigator and author of this paper.

Chapter 3

Nonequilibrium dual-fermion approach

3.1 Introduction

Since its theoretical conception [36] and the first experimental evidence of measurements on single-molecule junctions [37], molecular electronics has challenged theory for a proper description of response in open molecular systems far form equilibrium. Theoretical treatments are often based on a perturbative expansion in a small parameter, such as the strength of intra-molecular interactions or molecule-contact couplings. The former can be conveniently treated within the standard nonequilibrium Green function (NEGF) technique [38, 39], while the latter are handled at the nonequilibrium molecular limit [40] by many-body flavors of Green function (GF) methodology including pseudo-particles (PP) [6, 41] or Hubbard NEGF [42, 43] techniques. These two limits account for the majority of experimental measurements. For example, inelastic electron tunneling spectroscopy [44] is usually treated within NEGF [45, 46], while Coulomb blockade [47], single molecule strong coupling in plasmonic nanocavities [48] and coherent electron-nuclear dynamics [49] require many-body local analysis [50, 51]. In the absence of a small parameter, theoretical treatment is more involved. For example, this is the situation one encounters in describing Kondo physics in molecular junctions [52–58].

Dual-fermion (DF) approach [59] was originally proposed to account for non-local correlation beyond DMFT and was formulated for equilibrium systems [61,62]. A nonequilibrium version of the method (DF-inspired superperturbation theory) was later proposed in Ref. [32] as a way to solve impurity/transport problems. An attractive feature of the latter formulation is its applicability in the absence of a small parameter. At the heart of the approach is *a reference system*, which includes the molecule and a finite number of states representing leads. Such finite problem can be solved exactly, though the leads represented by a few states are a very rough approximation of the original ones. DF introduces an auxiliary zero order Hamiltonian around which standard diagrammatics can be formulated. The resulting expansion accounts for the difference between the true system-lead hybridization and its approximation within the reference system (see Ref. [32]).

When the steady-state is of interest, the nonequilibrium DF approach of Ref. [32] requires significant numerical effort. Because only a few sites represent infinite baths in the reference system, the hybridization function differs significantly from the true one. Furthermore, the finite reference system necessarily yields periodic solution and hence doesn't has steady state solution.

Based on the Markovian bath mapping developed in the previous chapter, we propose to approximate the true bath by a few dissipative auxiliary modes, and utilize the solution of corresponding auxiliary Lindblad QME for the DF approach in steady-state (compare Figs. 3.1b and c). These auxiliary dissipative modes effectively represent infite bath and hence yield a description of the bath which is much closer to the true one than any finite reference system. Furthermore, time propagation is completely avoided.

3.2 Nonequilibrium DF

In the nonequilibrium DF approach (for details see Ref. [32] and Appendix C), one considers reduced dynamics of an open system with interactions confined to the molecular

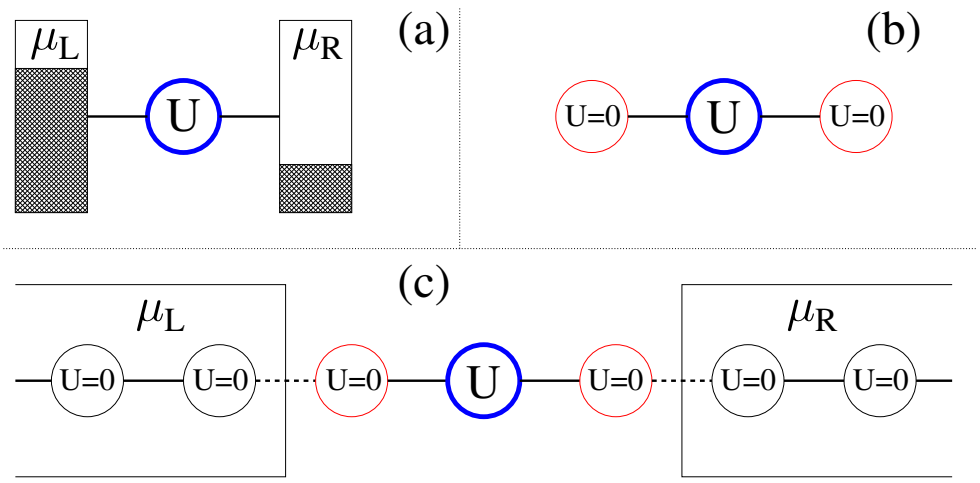

Figure 3.1: Nonequilibrium junction model. Shown are (a) Anderson impurity model; (b) Reference system within original DF approach [32]; and (c) Reference system within auxiliary QME-DF approach.

subspace and the effect of the leads entering via corresponding hybridization functions. The effective action on the Keldysh contour is [99]

$$S[d^*,d] = \sum_{1,2} d_1^* \left[G_0^{-1} - \Delta^B\right]_{12} d_2 + S^{int}[d^*,d], \tag{3.1}$$

where $i = (m_i, \tau_i)$ $(i = 1,2)$ is the index incorporating molecular orbital m_i and Keldysh contour variable τ_i, and the summation indicates sum over molecular orbitals and integral over the contour variables. $d_i^* = d_{m_i}^*(\tau_i)$ $(d_i = d_{m_i}(\tau_i))$ is the Grassmann variable corresponding to creation (annihilation) operator $\hat{d}_{m_i}^\dagger(\tau_i)$ $(\hat{d}_{m_i}(\tau_i))$ of an electron in orbital m_i in the Heisenberg picture [63]. G_0^{-1} is the inverse free GF [64]

$$\begin{aligned}\left[G_0^{-1}\right]_{12} &\equiv \delta(\tau_1,\tau_2)\left[i\overrightarrow{\partial}_{\tau_1}\delta_{m_1,m_2} - H^0_{m_1m_2}(\tau_1)\right] \\ &= \left[-i\overleftarrow{\partial}_{\tau_2}\delta_{m_1,m_2} - H^0_{m_1m_2}(\tau_2)\right]\delta(\tau_1,\tau_2)\end{aligned} \tag{3.2}$$

and $\Delta^B(\tau_1,\tau_2)$ is the self-energy due to coupling to contacts

$$\Delta^B_{m_1m_2}(\tau_1,\tau_2) = \sum_{k\in B} V_{m_1k} g_k(\tau_1,\tau_2) V_{km_2}. \tag{3.3}$$

In Eqs. (3.2) and (3.3), $H^0_{m_1m_2}(\tau)$ is the non-interacting part of the molecular Hamiltonian, V_{mk} is the matrix element for electron transfer between molecular orbital m and contact state k, and $g_k(\tau_1,\tau_2) \equiv -i\langle T_c\, \hat{c}_k(\tau_1)\, \hat{c}^\dagger_k(\tau_2)\rangle$ is the GF of free electron in state k of the contacts. All intra-molecular interactions are within the (unspecified) contribution to the action, $S^{int}[d^*,d]$.

The DF approach is based on two important steps. First, one introduces an exactly solvable reference system with baths represented by a finite number of states. Its known action $\tilde{S}[d^*,d]$ has the same general form (4.1) with true self-energy Δ^B substituted by its approximate representation $\tilde{\Delta}^B$. The desired action S can then be written as

$$S[d^*,d] = \tilde{S}[d^*,d] + \sum_{1,2} d^*_1 \left[\tilde{\Delta}^B - \Delta^B\right]_{12} d_2. \tag{3.4}$$

Second, direct application of standard diagrammatic expansion around the interacting reference system is not possible, because the Wick's theorem does not apply [65]. To resolve this, an artificial particle (*dual fermion*) is introduced which is used to unravel the term via the Hubbard-Stratonovich transformation [66]. Integrating out molecular fermions (d and d^*) and comparing the second order cumulant expansion of the resulting expression with the general form of action for dual fermions, $S^{DF}[f^*,f] = \sum_{1,2} f^*_1 \left[\left(G^{DF}_0\right)^{-1} - \Sigma^{DF}\right]_{12} f_2$, one gets

$$\left(G^{DF}_0\right)^{-1}_{12} = -g^{-1}_{12} - \sum_{3,4} g^{-1}_{13} \left[\tilde{\Delta}^B - \Delta^B\right]^{-1}_{34} g^{-1}_{42}, \tag{3.5}$$

$$\Sigma^{DF}_{12} = -\sum_{3,4} \Gamma_{13;24} \left[G^{DF}_0\right]_{43}. \tag{3.6}$$

Here g_{12} and $\Gamma_{13;24}$ are the single-particle GF and the two-particle vertex of the reference system,

respectively [39].

With $\left(G^{DF}\right) = \left[\left(G_0^{DF}\right)^{-1} - \Sigma^{DF}\right]^{-1}$ known, the single-particle GF of the molecule is obtained from the exact relation:

$$G = \left(\delta\Delta^B\right)^{-1} + \left[g\,\delta\Delta^B\right]^{-1} G^{DF} \left[\delta\Delta^B\, g\right]^{-1}, \tag{3.7}$$

where $\delta\Delta^B \equiv \tilde{\Delta}^B - \Delta^B$.

3.3 Auxiliary QME

The closer the reference system is to the real system, the higher accuracy of the associated DF approach. In this sense a finite reference system (see Fig. 3.1b) may not be optimal: its inability to represent dissipation and inevitably periodic solution makes reaching the steady-state difficult. We propose a reference system in which the physical leads are replaced by a set of auxiliary dissipative modes (A) under Lindblad QME. This reference system relies on Lindblad QME,

$$\frac{d\rho^{SA}(t)}{dt} = -i\mathcal{L}\rho^{SA}(t), \tag{3.8}$$

to simulate the extended system ($S+A$). Here, $\rho^{SA}(t)$ is the extended system density operator whose partial trace yields the reduced density matrix for the system S, and $\mathcal{L}$ is the Liouvillian. Our approach maintains all the advantages of Ref. [32] adding infinite baths, which results in a substantially more accurate and less numerically expensive computational scheme. Below, we focus on steady-state, where correlation functions depend on time differences, and work in the energy representation.

The nonequilibrium DF approach, Eqs. (3.5)-(3.6), requires single- and two-particle Green functions of the reference system as an input. To provide these we utilize the quantum regression

relation [35], as proved in Chapter 2:

$$\left\langle T_c \hat{A}(\tau_1)\hat{B}(\tau_2)\ldots\hat{Z}(\tau_n)\right\rangle = \mathrm{Tr}\left[O_n\,\mathcal{U}(t_n,t_{n-1})\ldots O_2\,\mathcal{U}(t_2,t_1)\,O_1\,\mathcal{U}(t_1,0)\,\rho^{SA}(0)\right] \tag{3.9}$$

Here $\rho^{SA}(0)$ is the steady-state density matrix of the extended system, $\mathcal{U}(t_i,t_{i-1})$ is the Liouville space evolution operator and times t_i are ordered so that $t_n > t_{n-1} > \ldots > t_2 > t_1 > 0$. O_i is the Liouville space super-operator corresponding to one of operators $\hat{A}\ldots\hat{Z}$ whose time is i-th in the ordering. It acts from the left (right) for the operator on the forward (backward) branch of the contour. The steady-state density matrix is found as a right eigenvector $|R_0\gg$ corresponding to the Liouvillian eigenvalue $\lambda_0 = 0$. Using spectral decomposition of the Liouvillian, the evolution operator can be presented in its eigenbasis as

$$\mathcal{U}(t_i,t_{i-1}) = \sum_\gamma |R_\gamma\gg\, e^{-i\lambda_\gamma(t_i-t_{i-1})}\, \ll L_\gamma|. \tag{3.10}$$

For evaluation of single- and two-particle GFs, besides the $\mathcal{L}$ of Eq. (3.8) we will also need Liouvillians $\mathcal{L}^{(\pm1)}$ and $\mathcal{L}^{(\pm2)}$. These are evolution operator generators for Liouville space vectors $|S_1S_2\gg$ with different number N_S of electrons in states $|S_1\rangle$ and $|S_2\rangle$. For example, for $\mathcal{L}^{(+1)}$, $N_{S_1} = N_{S_2} + 1$ [1].

Using (3.10) in (3.9) yields expressions for the GFs of the reference system (see [**?**] for details). Once single- and two-particle GFs of the reference system are known, the vertex required in (3.6) is given by

$$\Gamma_{13;24} = \sum_{\substack{1',2'\\3',4'}} g^{-1}_{11'}\, g^{-1}_{33'} \left[g^{(2)}_{1'3';2'4'} - g_{1'2'}\, g_{3'4'} + g_{1'4'}\, g_{3'2'}\right] g^{-1}_{2'2}\, g^{-1}_{4'4}.$$

Below we consider extended systems of size small enough that exact diagonalization can be

[1] Note, constructing the Liouvillians is helped by conservation of $N_{S_1} - N_{S_2}$ during evolution. Other symmetries (charge, spin) may help in understanding block structure within the Liouvillians [73].

employed. For larger systems more advanced methods (e.g. matrix product states [31]) may be used.

3.4 Model

We apply the QME-DF method to the Anderson impurity model: junction is constructed from quantum dot coupled to two paramagnetic leads each at its own equilibrium (see Fig. 3.1a). The Hamiltonian is

$$\hat{H} = \hat{H}_M + \sum_{K=L,R} \left(\hat{H}_K + \hat{V}_{MK}\right), \tag{3.11}$$

where $\hat{H}_M = \sum_{\sigma=\uparrow,\downarrow} \varepsilon_0 \hat{d}^\dagger_\sigma \hat{d}_\sigma + U\hat{n}_\uparrow \hat{n}_\downarrow$ and $\hat{H}_K = \sum_{k\in K}\sum_{\sigma=\uparrow,\downarrow} \varepsilon_k \hat{c}^\dagger_{k\sigma}\hat{c}_{k\sigma}$ are Hamiltonians of the quantum dot and contact K and $\hat{V}_{MK} = \sum_{k\in K}\sum_{\sigma=\uparrow,\downarrow}\left(V_k \hat{d}^\dagger_\sigma \hat{c}_{k\sigma} + H.c.\right)$ describes electron transfer between the dot and contact. The $\hat{d}^\dagger_\sigma$ ($\hat{d}_\sigma$) and $\hat{c}^\dagger_{k\sigma}$ ($\hat{c}_{k\sigma}$) creates (annihilates) electron of spin σ on the dot and in state k of the contacts, respectively. U is the Coulomb repulsion and $\hat{n}_\sigma = \hat{d}^\dagger_\sigma \hat{d}_\sigma$.

Using Eq. (3.7) we calculate the GF

$$G_\sigma(\tau_1,\tau_2) = -i\langle T_c\, \hat{d}_\sigma(\tau_1)\, \hat{d}^\dagger_\sigma(\tau_2)\rangle, \tag{3.12}$$

and use it to evaluate the level population n_σ, spectral function $A_\sigma(E)$, and current $I_L = -I_R$ [67] in steady-state

$$\begin{aligned} n_\sigma &= -i\int \frac{dE}{2\pi} G^<_\sigma(E); \quad A_\sigma(E) = -\frac{1}{\pi}\mathrm{Im}\, G^r_\sigma(E), \\ I_K &= \sum_\sigma \int \frac{dE}{2\pi}\left(\Delta^<_K(E)\, G^>_\sigma(E) - \Delta^>_K(E)\, G^<_\sigma(E)\right). \end{aligned} \tag{3.13}$$

Here $<$, $>$ and r are respectively lesser, greater and retarded projections of the GF. $\Delta^{\gtrless}_K(E)$ is the greater/lesser projection of the self-energy due to lead $K \in \{L,R\}$. Following Ref. [68], we model the leads as semi-infinite tight-binding chains with on-site energies ε_K and hopping parameter t_K

($K = L, R$); the electron hopping between the quantum dot and chain is t_{MK}.

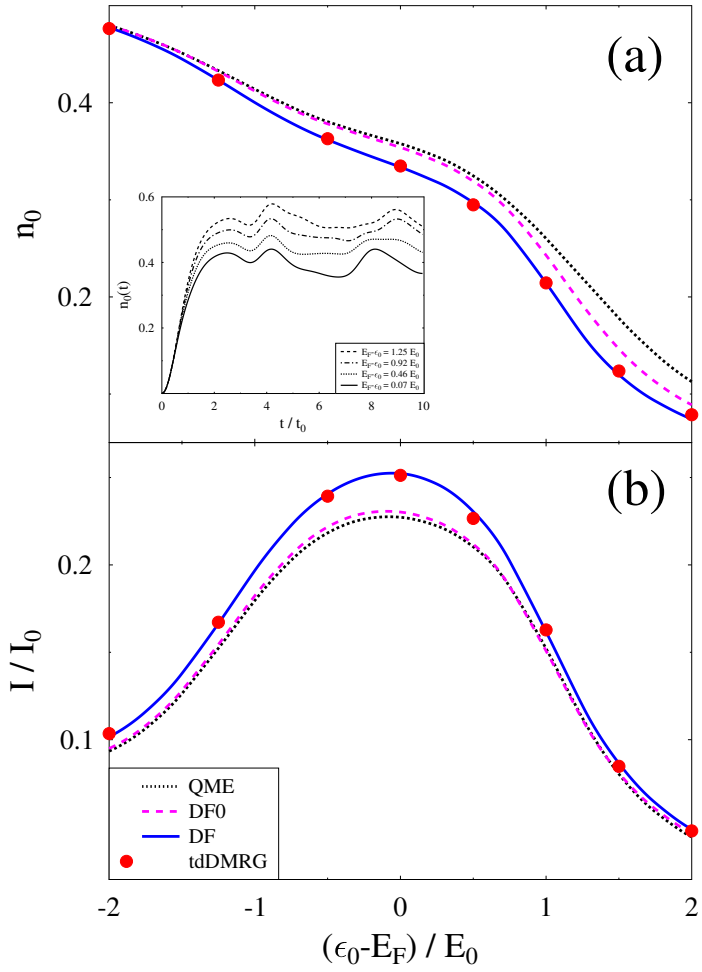

Figure 3.2: Steady-state transport characteristics vs. gate voltage at fixed bias. Shown are (a) population and (b) current vs. level position, as calculated from auxiliary QME (dotted line); and zero (dashed line) and first (solid line) order QME-DF approaches. Circles (red) represent results of numerically exact tdDMRG simulations. The inset in panel (a) shows the results of the original nonequilibrium DF simulation, where at $t = 0$ coupling between system and contacts is switched on for several level positions.

3.5 Numerical results.

We compare the QME-DF approach to the Anderson impurity model with the original nonequilibrium DF scheme and with numerically exact tdDMRG and CT-QMC calculations.

The former were performed using ALPS-MPS [33, 34], while the latter utilize the Inchworm algorithm introduced in Ref. [18]. The units are set by the maximum total escape rate, $\Gamma_0 = 2t_{ML}^2/t_L + 2t_{MR}^2/t_R$: in particular, we employ units of energy, $E_0 = \Gamma_0$, time $t_0 = \hbar/E_0$, voltage $V_0 = E_0/|e|$ and current $I_0 = |e|E_0/\hbar$. We show two flavors of the QME-DF results: zero order, where one neglects self-energy Σ^{DF}, and first order, where the self-energy is evaluated using Eq. (3.6).

Unless stated otherwise, the parameters are as follows: $U = 5E_0$, $\varepsilon_0 = -U/2$, $t_{ML} = t_{MR} = 0.79E_0$ and $t_L = t_R = 2.5E_0$. The positions of the on-site energies in the leads, ε_K, are given by the corresponding chemical potentials μ_K. The Fermi energy $E_F = 0$ is taken as the origin, and bias is assume dot be applied symmetrically such that $\mu_{L/R} = E_F \pm |e|V_{sd}/2$. The temperature is zero. The QME-DF simulations are performed on energy grid spanning range from $-12.5E_0$ to $12.5E_0$ with step $0.0125E_0$.

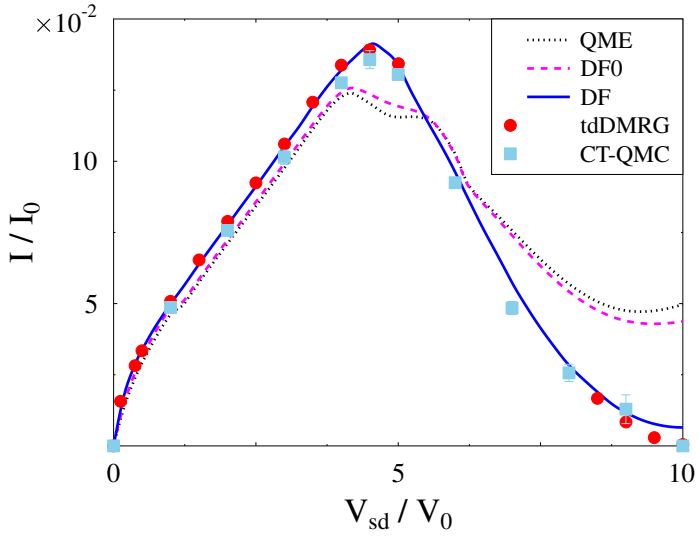

Figure 3.3: Current voltage characteristics. We show the auxiliary QME (dotted line), zero (dashed line) and first (solid line) order QME-DF approaches. For comparison, circles and squares represent respectively tdDMRG and CT-QMC results.

Figure 3.2a shows QME-DF level populations $n_\uparrow = n_\downarrow \equiv n_0$ under a bias $V_{sd} = 2.5V_0$, at several level positions ε_0, evaluated directly in steady-state. In contrast, the inset of Fig. 3.2a displays the corresponding time propagation of the population following a molecule-lead coupling

quench simulation of Ref. [32], illustrating the difficulty of reaching steady-state within the orginial nonequilibirum DF approach. Figure 3.2b shows the current at identical parameters. In both panels of Figure 3.2, we compare the zero (DF0, dashed line) with the first (DF, solid line) order QME-DF approach, the auxiliary QME (QME, dotted line) and numerically exact tdDMRG results at $t = 8t_0$. The first order QME-DF approach is quite accurate in predicting both level populations and currents, while being substantially less expensive numerically than the original DF formulation and having the added advantage of direct access to steady-state.

In Figure 3.3, we consider current-voltage characteristics in the particle-hole symmetric case, within the auxiliary QME (dotted line), the zero (dashed line) and first (solid line) order QME-DF. The latter is quite close to numerically exact tdDMRG (circles) and CT-QMC calculations (squares). Interestingly, the first order QME-DF calculation with three auxiliary sites yields result similar to a much more expensive six-site QME simulation (compare with Fig. 3 of Ref. [8]).

Finally, we consider spectral function: Fig. 3.4a shows results of equilibrium ($V_{sd} = 0$, solid line) and nonequilibrium ($V_{sd} = 2.5V_0$, dtted line) simulations; Fig. 3.4b shows the spectral function varying with bias. At low biases equilibrium Kondo peak splits and follows corresponding chemical potentials, while higher biases destroy the correlation. Similar results were obtained in Refs. [10, 69–72]. Note that results in Fig. 3.4 are only qualitative representation of true Kondo physics, but equilibrium DF studies, e.g., Ref. [61], have shown that accurate results in the correlated regime can be obtained efficiently by accounting for higher order diagrams.

3.6 Conclusion.

The nonequilibirum dual fermion approach introduced originally in Ref. [32] is a promising method for simulating strongly correlated open systems. Contrary to usual diagrammatic expansions in small interaction (e.g., intra-system interaction in NEGF or system-bath couplings

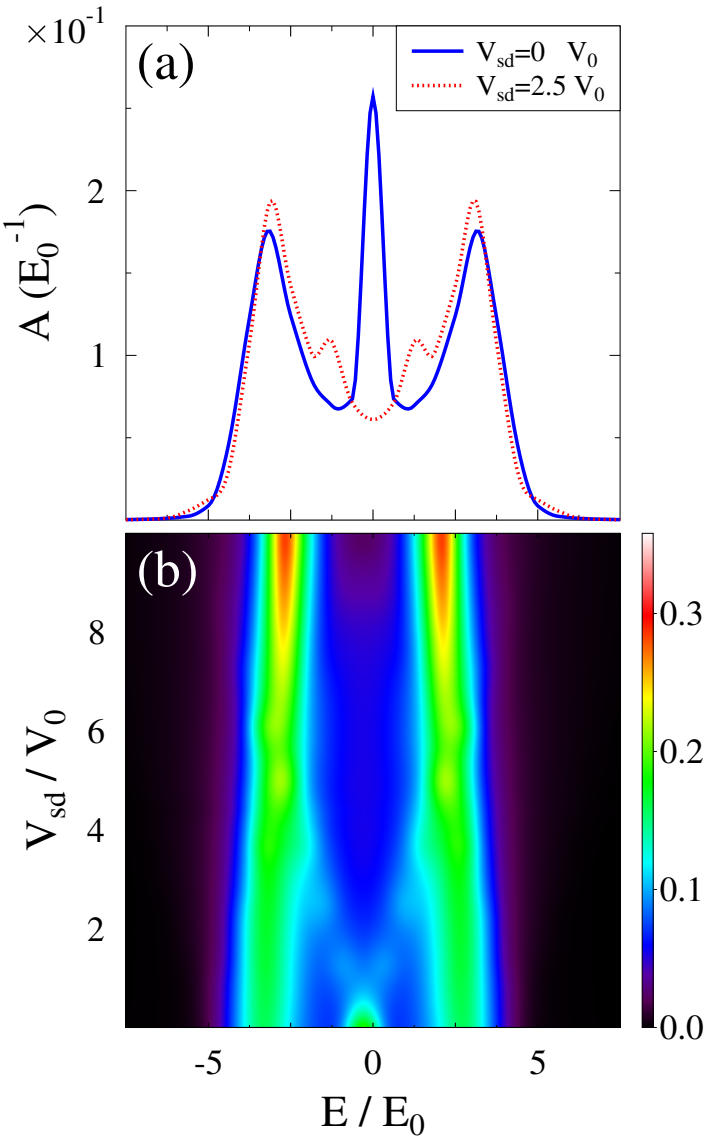

Figure 3.4: Spectral function of Anderson impurity model. Shown are results of QME-DF simulations for (a) The spectral function of the unbiased ($V_{sd} = 0$, solid line) and biased junction ($V_d/V_0 = 2.5$, dotted line); and (b) The spectral function vs. energy and applied bias.

in PP- or Hubbard NEGF), the method can treat systems with no small parameter by expanding around an exactly solvable reference system. The choice of a finite reference system in the original DF formulation cannot properly describe bath induced dissipation and results in periodic dynamics, which, together with the necessity to consider time propagation starting from a decoupled initial state, complicates reaching steady-state.

We proposed complementing finite reference system with infinite Markovian baths and use auxiliary quantum master equation to solve the reference problem. We argued that the approach is advantageous in treating the steady-states because it yields reference system which is much closer to the true nonequilibirum state than that in the original formulation. Also, infinite size of the modified reference system results in more accurate description of bath induced dissipation. Finally, the approach allows to avoid long time propagations necessary to reach steady-state solution in the original formulation.

For the Anderson impurity model, we tested our approach by comparing QME-DF simulations with numerically exact tdDMRG and CT-QMC results. This showed that the new scheme is both accurate and inexpensive. Further development of the method and its application to realistic systems is a goal for future research.

This chapter, in part, is a reprint of the material as it appears in 'Feng Chen, Guy Cohen, Michael Galperin. Phys. Rev. Lett. 122, 186803 (2019)'. The dissertation author was the primary investigator and author of this paper.

Chapter 4

Nonequilibrium Dual-boson Approach

4.1 Introduction

Fast development of nano-fabrication techniques combined with advances in laser technology lead to tremendous progress in optical studies of nanoscale systems. Optical spectroscopy of single molecules in current carrying junctions became reality. Surface [74–76] and tip [77–79] enhanced Raman spectroscopies (SERS and TERS) as well as bias-induced electroluminescence [80–86] measurements yield information on extent of heating of vibrational and electronic degrees of freedom in biased junctions, electron transport noise characteristics, molecular structure, dynamics and chemistry. Combination of molecular electronics with optical spectroscopy resulted in emergence of a new field of research coined optoelectronics [87, 88].

Optical response of single-molecule junctions is only possible due to strong enhancement of the signal by surface plasmons [89]. Large fields and confinement result in strong interaction between molecular and plasmonic excitations. Note also recent experiments on ultra-strong light-matter interaction in single-molecule nano-cavities (at the moment, in the absence of electron current) [48, 90]. At nanoscale classical electrodynamics becomes inadequate as it cannot describe quantum coherence and mixing between plasmon and molecular exciton, while strong

interactions require to go beyond perturbation theory. Note that focus of dual-fermion approach (DF) introduced in last chapter is electron transport. Whereas simulations of optoelectronic devices require accounting also for energy transfer.

In this chapter, we generalize dual-fermion method to take into account also the bosonic environment that the impurity is coupled to. And we call this generalization *auxiliary quantum master equation (QME) - nonequilibrium dual boson (aux-DB) method* - a universal nonequilibrium impurity solver which accounts for both charge and energy transport in strongly correlated open systems. Similar to DF of Ref. [32] being nonequilibrium version of the equilibrium DF method [59–62] (DF inspired superperturbation theory), aux-DB has its origin in equilibrium DB approach [91–98]. Below, after introducing nonequilibrium DB we present auxiliary quantum master equation (QME) treatment within the method. Theoretical considerations are followed by illustrative numerical simulations within generic junction models.

4.2 Formalism

Here we present a short description of the aux-DB method. Detailed derivations are given in the Appendix D. Similar to the DF method, in the nonequilibrium DB approach one considers reduced dynamics of an open quantum system with interactions confined to the

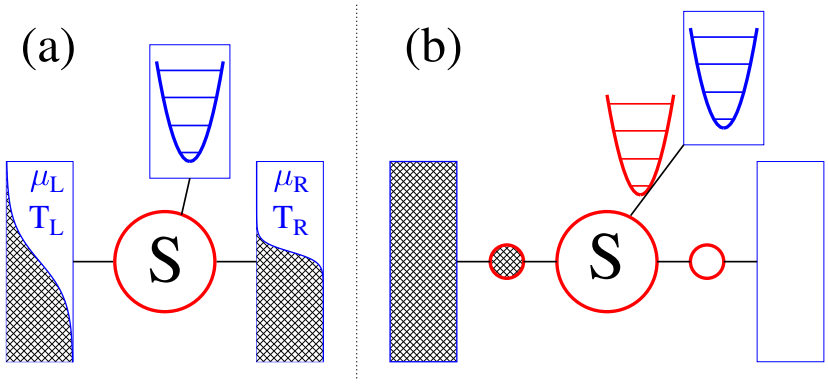

Figure 4.1: Nonequilibrium junction model. Shown are (a) Physical model and (b) Reference system within aux-DB approach.

molecular subspace. Contrary to the DF method, in addition to contacts (Fermi baths) the system is coupled also to Bose bath(s). Effect of the baths enters the effective action defined on the Keldysh contour [99] via corresponding self-energies Δ (for Fermi baths) and Π (for Bose baths)

$$S[\bar{d},d] = \bar{d}_1 \left[G_0^{-1} - \Delta^B\right]_{12} d_2 - \bar{b}_1 \Pi^B_{1,2} b_2 + S^{int}[\bar{d},d] \tag{4.1}$$

Here and below summation of repeating indices is assumed. In (4.1) $\bar{d}_i \equiv d_{m_i}(\tau_i)$ ($d_i \equiv d_{m_i}(\tau_i)$) is the Grassmann variable corresponding to creation (annihilation) operator $\hat{d}^\dagger_{m_i}(\tau_i)$ ($\hat{d}_{m_i}(\tau_i)$) represents both molecular (spin-)orbital m_i and contour variable τ_i, of an electron in orbital m_i in the Heisenberg picture [63]. $b_i = b_{m_1^i m_2^i}(\tau_i) \equiv \bar{d}_{m_1^i}(\tau_i) d_{m_2^i}(\tau_i)$ represents optical transition within the molecule from orbital m_2^i to orbital m_1^i at contour variable τ_i. Sum over indices includes summation over molecular orbitals (optical transitions) and contour integration: $\sum_i \ldots \equiv \sum_{m_i} \int_c d\tau_i \ldots$ ($\sum_{m_1^i, m_2^i} \int_c d\tau_i \ldots$). G_0^{-1} is the inverse free Green's function (GF) [64]

$$\left[G_0^{-1}\right]_{12} \equiv \delta(\tau_1,\tau_2)\left[i\partial_{\tau_1}\delta_{m_1,m_2} - H^0_{m_1 m_2}(\tau_1)\right] \tag{4.2}$$

Δ^B and Π^B are respectively self-energies due to coupling to Fermi (contacts) and Bose (plasmon) baths,

$$\begin{aligned} \Delta^B_{m_1 m_2}(\tau_1,\tau_2) &= V_{m_1 k} g_k(\tau_1,\tau_2) V_{k m_2} \\ \Pi^B_{m_1 m_2, m_3 m_4}(\tau_1,\tau_2) &= V_{m_1 m_2, \alpha} d_\alpha(\tau_1,\tau_2) V_{\alpha, m_3 m_4}. \end{aligned} \tag{4.3}$$

In Eqs. (4.2)-(4.3), $H^0_{m_1 m_2}(\tau)$ is the non-interacting part of the molecular Hamiltonian, V_{mk} and $V_{m_1 m_2,\alpha}$ are matrix elements for electron transfer from contact state k to molecular orbital m and for optical electron transfer from orbital m_1 to m_2 with absorption of phonon in mode α, respectively. $g_k(\tau_1,\tau_2) \equiv -i\langle T_c\, \hat{c}_k(\tau_1)\, \hat{c}^\dagger_k(\tau_2)\rangle$ and $d_\alpha(\tau_1,\tau_2) \equiv -i\langle T_c\, \hat{a}_\alpha(\tau_1)\, \hat{a}^\dagger_\alpha(\tau_2)\rangle$ are GFs of free electron in state k of the contacts and free phonon in mode α. All intra-molecular interactions

are within the (unspecified) contribution to the action $S^{int}[\bar{d},d]$.

As in equilibrium DB [92], one introduces an exactly solvable *reference system* (see below). Similarly to aux-DF [22], the true baths are approximated by a finite number of auxiliary discrete modes subject to Lindbladian evolution (see Fig. 4.1b). Thus, action of the reference system $\tilde{S}[\bar{d},d]$ is known and has the same general form (4.1) with true self-energies Δ^B and Π^B substituted by their approximate representations $\tilde{\Delta}^B$ and $\tilde{\Pi}^B$. The desired action S can then be written as

$$S[\bar{d},d] = \tilde{S}[\bar{d},d] + \bar{d}_1\,\delta\Delta^B_{12}\,d_2 + \bar{b}_1\,\delta\Pi^B_{12}\,b_2. \tag{4.4}$$

where $\delta\Delta^B \equiv \tilde{\Delta}^B - \Delta^B$ and $\delta\Pi^B \equiv \tilde{\Pi}^B - \Pi^B$.

Because direct application of standard diagrammatic expansion around the interacting reference system is not possible (the Wick's theorem does not apply [65]), two artificial particles, *dual fermion* (f) and *dual boson* (η), are introduced which is used to unravel last two terms in (4.4) via the Hubbard-Stratonovich transformation [66]. Integrating out molecular fermions (d and $\bar{d}$) and comparing the fourth order cumulant expansion of the resulting expression with the general form of action for dual particles,

$$\begin{aligned} S^D[f^*,f] = \bar{f}_1 \left[\left(G_0^{DF}\right)^{-1} - \Sigma^{DF}\right]_{12} f_2 \\ + \bar{\eta}_1 \left[\left(D_0^{DB}\right)^{-1} - \Pi^{DB}\right]_{12} \eta_2, \end{aligned} \tag{4.5}$$

one gets

$$
\begin{aligned}
\left(G_0^{DF}\right)^{-1}_{12} &= -g^{-1}_{12} - g^{-1}_{13}\left[\delta\Delta^B\right]^{-1}_{34} g^{-1}_{42}, \\
\left(D_0^{DB}\right)^{-1}_{12} &= -\chi^{-1}_{12} - \chi^{-1}_{13}\left[\delta\Pi^B\right]^{-1}_{34} \chi^{-1}_{42}, \\
\Sigma^{DF}_{12} &= \Bigg(\Gamma_{13;42} + i\big(\gamma_{514}\,\delta_{326} - \gamma_{512}\,\delta_{346} \\
&\qquad + \gamma_{532}\,\delta_{146} - \gamma_{534}\,\delta_{126}\big)\left[D_0^{DB}\right]_{65}\Bigg)\left[G_0^{DF}\right]_{43} \\
&\qquad - \left(\langle \hat{b}^\dagger_5\rangle \chi^{-1}_{54}\gamma_{312} + \chi^{-1}_{35}\langle \hat{b}_5\rangle \delta_{124}\right)\left[D_0^{DB}\right]_{43} \\
\Pi^{DB}_{12} &= -i\,\gamma_{145}\,\delta_{632}\left[G_0^{DF}\right]_{34}\left[G_0^{DF}\right]_{56}
\end{aligned}
\tag{4.6}
$$

Here g_{12} and χ_{12} are single particle GFs of fermion and molecular excitation of the reference system, γ_{123}, δ_{123} and $\Gamma_{13;24}$ are vertices [39] (see Eq. S12 and Fig. S1 in the SM [**?**]).

With dual particles GFs,

$$
\begin{aligned}
\left(G^{DF}\right) &= \left[\left(G_0^{DF}\right)^{-1} - \Sigma^{DF}\right]^{-1} \\
\left(D^{DB}\right) &= \left[\left(D_0^{DB}\right)^{-1} - \Pi^{DB}\right]^{-1},
\end{aligned}
\tag{4.7}
$$

known, the single-particle (G) and two-particle (D) GFs of the molecule are obtained from

$$
\begin{aligned}
G &= \left(\delta\Delta^B\right)^{-1} + \left[g\,\delta\Delta^B\right]^{-1} G^{DF}\left[\delta\Delta^B\, g\right]^{-1} \\
D &= \left(\delta\Pi^B\right)^{-1} + \left[\chi\,\delta\Pi^B\right]^{-1} D^{DF}\left[\delta\Pi^B\,\chi\right]^{-1}
\end{aligned}
\tag{4.8}
$$

Note, here the two-particle GF is correlation function of molecular optical transition operators. G yields information on orbital populations, spectral functions and electron current in the junction, while D is used in calculation of boson (phonon) flux.

Reference system. Construction of a reference system to a large extent relies on accurate reproduction of the physical system's hybridization functions Δ^B and Π^B. Accurate choice of the reference system parameters was recently discussed in Refs. [29, 100] for Bose baths and in

Refs. [21,27,31,101] for Fermi baths. Here we combine both considerations by introducing as the reference system physical system complemented with a finite number of auxiliary unitary modes (A) subject to Lindbladian evolution. This includes finite number of sites representing Fermi baths and modes representing Bose bath (see Fig. 4.1b and SM [**?**]). Dynamics of the extended SA system (molecule plus finite number of sites and modes) is driven by Markov Lindblad-type evolution

$$\frac{d\rho^{SA}(t)}{dt} = -i\mathcal{L}\rho^{SA}(t). \tag{4.9}$$

Here, $\rho^{SA}(t)$ is the extended system density operator and $\mathcal{L}$ is the Liouvillian. Note that Refs. [29] and [101] prove that, in principle, Markov dynamics of the extended system can exactly reproduce non-Markov unitary dynamics of the physical system S as long as free correlation function of the auxiliary modes accurately reproduces the correlation function of the full baths. However, in realistic calculations this representation is approximate due to restriction on number of auxiliary sites and modes which can be taken in consideration computationally. Thus, the aux-DB accounting for the difference between true and reference system hybridization functions, Eq. (4.6), is very useful in correcting the approximate mapping.

The aux-DB approach, Eqs. (4.5)-(4.8), requires single- and two-particle GFs g and χ and vertices Γ, γ and δ of the reference system as an input. Those are obtained by solving the QME (4.9) and employing the quantum regression relation (see Appendix C for details).

4.3 Model

We apply the aux-DB method to generic junction models constructed from a system S coupled to two Fermi (L and R) and one Boson bath (P) (see Fig. 4.1a). The Hamiltonian is $\hat{H} = \hat{H}_S + \sum_{B=L,R,P}\left(\hat{H}_B + \hat{V}_{SB}\right)$, where $\hat{H}_{L(R)} = \sum_{k\in L(R)} \varepsilon_k \hat{c}_k^\dagger \hat{c}_k$ and $\hat{H}_P = \sum_{\alpha\in P} \omega_\alpha \hat{a}_\alpha^\dagger \hat{a}_\alpha$ are Hamiltonians of the contact L (R) and phonon bath P. $\hat{V}_{SL(R)} = \sum_m \sum_{k\in L(R)} \left(V_{mk}\hat{d}_m^\dagger \hat{c}_k + H.c.\right)$ describes electron transfer between the system and contact L (R). $\hat{V}_{SP} = \sum_{m_1,m_2}\sum_{\alpha\in P} V^\alpha_{m_1m_2}(\hat{b}_{m_1m_2} +$

$\hat{b}^\dagger_{m_1m_2})(\hat{a}_\alpha + \hat{a}^\dagger_\alpha)$ describes coupling to phonon α in the thermal bath P ($\hat{b}_{m_1m_2} = \hat{d}^\dagger_{m_1}\hat{d}_{m_2}$). The $\hat{d}^\dagger_m$ ($\hat{d}_m$) and $\hat{c}^\dagger_k$ ($\hat{c}_k$) creates (annihilates) electron in orbital m on the system and in state k of the contacts, respectively. $\hat{a}^\dagger_\alpha$ ($\hat{a}_\alpha$) creates annihilates phonon in mode α.

For the system Hamiltonian we consider resonant level (RLM), $\hat{H}_S = \varepsilon_0 \hat{n}$, and Anderson impurity (AIM), $\hat{H}_S = \sum_{m=1,2} \varepsilon_0 \hat{n}_m + U\hat{n}_1\hat{n}_2$, models. Here $\hat{n}_m = \hat{d}^\dagger_m \hat{d}_m$ and U is the Coulomb repulsion. In the AIM two types of coupling to the thermal bath are considered: symmetric, $V^\alpha_{m_1m_2} = \delta_{m_1,m_2} V^\alpha_{m_1}$, and anti-symmetric, $V^\alpha_{m_1m_2} = \delta_{m_1,m_2}(-1)^{m_1} V^\alpha_{m_1}$.

Using Eq. (4.8) we calculate single- and two-particle GFs and employ them to evaluate the spectral functions, $A_m(E) = -\frac{1}{\pi}\mathrm{Im}\, G^r_{mm}(E)$, electron current [67],

$$I_L = -I_R = \int \frac{dE}{2\pi} \mathrm{Tr}\left[\Sigma^<_L(E)\, G^>(E) - \Sigma^{B>}_L(E)\, G^<(E)\right] \tag{4.10}$$

and phonon energy flux [88]

$$J_P = \int \frac{dE}{2\pi} E\, \mathrm{Tr}\left[\Pi^<_P(E)\, D^>(E) - \Pi^>_P(E)\, D^<(E)\right] \tag{4.11}$$

at steady-state. Here $<$, $>$ and r are respectively lesser, greater and retarded projections of the GFs, self-energies Σ and Π are defined in Eq.(4.3), and trace is over molecular orbitals in expression for $I_{L(R)}$ and over intra-molecular transitions in expression for J_P.

4.4 Numerical Results

We start from consideration of one spinless level coupled to both electron baths and boson bath as studied within numerically exact QMC approach in Ref. [102]. Parameters (in arbitrary energy units E_0) are $k_BT = 0.2$ and $\varepsilon_0 = 3.2$. Following Ref. [102] Fermi baths are treated within the wide-band approximation (WBA) with a smooth cut-off: $\Gamma_{L/R}(E) = \Gamma_{L/R}/[1 + e^{\nu(E-E_C)}][1 + e^{-\nu(E-E_C)}]$ with $\nu = 5$, $E_C = 20$ and $\Gamma_L = \Gamma_R = 0.5$; Bose bath is composed of a

primary phonon mode coupled to a secondary bath. Its spectral density is $J(\omega) = \gamma\omega/\left([(\omega/\omega_0)^2 - 1]^2 + [\gamma\omega_0\omega/(2M_0^2)]^2\right)$ with $\gamma = 0.1$, $\omega_0 = 5$ and $M_0 = 4$. Here ω_0 is the frequency of the primary phonon mode; M_0 is the coupling strength between the impurity and this mode; γ is the coupling strength between the secondary bath and the primary mode. Bias was applied symmetrically: $\mu_L = -\mu_R = V/2$. Results of simulation are presented in terms of units of bias $V_0 = E_0/|e|$, flux $I_0 = E_0/\hbar$, and energy flux $J_0 = E_0^2/\hbar$. Fig. 4.2a compares aux-DB results (solid line) with numerically exact QMC (circles) simulations of Ref. [102], and shows excellent agreement. Here we see steps at $V = 2\omega_0$ because at these values electrons at the fermi surface of left lead can lose energy to excite the primary phonon mode and become resonant with the impurity level. This step is the first Frank-Condon step [103]. Similarly as the inelastic transport in single-level Holstein model introduced in Chapter 1.

Aux-DB simulations of the AIM with symmetric coupling to Bose bath for $U = 0$ (dotted line) and $U = 7.5$ (dashed line) Coulomb interaction are shown in Fig. 4.2b. Note that even in the absence of Coulomb interaction results of simulations are significantly different from results of the RLM (compare dotted and solid lines). This is due to effective electron-electron interaction induced by coupling to common Bose bath and the effect can be understood within an effective negative-U model ($\tilde{\varepsilon}_0 = \varepsilon_0 - M_0^2/\omega_0$ and $\tilde{U} = U - 2M_0^2/\omega_0$) which predicts doubly populated state $E_2 = 2\tilde{\varepsilon}_0 + \tilde{U} = -6.4$ to be the ground state of $U = 0$ quantum dot with energy gap of 6.4 to its singly populated state $E_1 = \tilde{\varepsilon}_0 = 0$. For $U = 7.5$ (dash-dotted line) no current blockade is observed because electron transition between empty state ($E_0 = 0$) and singularly occupied state($E_1 = \tilde{\varepsilon}_0 = 0$) is gapless. Now doubly occupied state ($E_2 = 1.1$) is excited state. It is interesting to note that in blockaded region energy (phonon) flux is higher than for resonant tunneling (compare double-dotted and dash-double-dotted lines in Fig. 4.2b), which indicates predominantly elastic character of resonant transport.

4.5 Conclusion

The nonequilibirum DF approach introduced originally in Ref. [32] and its optimization for steady-state simulations - the aux-DF approach [22] - are promising methods for modeling strongly correlated open fermionic systems. Contrary to usual diagrammatic expansions the methods can treat systems with no small parameter available. This is the situation often encountered in single-molecule optoelectronic devices, which are at the forefront of experimental and theoretical research due to interesting fundamental problems and applicational perspectives in energy nano-materials, spintronics, and quantum computation. However, application of the aux-DF to simulations of optoelectronic devices is hindered by its inability to account for energy exchange between molecule and plasmonic field. The latter is crucial in modeling of the devices.

Here we proposed a new nonequilibrium method, *the aux-DB approach*, which accounts for both electron and boson fluxes between system and baths. The nonequilibrium aux-DB is a super-perturbation theory inspired by equilibrium DB method [91] proposed as generalization of the extended DMFT. Employing auxiliary QME and choosing infinite reference system makes the approach advantageous in treating the steady-states. We utilized generic junction models of a molecule coupled to two Fermi leads and one Bose phonon bath. The aux-DB was benchmarked vs. numerically exact QMC results of Ref. [102]. We showed that the new scheme is both accurate and relatively numerically inexpensive. Further development of the method and its application to realistic systems is a goal for future research.

This chapter, in part, is a reprint of the material as it appears in 'Feng Chen, Mikhail I. Katsnelson, Michael Galperin. arXiv:1912.08203(2019)'. The dissertation author was the primary investigator and author of this paper.

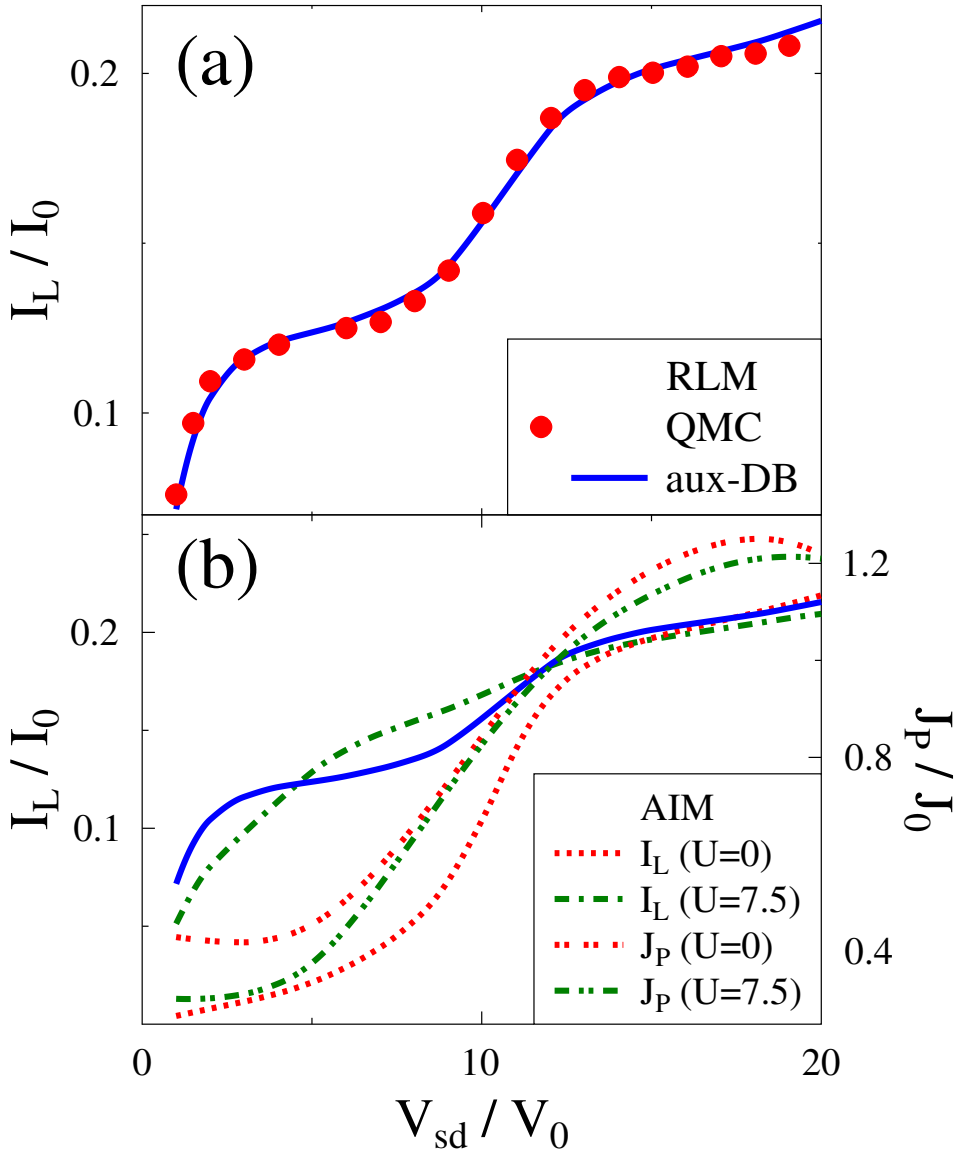

Figure 4.2: Electron I_L and phonon I_P fluxes. Shown are results for (a) RLM and (b) AIM. In panel (a) aux-DB results (solid line, blue) are benchmarked vs. numerically exact QMC calculation of Ref. [102]. Panel (b) compares aux-DB results for AIM with $U = 0$ and $U = 7.5$.

Chapter 5

Auxiliary Quantum Master Equation for Full Counting Statistics

5.1 Background

Electron transport in mesoscopic system such as molecular junctions is fundamentally a stochastic process—for a given period of time t, the number of electrons flowing out of a lead, Δn, is described by certain probability distribution $P(\Delta n, t)$. While current is related to the first cumulant of this distribution, higher cumulants can yield additional important information about the transport properties. For example, current fluctuation, so-called noise, can reveal the charge of effective quasiparticles that participate in the transport process, such as Cooper-pair in superconducting junctions ($e^* = 2e$) [104–106] and fractional charge in fractional quantum Hall effect [107].

The theory of studying cumulants of all orders in a transport process is called full-counting statistics [108, 109]. Its central goal is to calculate the generating function (GF)

$Z(\lambda,t) \equiv \sum_n e^{i\lambda n} P(n,t)$, from which j-th cumulant $C_j(t)$ can be obtained by

$$C_j(t) \equiv \langle\langle (\Delta n)^j \rangle\rangle(t) = \left. \frac{\partial^j \ln Z(\lambda,t)}{\partial (i\lambda)^j} \right|_{\lambda=0} \tag{5.1}$$

where λ is called "counting field".

In this thesis, I'll consider an impurity coupled to two noninteracting electronic leads L and R, and count electrons in the L lead. We adopt the two-time measurement scheme: we measure the electron number operator of L lead, $\hat{N}_L$, at two different times 0 and t, and formulate the GF for change of electron number, $\Delta n(t) = N_L(t) - N_L(0)$. The whole system is initially prepared at time 0 in decoupled equilibrium states $\hat{\rho}_0 = \hat{\rho}_L \otimes \hat{\rho}_I \otimes \hat{\rho}_R$, where $\hat{\rho}_\alpha = \frac{e^{-\beta(\hat{H}_\alpha - \mu_\alpha \hat{N}_\alpha)}}{\mathrm{Tr} e^{-\beta(\hat{H}_\alpha - \mu_\alpha \hat{N}_\alpha)}}$, and initial state of the impurity $\hat{\rho}_I$ can be arbitrary. After time 0 the coupling between impurity and leads is turned on.

It can be shown that $Z(\lambda,t)$ can be given by [110]

$$Z(\lambda,t) = \mathrm{Tr}(e^{-i\hat{H}_\lambda t} \hat{\rho}_0 e^{i\hat{H}_{-\lambda} t}) \tag{5.2}$$

where $\hat{H}_\lambda \equiv e^{i\frac{\lambda}{2}\hat{N}_L} \hat{H} e^{-i\frac{\lambda}{2}\hat{N}_L}$. The transient electron flux into left lead, $I_L(t) \equiv \langle \frac{d\hat{N}_L(t)}{dt} \rangle$ is then given by $I_L(t) = \frac{d\Delta n(t)}{dt} = \frac{dC_1(t)}{dt}$. In the long-time limit $t \to \infty$, each of these cumulants become linear in time. For example, $S = \lim_{t\to\infty} \frac{C_2(t)}{t}$, where S is the zero-frequency noise

$$S \equiv \lim_{t\to\infty} \int_{-\infty}^{+\infty} d\tau \langle \Delta\hat{I}_L(t+\tau) \Delta\hat{I}_L(t) \rangle \tag{5.3}$$

and $\Delta\hat{I}_L \equiv \hat{I}_L - \langle \hat{I}_L \rangle$.

In this chapter, I propose that based on the mapping scheme in Chapter 2 and by dressing the corresponding Lindblad quantum master equation (QME) with counting field, $Z(\lambda,t)$ can be calculated exactly. An accurate mapping of the baths requires a large number of auxiliary sites, which renders exact diagonalization impossible due to the exponential increase of Hilbert space.

To deal with this difficulty, matrix product state (MPS) representation of the dressed Lindblad QME in super-fermion representation [111] is adopted.

5.2 Dressed Auxiliary Quantum Master Equation

In full-counting statistics for impurity models, the noninteracting electronic baths are fully characterized by the hybridization function (HF) of each bath [**?**, 112]. Now if I map each of the original leads L and R into a set of auxiliary sites additionally coupled to full and empty baths with constant density of states, as long as the HFs of the auxiliary baths (auxiliary modes+full+empty bath) give good approximation for those of original baths, GF of the original system can be well approximated by GF of the auxiliary system ($\mathrm{IM_{aux}}$). The advantage of this mapping is that GF of $\mathrm{IM_{aux}}$ can be calculated by solving a small-size Lindblad QME dressed with counting field, which will be proved in the following.

In the auxiliary configuration, L lead is mapped into some auxiliary modes (A_L) additionally coupled to one full (F_L) and one empty (E_L) electron bath. Similarly, R lead is mapped into A_R coupled to F_R and E_R (see Fig.(5.1)). Compared with the strategy in [27, 31] of mapping two leads together, the mapping scheme here has the advantage of distinguishing leads L and R, which is necessary for FCS. The Hamiltonian of the total $\mathrm{IM_{aux}}$ is

$$
\begin{aligned}
\hat{H}^{\mathrm{aux}} &= \hat{H}_I + \sum_{\alpha=L,R}\left(\hat{T}^{\alpha} + \hat{H}_A^{\alpha} + \sum_{B=F,E}\left(\hat{H}_B^{\alpha} + \hat{V}_B^{\alpha}\right)\right) \\
\hat{H}_A^{\alpha} &= \sum_{m_1,m_2\in A_\alpha} E^{\alpha}_{m_1m_2}\hat{a}^{\dagger}_{\alpha m_1}\hat{a}_{\alpha m_2} \\
\hat{H}_B^{\alpha} &= \sum_k \varepsilon^{B}_{\alpha k}\hat{c}^{\dagger}_{B_\alpha k}\hat{c}_{B_\alpha k} \\
\hat{T}^{\alpha} &= \sum_{i\in I}\sum_{m\in A_\alpha}\left(t^{\alpha}_{im}\hat{d}^{\dagger}_i\hat{a}_{\alpha m} + \mathrm{h.c.}\right) \\
\hat{V}_B^{\alpha} &= \sum_{m\in A_\alpha}\sum_{k\in B_\alpha}\left(V^{\alpha}_{Bm}\hat{a}^{\dagger}_{\alpha m}\hat{c}_{B_\alpha k} + \mathrm{h.c.}\right)
\end{aligned}
\tag{5.4}
$$

where $\hat{H}_I, \hat{H}_A^\alpha$ and $\hat{H}_B^\alpha$ are the Hamiltonians of the impurity, auxiliary modes, and full/empty baths respectively; $\hat{T}^\alpha$ is the coupling between the impurity and auxiliary modes; $\hat{V}_B^\alpha$ is the coupling between full/empty baths and auxiliary modes. Density of states of full/empty baths are constant

$$N_B^\alpha(E) = \sum_{k\in B_\alpha} \delta(E - \varepsilon_{\alpha k}^B) = \text{const} \tag{5.5}$$

Let's define

$$\hat{O}_\lambda(t) \equiv e^{i\hat{H}_{-\lambda}^{\text{aux}} t} \hat{O} e^{-i\hat{H}_\lambda^{aux} t} \tag{5.6}$$

where $\hat{O}$ is an Bose-type operator (i.e., consists of even number of fermi creation/annination operators) belong to $I + A$, and

$$\begin{aligned}
\hat{N}_L^{\text{aux}} &\equiv \sum_{m\in A_L} \hat{a}_{Lm}^\dagger \hat{a}_{Lm} + \sum_{B=F,E} \sum_{k\in B_L} \hat{c}_{B_L k}^\dagger \hat{c}_{B_L k} \\
\hat{T}_\lambda^L &\equiv \sum_{i\in I} \sum_{m\in A_L} t_{im}^L e^{-i\frac{\lambda}{2}} \hat{d}_i^\dagger \hat{a}_{Lm} + \text{h.c.} \\
\hat{H}_\lambda^{\text{IA}} &\equiv \hat{H}_I + \hat{H}_A^L + \hat{H}_A^R + \hat{T}^R + \hat{T}_\lambda^L \\
\hat{H}_\lambda^{\text{aux}} &\equiv e^{i\frac{\lambda}{2}\hat{N}_L^{\text{aux}}} \hat{H}^{\text{aux}} e^{-i\frac{\lambda}{2}\hat{N}_L^{\text{aux}}} \\
&= \hat{H}_I + \sum_{\alpha=L,R} \left[\hat{H}_A^\alpha + \sum_{B=F,E} \left(\hat{H}_B^\alpha + \hat{V}_B^\alpha \right) \right] + \hat{T}^R + \hat{T}_\lambda^L \\
&\equiv \hat{H}_\lambda^{\text{IA}} + \sum_{\alpha=L,R} \sum_{B=F,E} \left(\hat{H}_B^\alpha + \hat{V}_B^\alpha \right)
\end{aligned} \tag{5.7}$$

Then the equation of motion (EOM) for $\hat{O}_\lambda(t)$ is

$$\begin{aligned}
\frac{d}{dt}\hat{O}_\lambda(t) &= e^{i\hat{H}_{-\lambda}^{\text{aux}} t} (i\hat{H}_{-\lambda}^{\text{aux}} \hat{O} - i\hat{O}\hat{H}_\lambda^{\text{aux}}) e^{-i\hat{H}_\lambda^{aux} t} \\
&= e^{i\hat{H}_{-\lambda}^{\text{aux}} t} (i\hat{H}_{-\lambda}^{\text{IA}} \hat{O} - i\hat{O}\hat{H}_\lambda^{\text{IA}}) e^{-i\hat{H}_\lambda^{aux} t} + \\
&\sum_{\alpha,B,m,k} e^{i\hat{H}_{-\lambda}^{\text{aux}} t} \left[i(V_{Bm}^\alpha \hat{a}_{\alpha m}^\dagger \hat{c}_{B_\alpha k} + V_{Bm}^{\alpha *} \hat{c}_{B_\alpha k}^\dagger \hat{a}_{\alpha m}) \hat{O} - i\hat{O}(V_{Bm}^\alpha \hat{a}_{\alpha m}^\dagger \hat{c}_{B_\alpha k} + V_{Bm}^{\alpha *} \hat{c}_{B_\alpha k}^\dagger \hat{a}_{\alpha m}) \right] e^{-i\hat{H}_\lambda^{aux} t}
\end{aligned} \tag{5.8}$$

Let's look at one of the terms in the last equation explicitly,

$$
\begin{aligned}
&\sum_{B,k} e^{i\hat{H}^{\rm aux}_{-\lambda}t}\left(iV^{\alpha}_{Bm}\hat{a}^{\dagger}_{\alpha m}\hat{c}_{B\alpha k}\hat{O}\right)e^{-i\hat{H}^{\rm aux}_{\lambda}t}\\
=&\sum_{k} e^{i\hat{H}^{\rm aux}_{-\lambda}t}\left(-iV^{\alpha}_{Fm}\hat{c}_{F_\alpha k}\hat{a}^{\dagger}_{\alpha m}\hat{O}+iV^{\alpha}_{Em}\hat{a}^{\dagger}_{\alpha m}\hat{O}\hat{c}_{E_\alpha k}\right)e^{-i\hat{H}^{\rm aux}_{\lambda}t}\\
=&\sum_{k} e^{i\hat{H}^{\rm aux}_{-\lambda}t}\left(-iV^{\alpha}_{Fm}\hat{c}_{F_\alpha k}e^{-i\hat{H}^{\rm aux}_{-\lambda}t}e^{i\hat{H}^{\rm aux}_{-\lambda}t}\hat{a}^{\dagger}_{\alpha m}\hat{O}+iV^{\alpha}_{Em}\hat{a}^{\dagger}_{\alpha m}\hat{O}e^{-i\hat{H}^{\rm aux}_{\lambda}t}e^{i\hat{H}^{\rm aux}_{\lambda}t}\hat{c}_{F_\alpha k}\right)e^{-i\hat{H}^{\rm aux}_{\lambda}t}\\
\overset{(A.2)}{=}&-iV^{\alpha}_{Fm}\sum_{k}\left(e^{-i\varepsilon^{F}_{\alpha k}t}\hat{c}_{F_\alpha k}-i\sum_{n\in A_\alpha}V^{\alpha *}_{Fn}\int_0^t ds e^{-i\varepsilon^{F}_{\alpha k}(t-s)}e^{i\hat{H}^{\rm aux}_{-\lambda}s}\hat{a}_{\alpha n}e^{-i\hat{H}^{\rm aux}_{-\lambda}s}\right)e^{i\hat{H}^{\rm aux}_{-\lambda}t}\hat{a}^{\dagger}_{\alpha m}\hat{O}e^{-i\hat{H}^{\rm aux}_{\lambda}t}\\
&+iV^{\alpha}_{Em}e^{i\hat{H}^{\rm aux}_{-\lambda}t}\hat{a}^{\dagger}_{\alpha m}\hat{O}e^{-i\hat{H}^{\rm aux}_{\lambda}t}\sum_{k}\left(e^{-i\varepsilon^{E}_{\alpha k}t}\hat{c}_{E_\alpha k}-i\sum_{n\in A_\alpha}V^{\alpha *}_{En}\int_0^t ds e^{-i\varepsilon^{F}_{\alpha k}(t-s)}e^{i\hat{H}^{\rm aux}_{\lambda}s}\hat{a}_{\alpha n}e^{-i\hat{H}^{\rm aux}_{-\lambda}s}\right)\\
\overset{(A.4)}{=}&-iV^{\alpha}_{FM}\sqrt{2\pi N^{\alpha}_{F}}\hat{c}^{(\rm in)}_{F_\alpha}(0)e^{i\hat{H}^{\rm aux}_{-\lambda}t}\hat{a}^{\dagger}_{\alpha m}\hat{O}e^{-i\hat{H}^{\rm aux}_{\lambda}t}-\sum_{n\in A_\alpha}\Gamma^{F\alpha}_{mn}e^{i\hat{H}^{\rm aux}_{-\lambda}t}\hat{a}_{\alpha n}\hat{a}^{\dagger}_{\alpha m}\hat{O}e^{-i\hat{H}^{\rm aux}_{\lambda}t}\\
&+iV^{\alpha}_{EM}e^{i\hat{H}^{\rm aux}_{-\lambda}t}\hat{a}^{\dagger}_{\alpha m}\hat{O}e^{-i\hat{H}^{\rm aux}_{\lambda}t}\sqrt{2\pi N^{\alpha}_{E}}\hat{c}^{\rm in}_{E_\alpha}(0)+\sum_{n\in A_\alpha}\Gamma^{E\alpha}_{mn}e^{i\hat{H}^{\rm aux}_{-\lambda}t}\hat{a}^{\dagger}_{\alpha m}\hat{O}\hat{a}_{\alpha n}e^{-i\hat{H}^{\rm aux}_{\lambda}t}
\end{aligned}
\tag{5.9}
$$

where $\Gamma^{B\alpha}_{mn}=\pi N^{\alpha}_{B}V^{\alpha}_{Bm}V^{\alpha *}_{Bn},\quad B=F,E$. Treating others terms in Eq.(5.8) similarly, we can get an equation similar as Eq.(A.9), and follow the same procedure as (A.10-13), we have EOM for $\hat{\rho}^{\rm IA}_{\lambda}(t)\equiv {\rm Tr}_{L_EL_FR_ER_F}\left(e^{-i\hat{H}^{\rm aux}_{\lambda}t}\hat{\rho}^{\rm aux}_{0}e^{i\hat{H}^{\rm aux}_{-\lambda}t}\right)$, where $\hat{\rho}^{\rm aux}_{0}=\hat{\rho}_{L_E}\otimes\hat{\rho}_{L_F}\otimes\hat{\rho}^{\rm IA}(0)\otimes\hat{\rho}_{R_E}\otimes\hat{\rho}_{R_F}$ is the initial state of the whole IM$_{\rm aux}$ and $\hat{\rho}_{\alpha_E}=|{\rm empty}\rangle\langle{\rm empty}|,\hat{\rho}_{\alpha_F}=|{\rm full}\rangle\langle{\rm full}|$:

$$
\begin{aligned}
\frac{d}{dt}\hat{\rho}^{IA}_{\lambda}(t) \quad &= -i\hat{H}^{IA}_{\lambda}\hat{\rho}^{IA}_{\lambda}(t)+i\hat{\rho}^{IA}_{\lambda}(t)\hat{H}^{IA}_{-\lambda}\\
&+\sum_{\alpha=L,R}\sum_{m_{1,2}\in A_\alpha}\Bigg[\Gamma^{E\alpha}_{m_1m_2}\left(2\hat{a}_{\alpha m_2}\hat{\rho}^{IA}_{\lambda}(t)\hat{a}^{\dagger}_{\alpha m_1}-\left\{\hat{\rho}^{IA}_{\lambda}(t),\hat{a}^{\dagger}_{\alpha m_1}\hat{a}_{\alpha m_2}\right\}\right) \qquad (5.10)\\
&\qquad +\Gamma^{F\alpha}_{m_1m_2}\left(2\hat{a}^{\dagger}_{\alpha m_1}\hat{\rho}^{IA}_{\lambda}(t)\hat{a}_{\alpha m_2}-\left\{\hat{\rho}^{IA}_{\lambda}(t),\hat{a}_{\alpha m_2}\hat{a}^{\dagger}_{\alpha m_1}\right\}\right)\Bigg] \qquad (5.11)
\end{aligned}
$$

The differences between Eq.(5.10) and Eq.(A.13) are: 1. lead L and R are distinguished; 2. $\hat{H}^{\rm IA}$

is now dressed with counting field $\pm\lambda$ when it appears to the left/right side of $\hat{\rho}^{\text{aux}}_{\lambda}$ respectively.

The GF of FCS for IM_{aux} satisfies

$$\begin{aligned}\tilde{Z}(\lambda,t) &= \text{Tr}\left(e^{-i\hat{H}^{\text{aux}}_{\lambda}t}\hat{\rho}^{\text{aux}}_{0}e^{i\hat{H}^{\text{aux}}_{-\lambda}t}\right)\\ &= \text{Tr}_{IA}\hat{\rho}^{\text{IA}}_{\lambda}(t)\end{aligned} \tag{5.12}$$

Hence by solving Eq.(5.10) I have access to the GF of the IM_{aux}, which is equal to the GF of the original system if the mapping is exact.

5.3 Bath Mapping

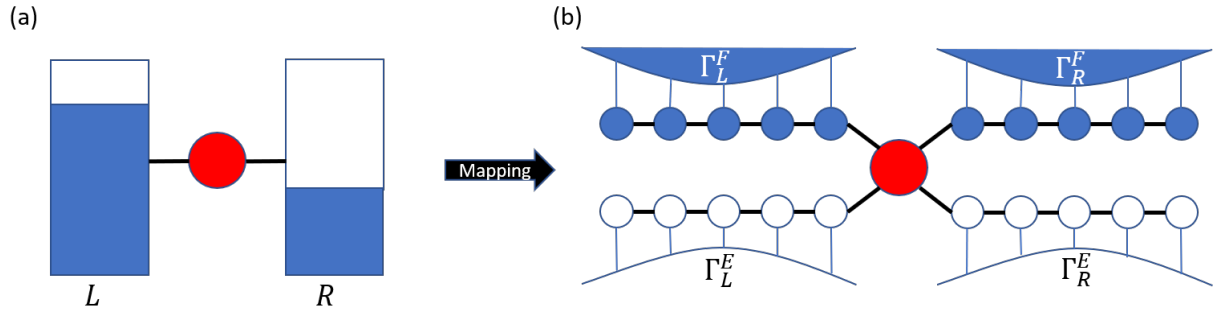

Figure 5.1: (a) Original system: the impurity is coupled to two leads L and R; (b) Auxiliary system: each lead is mapped into a full bath and an empty bath. The impurity is displayed as red circles, the full and empty bath sites as blue and white ones.

Mapping procedure is discussed in [27] in detail. Here for simplicity I'll assume that each bath is only coupled to one site in the impurity. The original baths start from the thermal equilibrium, the corresponding HFs only depend on the time difference, i.e. $\Delta^{R/K}_{L/R}(t_1,t_2) = \Delta^{R/K}_{L/R}(t_1-t_2)$. Correspondingly, the initial states of the auxiliary modes should be the stationary states when they are evolving without coupling to the impurity but is purely driven by the full and empty baths. To simplify the preparation of the initial state, I map the original lead $\alpha(\alpha = L,R)$ into one full and one empty bath, see Fig. 5.1. The full bath is composed of some dissipative auxiliary modes (A^F_{α}) which are initially occupied and are characterized by Hamiltonian matrix

$\boldsymbol{E}_\alpha^F$ and $\boldsymbol{\Gamma}_\alpha^F$; for the empty bath, auxiliary modes are initially unoccupied and are characterized by $\boldsymbol{E}_\alpha^E$ and $\boldsymbol{\Gamma}_\alpha^E$. Note that here and in the following bold $\boldsymbol{E}$ denotes Hamiltonian matrix of the auxiliary modes and ordinary E appearing in the superscript denotes empty bath.

According to Eq.(1.8), the greater(lesser) component of the HF of the full(empty) bath vanishes. Hence the full(empty) bath accounts for the lesser(greater) component of the HF of the lead respectively, i.e. $\tilde{\Delta}_\alpha^F$ and $\tilde{\Delta}_\alpha^E$ of the full and empty bath for lead α should achieve

$$\begin{aligned}\tilde{\Delta}^<_{F\alpha}(\omega) &\to -2if(\omega;\mu_\alpha,T_\alpha)\mathrm{Im}\Delta^R_\alpha(\omega)\\ \tilde{\Delta}^>_{E\alpha}(\omega) &\to 2i\left[1-f(\omega;\mu_\alpha,T_\alpha)\right]\mathrm{Im}\Delta^R_\alpha(\omega)\end{aligned} \tag{5.13}$$

Due to fluctuation-dissipation theorem, this relation can be equivalently written in terms of the retarded components:

$$\begin{aligned}\mathrm{Im}\tilde{\Delta}^R_{F\alpha}(\omega) &\to f(\omega;\mu_\alpha,T_\alpha)\mathrm{Im}\Delta^R_\alpha(\omega)\\ \mathrm{Im}\tilde{\Delta}^R_{E\alpha}(\omega) &\to \left[1-f(\omega;\mu_\alpha,T_\alpha)\right]\mathrm{Im}\Delta^R_\alpha(\omega)\end{aligned} \tag{5.14}$$

However, with finite number of auxiliary modes, the mapping can only be achieved approximately, and the retarded HF of the full/empty bath is given by [27]

$$\begin{aligned}\tilde{\Delta}^R_{F\alpha}(\omega) &= \sum_{m\in A^F_\alpha}|t^{F\alpha}_m|^2(\omega\mathbf{I}-\boldsymbol{E}^F_\alpha+\frac{i}{2}\boldsymbol{\Gamma}^F_\alpha)^{-1}_{mm}\\ \tilde{\Delta}^R_{E\alpha}(\omega) &= \sum_{m\in A^E_\alpha}|t^{E\alpha}_m|^2(\omega\mathbf{I}-\boldsymbol{E}^E_\alpha+\frac{i}{2}\boldsymbol{\Gamma}^E_\alpha)^{-1}_{mm}\end{aligned} \tag{5.15}$$

where $t^{F\alpha}_m(t^{E\alpha}_m)$ is the coupling strength between the impurity and the auxiliary mode m in full(empty) bath for lead α.

The central task of bath mapping is adjusting parameters $t,\boldsymbol{E},\boldsymbol{\Gamma}$ in Eq.(5.15) to achieve

Eq.(5.14), and this can be done by minimize the following cost functions:

$$\begin{aligned}\chi_{F\alpha} &= \int d\omega \left[\mathrm{Im}\tilde{\Delta}^R_{F\alpha}(\omega) - f(\omega;\mu_\alpha,T_\alpha)\mathrm{Im}\Delta^R_\alpha(\omega)\right]^2 \\ \chi_{E\alpha} &= \int d\omega \left\{\mathrm{Im}\tilde{\Delta}^R_{E\alpha}(\omega) - [1-f(\omega;\mu_\alpha,T_\alpha)]\mathrm{Im}\Delta^R_\alpha(\omega)\right\}^2\end{aligned} \tag{5.16}$$

In favor of the applicability of MPS methods, one should avoid long-range hoppings and I thus restrict $\boldsymbol{E}$ to tridiagonal form. Furthermore, hermiticity and gauge degrees of freedom allow $\boldsymbol{E}$ to be real symmetric. And for reasons that we will see later in section 5.5, $\boldsymbol{\Gamma}$ is restricted to be diagonal. Hence for N_B auxiliary bath modes, the number of parameters assigned to $t, \boldsymbol{E}, \boldsymbol{\Gamma}$ is respectively $1, 2N_B-1, N_B$; totally there are $3N_B$ parameters. So Eq.(5.16) constitutes a multi-dimensional minimization problem, which is very demanding. An efficient numerical strategy based on parallel tempering algorithm was put forward for this bath mapping problem in [27], and is adopted in this thesis.

5.4 Super-fermion Representation

Once the bath parameters $t, \boldsymbol{E}, \boldsymbol{\Gamma}$ are set, the next step is to solve the corresponding Lindblad QME (5.10). Here I exploit the so-called super-fermion representation [31, 111] in which Lindblad QME can be cast into a Schrödinger-type equation. Explicitly, this can be done by introducing an augmented fermionic Fock space with twice as many sites as in $\mathrm{IM}_{\mathrm{aux}}$. The additional sites are a copy of the physical sites and are labeled by a tilde. A fundamental object in this augmented space is the so-called left vacuum:

$$|I\rangle = \sum_{\{n_i\}} (-i)^{N(\{n_i\})} |\{n_i\}\rangle \otimes \widetilde{|\{\bar{n}_i\}\rangle} \tag{5.17}$$

The summation runs over all possible configurations in occupation basis $|\{n_i\}\rangle$ of the physical system and $\widetilde{|\{\bar{n}_i\}\rangle}$ is the corresponding state of the tilde system with inverted occupation $\bar{n}_i =$

$1-n_i$. And $N(\{n_i\}) = \sum_i n_i$ is the total number of electrons in the non-tilde system at state $|\{n_i\}\rangle$. The following rules is satisfied for left-vacuum:

$$c_j|I\rangle = -i\tilde{c}_j|I\rangle, \qquad c_j^\dagger|I\rangle = -i\tilde{c}_j^\dagger|I\rangle \tag{5.18}$$

One can define the following state vector for the dressed density operator (expecting no danger of causing confusion, I'll drop the "IA" superscript and hat on operators from now on):

$$|\rho_\lambda(t)\rangle \equiv \rho_\lambda(t)|I\rangle \tag{5.19}$$

Then by multiplying both sides of Eq.(5.10) by $|I\rangle$, and applying the commutation relation $[\tilde{c}_j, \rho_\lambda(t)] = 0$ and $[\tilde{c}_j^\dagger, \rho_\lambda(t)] = 0$, the dressed Lindblad QME is transformed into the following form:

$$\frac{d}{dt}|\rho_\lambda(t)\rangle = \mathcal{L}_\lambda|\rho_\lambda(t)\rangle \tag{5.20}$$

where $\mathcal{L}_\lambda$ is a non-hermitian operator in the augmented space. A nice property of $\mathcal{L}_\lambda$ is that it preserves the Abelian symmetry (charge conservation) of the original Hamiltonian, and by making use of symmetries the computational cost can be greatly reduced.

Note also the following important relation:

$$Z(\lambda,t) = \mathrm{Tr}\,(\rho_\lambda(t)) = \langle I|\rho_\lambda(t)\rangle, \qquad \langle I|O|\rho_\lambda(t)\rangle = \mathrm{Tr}\,(\rho_\lambda(t)O) \tag{5.21}$$

5.5 MPS and TEBD

With QME written in Schrödinger-type form, we are ready to employ matrix product state (MPS) [15] representation of the state vector $|\rho_\lambda(t)\rangle$. MPS is designed to describe the many-body states of one-dimensional systems, so we map $\mathrm{IM}_{\mathrm{aux}}$ shown in Fig.(5.1) into a chain in the augmented space of SF representation, as in Fig.(5.2). Since each lead is split into two

auxiliary baths (full and empty), there are inevitably long-range hopping between one of the two and the impurity. The diagonal elements of $\mathbf{\Gamma}$ provide nearest-neighbor couplings between a physical site and its tilt copy because

$$\begin{aligned}\Gamma^E_{jj} c_j \rho_\lambda(t) c_j^\dagger |I\rangle &= \Gamma^E_{jj} c_j \rho_\lambda(t)(-i)\tilde{c}_j^\dagger |I\rangle = i\Gamma^E_{jj}\tilde{c}_j^\dagger c_j |\rho_\lambda(t)\rangle \\ \Gamma^F_{jj} c_j^\dagger \rho_\lambda(t) c_j |I\rangle &= \Gamma^F_{jj} c_j^\dagger \rho_\lambda(t)(-i)\tilde{c}_j |I\rangle = -i\Gamma^F_{jj} c_j^\dagger \tilde{c}_j |\rho_\lambda(t)\rangle\end{aligned} \tag{5.22}$$

Off-diagonal elements of $\mathbf{\Gamma}$ like $\mathbf{\Gamma}_{i,i+1}$ will result in interactions beyond next-nearest neighbors. But long-range interactions are cumbersome to deal with in MPS, and my experience is that adding these terms as parameters only slightly improve the bath fitting. So it improves the computational efficiency by restricting $\mathbf{\Gamma}$ to be diagonal.

Next-nearest-neighbor couplings between two non-tilde sites or two tilde sites are due to the non-diagonal hopping terms of the tridiagonal matrix $\boldsymbol{E}$. The diagonal elements of both $\boldsymbol{E}$ and $\mathbf{\Gamma}$ contribute to the on-site terms.

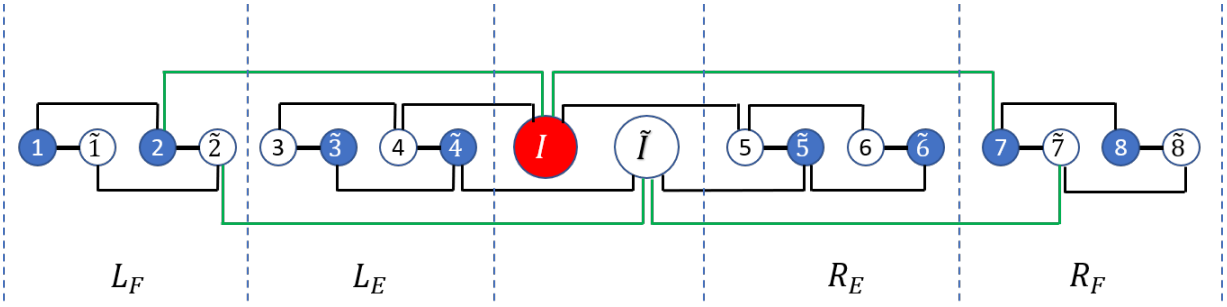

Figure 5.2: Auxiliary system with a chain geometry in augmented space. For the full baths L_F and R_F, non-tilde sites are initially occupied while tilde sites are initially unoccupied. For empty baths L_E and R_E, it's the other way around.

The formal solution of Eq.(5.20) is

$$|\rho_\lambda(t)\rangle = e^{\mathcal{L}_\lambda t}|\rho_0\rangle \tag{5.23}$$

Initially, all non-tilde bath sites of the full baths are occupied but those of the empty baths are

unoccupied. We have freedom of the initial occupation of the impurity site, and here I choose it to be occupied. The initial density matrix operator of $\mathrm{IM}_{\mathrm{aux}}$ is thus

$$\rho_0 = \left(\prod_{i \in L_F \cup R_F} |1_i\rangle\langle 1_i| \right) \otimes \left(\prod_{j \in L_E \cup R_E} |0_j\rangle\langle 0_j| \right) \otimes (|1_I\rangle\langle 1_I|)$$

which means

$$|\rho_0\rangle = \rho_0 |I\rangle = (-i)^N \left(\prod_{i \in L_F \cup R_F} |1_i\rangle \otimes \widetilde{|0_i\rangle} \right) \otimes \left(\prod_{j \in L_E \cup R_E} |0_j\rangle \otimes \widetilde{|1_j\rangle} \right) \otimes \left(|1_I\rangle \otimes \widetilde{|0_I\rangle} \right)$$

where N is the total occupation number of the non-tilde sites. A convenient way to construct MPS for left vacuum state is using the following relation:

$$|I\rangle = \exp(-i \sum_j c_j^\dagger \tilde{c}_j) |\{0\}\rangle \otimes \widetilde{|\{1\}\rangle} \tag{5.24}$$

With chain geometry of $\mathrm{IM}_{\mathrm{aux}}$ and MPS representation of initial state vector $|\rho_0\rangle$, I then implement time-evolving block decimation technique (TEBD) [113] to propagate the state. TEBD is realised by decomposing a short-time evolution operator $e^{\mathcal{L}_\lambda \Delta t}$ into a sequence of Trotter gates, which act on two nearest-neighbor sites. The application of Trotter gates enlarges the matrix dimension of MPS, so a singular value decomposition (SVD) is performed to fix the bond dimension. Particularly, I'll adopt the second-order Trotter decomposition (TEBD2) [115], which has error $O(\Delta t^2)$ accumulated over the entire time interval.

Long-range interactions can be treated by swap gates [114] $S(ij) = \delta_{s_i s'_j} \delta_{s_j s'_i}$: each swap gate exchange two neighboring sites i and j, and a series of them can move the long-range interacting sites next to each other. For example, the next-nearest-neighbor interactions in $\mathcal{L}_\lambda$ can be efficiently treated by swap gates (see Fig.5.3).

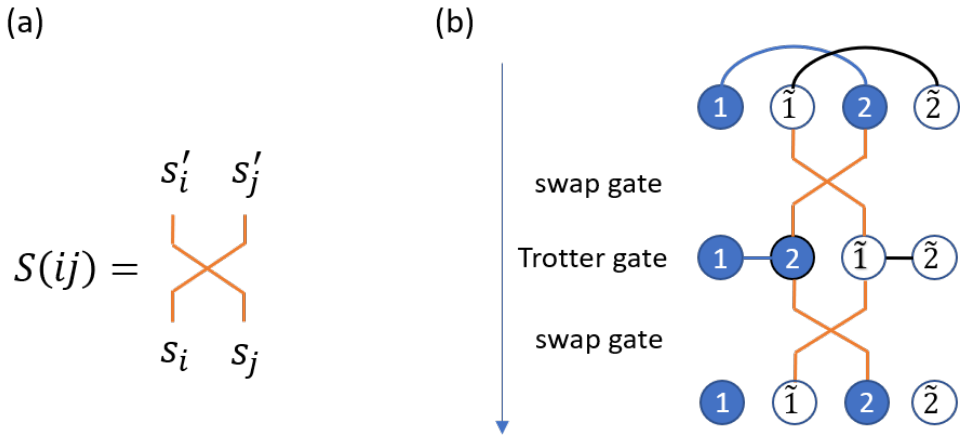

Figure 5.3: (a) Swap gate exchange the states on two identical nearest-neighboring sites i and j; (b) By applying swap gate, two pairs of next-nearest neighbors (12) and $(\tilde{1}\tilde{2})$ become nearest ones. We can then act on them Trotter gates corresponding to terms $e^{\mathcal{L}_{12}\Delta t}$ and $e^{\mathcal{L}_{\tilde{1}\tilde{2}}\Delta t}$. Finally, I swap sites back to their original positions.

5.6 Noise

With the time-evolved state $|\rho_\lambda(t)\rangle\rangle$, we can calculate GF of FCS by Eq.(5.21), from which all cumulants of electron transport are accessible. Particularly, zero-frequency noise S is given by

$$S = \lim_{t\to\infty} \frac{dC_2(t)}{dt}, \qquad C_2(t) = \frac{\partial^2 \ln Z(\lambda,t)}{\partial(i\lambda)^2}\bigg|_{\lambda=0} \tag{5.25}$$

In practice, we could compute $Z(\lambda,t)$ for a small λ, and then $S \approx 2\frac{\ln Z(\lambda,t+\Delta t/2)-\ln Z(\lambda,t-\Delta t/2)}{\Delta t(i\lambda)^2}$ for sufficiently large t.

A numerically more realiable way to calculate S is

$$S = 2\frac{\partial}{\partial\lambda}\lim_{t\to\infty} \mathrm{Im}J(\lambda,t), \qquad J(\lambda,t) \equiv \frac{\mathrm{Tr}(J\rho_\lambda(t))}{\mathrm{Tr}\rho_\lambda(t)} = \frac{\langle\langle I|J|\rho_\lambda(t)\rangle\rangle}{\langle\langle I|\rho_\lambda(t)\rangle\rangle} \tag{5.26}$$

where $J \equiv -i[N_L, H]$ is the current operator. In numerical practise, calculating S by Eq.(5.26) turns out to be less hampered by the truncation error of SVD than by Eq.(5.25).

5.6.1 Proof of Eq.(5.26)

First, I need following relations:

$$
\begin{aligned}
Z(\lambda,t) &= \mathrm{Tr}(e^{iH_{-\lambda}t}e^{-iH_{\lambda}t}\rho_0) \\
Z(0,t) &= 1 \\
\frac{dH_\lambda}{d\lambda} &= \frac{d\left(e^{iN_L\lambda/2}He^{-iN_L\lambda/2}\right)}{d\lambda} \\
&= e^{iN_L\lambda/2}\frac{i}{2}[N_L,H]e^{-iN_L\lambda/2} \\
&= -e^{iN_L\lambda/2}\frac{J}{2}e^{-iN_L\lambda/2}
\end{aligned}
\tag{5.27}
$$

Then

$$
\begin{aligned}
\frac{\partial}{\partial t}\frac{\partial^2 \ln Z(\lambda,t)}{\partial(i\lambda)^2} =& \frac{\partial^2}{\partial(i\lambda)^2}\left\{\frac{1}{Z(\lambda,t)}\mathrm{Tr}\left[-i(H_\lambda - H_{-\lambda})e^{-iH_\lambda t}\rho_0 e^{iH_{-\lambda}t}\right]\right\} \\
=& \frac{\partial^2}{\partial(i\lambda)^2}\left\{\frac{1}{Z(\lambda,t)}\mathrm{Tr}\left[-i(H_\lambda - H_{-\lambda})\rho_\lambda(t)\right]\right\} \\
=& \left(\frac{\partial^2}{\partial(i\lambda)^2}\frac{1}{Z(\lambda,t)}\right)\mathrm{Tr}\left[-i(H_\lambda - H_{-\lambda})\rho_\lambda(t)\right] \\
&+ \frac{1}{Z(\lambda,t)}\frac{\partial^2}{\partial(i\lambda)^2}\mathrm{Tr}\left[-i(H_\lambda - H_{-\lambda})\rho_\lambda(t)\right] \\
&+ 2\left(\frac{\partial}{\partial(i\lambda)}\frac{1}{Z(\lambda,t)}\right)\frac{\partial}{\partial(i\lambda)}\mathrm{Tr}\left[-i(H_\lambda - H_{-\lambda})\rho_\lambda(t)\right]
\end{aligned}
\tag{5.28}
$$

There are three terms after the last equal sign, but because

$$
(H_\lambda - H_{-\lambda})|_{\lambda=0} = 0, \qquad \frac{\partial^2}{\partial\lambda^2}(H_\lambda - H_{-\lambda})|_{\lambda=0} = 0 \tag{5.29}
$$

only following terms remain after taking $\lambda = 0$:

$$\begin{aligned}\frac{\partial}{\partial t}\frac{\partial^2 \ln Z(\lambda,t)}{\partial (i\lambda)^2}\bigg|_{\lambda=0} =& 2\mathrm{Tr}\left[J\,\frac{\partial \rho_\lambda(t)}{\partial i\lambda}\bigg|_{\lambda=0}\right] + 2\,\frac{\partial}{\partial (i\lambda)}\frac{1}{Z(\lambda,t)}\bigg|_{\lambda=0}\mathrm{Tr}\left[J\rho(t)\right] \\ =& 2\frac{\partial}{\partial (i\lambda)}\,\frac{\mathrm{Tr}\left[J\rho_\lambda(t)\right]}{\mathrm{Tr}\rho_\lambda(t)}\bigg|_{\lambda=0}\end{aligned} \tag{5.30}$$

Hence,

$$\begin{aligned}S =& \lim_{t\to\infty}\,\frac{\partial}{\partial t}\frac{\partial^2 \ln Z(\lambda,t)}{\partial (i\lambda)^2}\bigg|_{\lambda=0} \\ =& 2\lim_{t\to\infty}\,\frac{\partial}{\partial (i\lambda)}\,\frac{\mathrm{Tr}\left[J\rho_\lambda(t)\right]}{\mathrm{Tr}\rho_\lambda(t)}\bigg|_{\lambda=0} \\ =& 2\frac{\partial}{\partial \lambda}\lim_{t\to\infty}\mathrm{Im}\,\frac{\mathrm{Tr}\left[J\rho_\lambda(t)\right]}{\mathrm{Tr}\rho_\lambda(t)}\bigg|_{\lambda=0}\end{aligned} \tag{5.31}$$

where at the last step I used the fact that S is real. □

5.7 Example

In this section, I validate this method by benchmarking against the exact solution of GF for resonant level model, where a single spinless level is coupled to two leads L and R. Initially, the level and leads are decoupled and leads are in equilibrium. At $t = 0$, the coupling is turned on. Using the path-integral formalism, the GF based on two-time measurement scheme is given by [116]

$$Z(\lambda,t) = \det(\boldsymbol{G}\boldsymbol{G'}^{-1}) \tag{5.32}$$

where

$$\boldsymbol{G}^{-1} = \boldsymbol{g}^{-1} - \boldsymbol{\Delta}_L - \boldsymbol{\Delta}_R, \qquad \boldsymbol{G}_\lambda^{-1} = \boldsymbol{g}^{-1} - \boldsymbol{\Delta}'_L - \boldsymbol{\Delta}_R \tag{5.33}$$

Here $\boldsymbol{g}$ is the bare Green's function of isolated level, $\boldsymbol{\Delta}'_L$ is the hybridization function of lead L dressed with counting field. All quantities in the above expression are defined in the Keldysh

space with two time indices, which go from 0 to t:

$$\boldsymbol{A}(t,t') = \begin{pmatrix} A^R(t,t') & A^K(t,t') \\ 0 & A^A(t,t') \end{pmatrix} \tag{5.34}$$

Finally,

$$\boldsymbol{\Delta}'_L(t,t') = \exp[-i\sigma_x\lambda/2]\boldsymbol{\Delta}_L(t,t')\exp[i\sigma_x\lambda/2] \tag{5.35}$$

The implementation of dressed auxiliary QME for FCS starts from bath fitting. Here the leads are chosen to have a flat band with a smooth cutoff [117]:

$$\Gamma_{L/R}(\omega) = \frac{\Gamma_{L/R}}{(1+e^{\nu(\omega-\Omega_c)})(1+e^{-\nu(\omega+\Omega_c)})} \tag{5.36}$$

In what follows, I set $\Gamma_L = \Gamma_R = 1/2$ and $\Gamma \equiv \Gamma_L + \Gamma_R = 1$ is the energy unit. We take the leads' band cutoff Ω_c to be 10Γ, and the edge width $\frac{1}{\nu}$ to be 0.1Γ. e, $\hbar$, and k_B are taken to be unity. The voltage bias V is set to be 10Γ, and $\mu_L = -\mu_R = V/2$. Temperature is 0.02Γ.

Fig.(5.4) is the result of fitting the full and empty bath components of lead L, with $N_B = 10$. After bath fitting, we map the auxiliary system into a chain, write the Liouvillian in super-fermion representation and evolve the system in time by TEBD2. We evaluate GF and dressed current by Eq.(5.21) along the way, and when the dressed current becomes stable, we calculate noise by Eq.(5.26). There are three sources of error: imperfection of bath fitting, time-step error and truncation error. MPS calculation is performed using the ITensor Library [118]. The exact value of steady-state noise S is given by

$$S = \frac{e^2}{2\pi\hbar}\int_{-\infty}^{+\infty} d\omega\{T(\omega)[f_L(1-f_L)+f_R(1-f_R)]+T(\omega)[1-T(\omega)](f_L-f_R)^2\} \tag{5.37}$$

where $T(\omega) = 4\Gamma_L(\omega)G^R(\omega)\Gamma_R(\omega)G^A(\omega)$ and $G^{R/A}$ are the Green's functions of the impurity

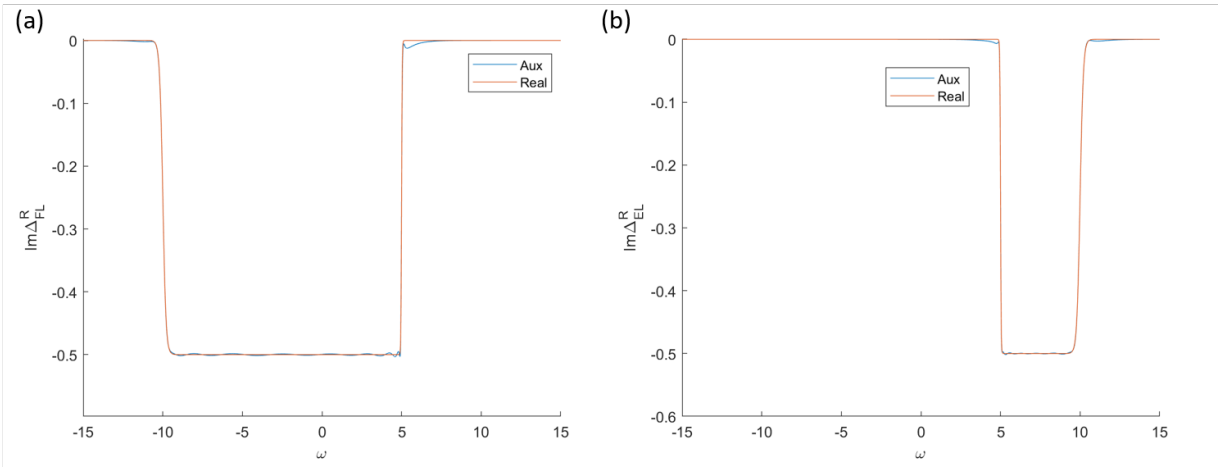

Figure 5.4: Results of fitting the full and empty bath components of lead L with $N_B = 10$. (a) Imaginary part of retarded HFs of the auxiliary full bath ('Aux', Eq.5.15) and full bath component of lead L ('Real', Eq.5.14); (b) Similarly for the empty bath.

level.

In Fig.(5.5), I compare the exact results by Eq.(5.32) with the ones from dressed QME calculation done for $\lambda = \pi/100$. Indeed, for very small λ, the imaginary part of GF grows linearly with time for large t. And the noise $S(t) \equiv dC_2(t)/dt$ calculated by Eq.(5.25) and Eq.(5.26) match very well in time and eventually reach the steady-state value given by Eq.(5.37).

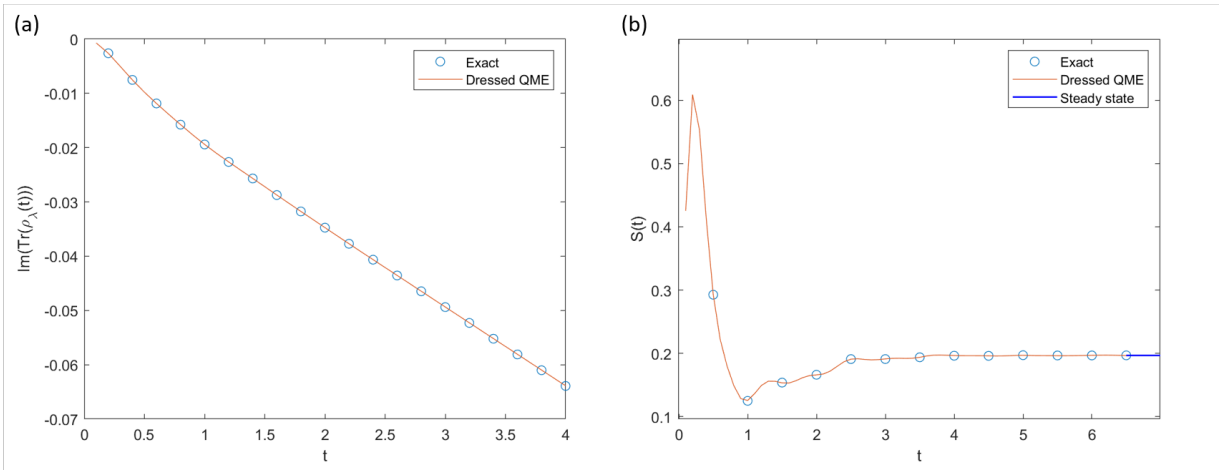

Figure 5.5: FCS for resonant level model: dressed QME versus exact results. $\lambda = \pi/100$. (a) Imaginary part of the generating function; (b) Noise $S(t) \equiv dC_2(t)/dt$ given by Eq.(5.25) and Eq.(5.26) display very nice agreement and converge to the steady value denoted by blue line.

5.8 Conclusion

Auxiliary QME was originally proposed to be an efficient method for solving nonequilibrium impurity problems. In this thesis, I generalize it to the realm of full counting statistics, which yields much more information about transport properties. Theoretical construction as well as implementation details are given. Particularly, I propose a bath mapping scheme (full + empty) which simplifies the preparation of bath in equilibrium. Super-fermion representation enables MPS representation of the density matrix of auxiliary system and applicability of standard time-evolution method TEBD2. I also prove that zero-frequency noise can be evaluated from the steady value of dressed current. Finally, I benchmark the new method with exact solution for resonant level model, and find nice agreement. In the future, I plan to apply this method to more interesting models such as two level bridge coupled to optical cavity, in which one can study the interplay between photon absorption/emission and electron tunneling.

This chapter is a preliminary draft, and will be coauthored with Michael Galperin. The dissertation author was the primary investigator and author of this draft.

Appendix A

Derivation of Lindblad QME Eq. (2.17)

Here we prove that reduced density matrix of $S+A$ in the *aux* model satisfies Markov Lindblad-type equation-of-motion (EOM), Eq. (2.17).

We start by considering unitary evolution of the *aux* model. Heisenberg EOM for bath annihilation operator $\hat{c}_{Ck}$ is

$$\frac{d}{dt}\hat{c}_{Ck}(t) = i[\hat{H}^{aux}(t), \hat{c}_{Ck}(t)] = -i\varepsilon_{Ck}\hat{c}_{Ck}(t) - i\sum_{m\in A}(t_m^C)^*\,\hat{a}_m(t) \tag{A.1}$$

Its formal solution is

$$\hat{c}_{Ck}(t) = e^{-i\varepsilon_{Ck}t}\hat{c}_{Ck}(0) - i\sum_{m\in A}(t_m^C)^*\int_0^t ds\, e^{i\varepsilon_{Ck}(t-s)}\hat{a}_m(s) \tag{A.2}$$

Thus, Heisenberg EOM for an arbitrary operator $\hat{O}$ on $S+A$ can be written as

$$\begin{aligned}\frac{d}{dt}\hat{O}(t) = i[\hat{H}_{SA}(t),\hat{O}(t)] - i\sum_{m\in A}\Bigg\{ \\ \sum_{k\in R}\Bigg[t^R_m[\hat{O}(t),\hat{a}^\dagger_m]_\zeta\Big(e^{-i\varepsilon_{Rk}t}\hat{c}_{Rk}(0) - i\sum_{m'\in A}(t^R_{m'})^*\int_0^t ds\, e^{-i\varepsilon_{Rk}(t-s)}\hat{a}_{m'}(s)\Big) \\ +\zeta(t^R_m)^*\Big(e^{i\varepsilon_{Rk}t}\hat{c}^\dagger_{Rk}(0) + i\sum_{m'\in A}t^R_{m'}\int_0^t ds\, e^{i\varepsilon_{Rk}(t-s)}\hat{a}^\dagger_{m'}(s)\Big)[\hat{O}(t),\hat{a}_m(t)]_\zeta\Bigg] \\ -\sum_{k\in L}\Bigg[(t^L_m)^*[\hat{O}(t),\hat{a}_m(t)]_\zeta\Big(e^{i\varepsilon_{Lk}t}\hat{c}^\dagger_{Lk}(0) + i\sum_{m'\in A}t^L_{m'}\int_0^t ds\, e^{i\varepsilon_{Lk}(t-s)}\hat{a}^\dagger_{m'}(s)\Big) \\ +\zeta t^L_m\Big(e^{-i\varepsilon_{Lk}t}\hat{c}_{Lk}(0) - i\sum_{m'\in A}(t^L_{m'})^*\int_0^t ds\, e^{-i\varepsilon_{Lk}(t-s)}\hat{a}_{m'}(s)\Big)[\hat{O}(t),\hat{a}^\dagger_m(t)]_\zeta\Bigg]\Bigg\}\end{aligned} \tag{A.3}$$

where $\zeta = +/-1$ if $\hat{O}$ contains even/odd number of fermion operators, and $[,]_\zeta$ is (anti)commutator for $\zeta = (-)1$.

For future reference we introduce

$$\hat{c}^{(in)}_C(t) \equiv \frac{1}{\sqrt{2\pi N_C}}\sum_{k\in C}e^{-i\varepsilon_{Ck}t}\hat{c}_{Ck}(0) \tag{A.4}$$

which satisfies anti-commutation relations

$$\left\{\hat{c}^{(in)}_{C_1}(t),\hat{c}^{(in)\,\dagger}_{C_2}(s)\right\} = \delta_{C_1,C_2}\,\delta(t-s) \tag{A.5}$$

$$\left\{\hat{c}^{(in)}_{C_1}(t),\hat{c}^{(in)}_{C_2}(s)\right\} = \left\{\hat{c}^{(in)\,\dagger}_{C_1}(t),\hat{c}^{(in)\,\dagger}_{C_2}(s)\right\} = 0 \tag{A.6}$$

The delta in time is due to the fact that the contact density of states N_C is constant, and, thus,

$$\sum_{k\in C}e^{-i\varepsilon_{Ck}t} \equiv \int d\varepsilon\, N_C(\varepsilon)e^{-i\varepsilon t} = 2\pi N_C\delta(t) \tag{A.7}$$

is satisfied. Note also that

$$\int_0^t ds\,\delta(t-s)f(s) = \frac{1}{2}f(t) \tag{A.8}$$

holds for arbitrary function $f(t)$.

Using (A.4), (A.7), and (A.8) in (A.3) leads to

$$\begin{aligned}
&\frac{d}{dt}\hat{O}(t) = i[\hat{H}_{SA}(t), \hat{O}(t)] \\
&-i\sum_{m\in A}\Big\{t_{Rj}[\hat{O}(t), \hat{a}_m^\dagger(t)]_\zeta\, \hat{c}_R^{(in)}(t) + \zeta(t_m^R)^* \hat{c}_R^{(in)\,\dagger}(t)[\hat{O}(t), \hat{a}_m(t)]_\zeta \\
&-(t_m^L)^*[\hat{O}(t), \hat{a}_m(t)]_\zeta \hat{c}_L^{(in)\,\dagger}(t) - \zeta t_m^L \hat{c}_L^{(in)}(t)[\hat{O}(t), \hat{a}_m^\dagger(t)]_\zeta\Big\} \qquad \text{(A.9)} \\
&-\sum_{m_1,m_2\in A}\Big\{\Gamma^R_{m_1m_2}[\hat{O}(t), \hat{a}_{m_1}^\dagger(t)]_\zeta\, \hat{a}_{m_2}(t) - \zeta\Gamma^R_{m_2m_1}\hat{a}_{m_2}(t)^\dagger[\hat{O}(t), \hat{a}_{m_1}(t)]_\zeta \\
&-\zeta\Gamma^L_{m_1m_2}\hat{a}_{m_2}(t)[\hat{O}(t), \hat{a}_{m_1}^\dagger(t)]_\zeta + \Gamma^L_{m_2m_1}[\hat{O}(t), \hat{a}_{m_1}(t)]_\zeta\, \hat{a}_{m_2}^\dagger(t)\Big\}
\end{aligned}$$

where we employed definition of the dissipation matrix, Eq. (2.19).

Next we are going to write EOM for expectation value of $\hat{O}$

$$\langle\hat{O}(t)\rangle \equiv \mathrm{Tr}\big[\hat{O}(t)\,\hat{\rho}^{aux}(0)\big] \qquad \text{(A.10)}$$

by averaging (A.9) with initial density operator of the *aux* model, Eq. (2.16). Because initially $S+A$ is from the baths and because bath L is full and R is empty (see Figure 2.1b)

$$\hat{c}_L^{(in)\,\dagger}(t)\,\hat{\rho}_L = \hat{\rho}_L\,\hat{c}_L^{(in)}(t) = \hat{c}_R^{(in)}(t)\,\hat{\rho}_R = \hat{\rho}_R\,\hat{c}_R^{(in)\,\dagger}(t) = 0 \qquad \text{(A.11)}$$

holds. Thus, second and third lines in (A.9) do not contribute, and EOM for the expectation value of $\hat{O}(t)$ is

$$\begin{aligned}
\left\langle\frac{d}{dt}\hat{O}(t)\right\rangle = \mathrm{Tr}\Big[\hat{\rho}^{aux}(0)\,i[\hat{H}_{SA}(t), \hat{O}(t)]\Big] - \sum_{m_1,m_2\in A}\mathrm{Tr}\Big[\hat{\rho}^{aux}(0)\Big\{ \\
\Gamma^R_{m_1m_2}[\hat{O}(t), \hat{a}_{m_1}^\dagger(t)]_\zeta\, \hat{a}_{m_2}(t) - \zeta\Gamma^R_{m_1m_2}\hat{a}_{m_1}^\dagger(t)[\hat{O}(t), \hat{a}_{m_2}(t)]_\zeta \qquad \text{(A.12)} \\
+\Gamma^L_{m_1m_2}[\hat{O}(t), \hat{a}_{m_2}(t)]_\zeta\, \hat{a}_{m_1}^\dagger(t) - \zeta\Gamma^L_{m_1m_2}\hat{a}_{m_2}(t)[\hat{O}(t), \hat{a}_{m_1}^\dagger(t)]_\zeta\Big\}\Big]
\end{aligned}$$

Because $\hat{O}$ is arbitrary in $S+A$, after transforming to Schrödinger picture (A.12) can be rewritten as EOM for $\hat{\rho}^{aux}(t)$

$$\begin{aligned}\frac{d}{dt}\hat{\rho}^{aux}(t) \quad &= -i[\hat{H}_{SA}(t),\hat{\rho}^{aux}(t)] \\ &+ \sum_{m_1,m_2\in A}\Bigg[\Gamma^{R}_{m_1m_2}\left(2\hat{a}_{m_2}\hat{\rho}^{aux}(t)\hat{a}^{\dagger}_{m_1} - \left\{\hat{\rho}^{aux}(t),\hat{a}^{\dagger}_{m_1}\hat{a}_{m_2}\right\}\right) \\ &\qquad +\Gamma^{L}_{m_1m_2}\left(2\hat{a}^{\dagger}_{m_1}\hat{\rho}^{aux}(t)\hat{a}_{m_2} - \left\{\hat{\rho}^{aux}(t),\hat{a}_{m_2}\hat{a}^{\dagger}_{m_1}\right\}\right)\Bigg]\end{aligned} \tag{A.13}$$

Finally, because only operators in $S+A$ subspace appear in the right side of (A.13), tracing out baths degrees of freedom leads to Eq. (2.17).

Appendix B

Derivation of quantum regression theorem

B.1 Derivation of Eq. (2.22)

Here we prove that two-time correlation function of two arbitrary operators in $S+A$, $\langle \hat{O}_1(t_1)\,\hat{O}_2(t_2)\rangle$ ($t_1 \geq t_2 \geq 0$), Eq. (2.20), can be equivalently obtained from reduced Lindblad-type evolution in the $S+A$ subspace of the *aux* model.

Let introduce $t \equiv t_1 - t_2 \geq 0$, then $\hat{O}_1(t_1)\hat{O}_2(t_2) = \hat{O}_1(t+t_2)\hat{O}_2(t_2)$ and using Eq. (A.9)

we get

$$\begin{aligned}\frac{d}{dt}\hat{O}_1(t+t_2)\hat{O}_2(t_2) = \quad & \Big\{ i[\hat{H}_{SA}(t+t_2),\hat{O}_1(t+t_2)] \\ & -i\sum_{m\in A}\Big(t_m^R[\hat{O}_1(t+t_2),\hat{a}_m^\dagger(t+t_2)]_{\zeta_1}\hat{c}_R^{(in)}(t+t_2) \\ & \quad +\zeta_1(t_m^R)^*\hat{c}_R^{(in)\,\dagger}(t+t_2)[\hat{O}_1(t+t_2),\hat{a}_m(t+t_2)]_{\zeta_1} \\ & \quad -(t_m^L)^*[\hat{O}_1(t+t_2),\hat{a}_m(t+t_2)]_{\zeta_1}\hat{c}_L^{(in)\,\dagger}(t+t_2) \\ & \quad -\zeta_1 t_m^L\hat{c}_L^{(in)}(t+t_2)[\hat{O}_1(t+t_2),\hat{a}_m^\dagger(t+t_2)]_{\zeta_1}\Big) \\ & -\sum_{m_1,m_2\in A}\Big(\Gamma^R_{m_1m_2}[\hat{O}_1(t+t_2),\hat{a}^\dagger_{m_1}(t+t_2)]_{\zeta_1}\hat{a}_{m_2}(t+t_2) \\ & \quad -\zeta_1\Gamma^R_{m_1m_2}\hat{a}^\dagger_{m_1}(t+t_2)[\hat{O}_1(t+t_2),\hat{a}_{m_2}(t+t_2)]_{\zeta_1} \\ & \quad +\Gamma^L_{m_1m_2}[\hat{O}_1(t+t_2),\hat{a}_{m_2}(t+t_2)]_{\zeta_1}\hat{a}^\dagger_{m_1}(t+t_2) \\ & \quad -\zeta_1\Gamma^L_{m_1m_2}\hat{a}_{m_2}(t+t_2)[\hat{O}_1(t+t_2),\hat{a}^\dagger_{m_1}(t+t_2)]_{\zeta_1}\Big)\Big\}\hat{O}_2(t_2)\end{aligned} \tag{B.1}$$

Note that for $t>0$

$$[\hat{c}_C^{(in)\,\dagger}(t+t_2),\hat{O}_2(t_2)]_{\zeta_2} = [\hat{c}_C^{(in)}(t+t_2),\hat{O}_2(t_2)]_{\zeta_2} = 0 \tag{B.2}$$

Indeed, because from Eq. (A.9) it is clear that $\hat{O}_2(t_2)$ depends on $\hat{O}_2(s)$ and $\hat{c}_C^{(in)\,(\dagger)}(s)$ only at earlier times ($s<t_2$) and because Eq. (A.5) shows that $\hat{c}_C^{(in)\,(\dagger)}(s)$ taken at different times anti-commute with each other, Eq. (B.2) holds.

Thus, while taking the expectation value of (B.1) with respect to $\hat{\rho}^{aux}(0)$, Eq. (2.16), $\hat{c}_L^{(in)\,\dagger}(t+t_2)$ and $\hat{c}_R^{(in)}(t+t_2)$ can be moved over $\hat{O}_2(t_2)$ for any $t>0$. So as in Appendix A, terms

with $\hat{c}_C^{(in)\,(\dagger)}(t)$ in (B.1) again don't contribute (see Eq. (A.11)), and we get for $t > 0$

$$\begin{aligned}\frac{d}{dt}\Big\langle \hat{O}_1(t+t_2)\hat{O}_2(t_2)\Big\rangle = \quad & \mathrm{Tr}\Bigg[\Bigg\{ i[\hat{H}_{SA}(t+t_2),\hat{O}_1(t+t_2)] \\ & -\sum_{m_1,m_2\in A}\Big(\Gamma^R_{m_1m_2}[\hat{O}_1(t+t_2),\hat{a}^\dagger_{m_1}(t+t_2)]_{\zeta_1}\hat{a}_{m_2}(t+t_2) \\ & -\zeta_1\Gamma^R_{m_1m_2}\hat{a}^\dagger_{m_1}(t+t_2)[\hat{O}_1(t+t_2),\hat{a}_{m_2}(t+t_2)]_{\zeta_1} \\ & +\Gamma^L_{m_1m_2}[\hat{O}_1(t+t_2),\hat{a}_{m_2}(t+t_2)]_{\zeta_1}\hat{a}^\dagger_{m_1}(t+t_2) \\ & -\zeta_1\Gamma^L_{m_1m_2}\hat{a}_{m_2}(t+t_2)[\hat{O}_1(t+t_2),\hat{a}^\dagger_{m_1}(t+t_2)]_{\zeta_1}\Big)\Bigg\}\times\hat{O}_2(t_2)\hat{\rho}^{aux}(0)\Bigg]\end{aligned} \tag{B.3}$$

Rearranging evolution operators, Eq. (2.21), and separating traces over $S+A$ and $L+R$ yields

$$\Big\langle \hat{O}_1(t+t_2)\,\hat{O}_2(t_2)\Big\rangle = \tag{B.4}$$
$$\mathrm{Tr}_{SA}\Big\{\hat{O}_1\,\mathrm{Tr}_{LR}\Big[\hat{U}^{aux}(t+t_2,0)\hat{O}_2(t_2)\,\hat{\rho}^{aux}(0)\hat{U}^{aux\,\dagger}(t+t_2)\Big]\Big\}$$
$$\frac{d}{dt}\Big\langle \hat{O}_1(t+t_2)\hat{O}_2(t_2)\Big\rangle = \tag{B.5}$$
$$\mathrm{Tr}_{SA}\Big\{\hat{O}_1\,\frac{d}{dt}\mathrm{Tr}_{LR}\Big[\hat{U}^{aux}(t+t_2,0)\hat{O}_2(t_2)\,\hat{\rho}^{aux}(0)\hat{U}^{aux\,\dagger}(t+t_2)\Big]\Big\}$$

So that (B.3) can be rewritten as

$$\begin{aligned}\mathrm{Tr}_{SA}\Big\{\hat{O}_1\,\tfrac{d}{dt}\mathrm{Tr}_{LR}[\ldots]\Big\} &= \mathrm{Tr}_{SA}\Big\{\Big(\mathcal{L}^\dagger_{SA}(t)\,\hat{O}_1\Big)\mathrm{Tr}_{LR}[\ldots]\Big\} \\ &\equiv \mathrm{Tr}_{SA}\Big\{\hat{O}_1\,\mathcal{L}_{SA}(t)\mathrm{Tr}_{LR}[\ldots]\Big\}\end{aligned} \tag{B.6}$$

where $\mathcal{L}^\dagger_{SA}(t)$ is adjoint [35] of the Liouvillian $\mathcal{L}_{SA}(t)$ defined in (2.17), and where $\mathrm{Tr}_{LR}[\ldots]$ is used as a shorthand notation for the full expression in (B.4)-(B.5).

Taking into account that $\hat{O}_1$ is an arbitrary operator, we get

$$\frac{d}{dt}\mathrm{Tr}_{LR}[\ldots] = \mathcal{L}_{SA}\,\mathrm{Tr}_{LR}[\ldots] \tag{B.7}$$

which has solution

$$\mathrm{Tr}_{LR}[\ldots](t) = \mathcal{U}_{SA}(t,0)\,\mathrm{Tr}_{LR}[\ldots](0) \equiv \mathcal{U}_{SA}(t,0)\,\hat{O}_2\,\hat{\rho}_{SA}(t_2) \tag{B.8}$$

Substituting (B.8) into (B.4) leads to

$$\left\langle \hat{O}_1(t+t_2)\,\hat{O}_2(t_2) \right\rangle = \mathrm{Tr}_{LR}\left[\hat{O}_1\,\mathcal{U}_{SA}(t_1,t_2)\left(\hat{O}_2\,\hat{\rho}_{SA}(t_2)\right)\right] \tag{B.9}$$

This relation expresses two-time correlation function defined from unitary evolution of the *aux* model in terms of Lindblad-type evolution of $S+A$ subspace of the *aux* model. Finally, we note that while we had restriction $t > 0$ in derivation of (B.3), the result is correct also for $t = 0$, as one can see by direct comparison of the two sides in (B.9). Eq. (B.9) together with (2.17) leads to (2.22).

Similarly, for $t_2 \geq t_1 \geq 0$ one can prove that

$$\langle \hat{O}_1(t_1)\hat{O}_2(t_2)\rangle = \langle\langle I|\,O_2^-\,\mathcal{U}_{SA}(t_1,t_2)\,O_1^+\,\mathcal{U}_{SA}(t_2,0)\,|\rho_{SA}(0)\rangle\rangle \tag{B.10}$$

B.2 Derivation of Eq. (2.27)

Here we prove that multi-time correlation functions of arbitrary operators $\hat{O}_i$ in $S+A$ of the *aux* model defined on the Keldysh contour,

$$\left\langle T_c \hat{O}_1(\tau_1)\,\hat{O}_2(\tau_2)\ldots\hat{O}_N(\tau_N) \right\rangle, \tag{B.11}$$

can be evaluated from Markov Lindblad-type evolution in the $S+A$ subspace. Here operators $\hat{O}_i$ are in the Heisenberg picture. Projections (one-the-contour time orderings) of multi-time

correlation functions (B.11) will have the following form

$$\begin{aligned}&\left\langle \hat{B}_1(s_1)\hat{B}_2(s_2)..\hat{B}_m(s_m)\hat{C}_n(t_n)...\hat{C}_2(t_2)\hat{C}_1(t_1)\right\rangle \\ &= \mathrm{Tr}\left[\hat{C}_n(t_n)...\hat{C}_2(t_2)\hat{C}_1(t_1)\hat{\rho}^{aux}(0)\hat{B}_1(s_1)\hat{B}_2(s_2)...\hat{B}_m(s_m)\right]\end{aligned} \tag{B.12}$$

where $\hat{B}_j(s_j)$ and $\hat{C}_i(t_i)$ are used for operators $\hat{O}_i$ on the backward and forward branches of the contour, respectively (see Figure 1.3) and where

$$\begin{aligned}&t_n > t_{n-1} > ... > t_1 \geq 0 \\ &s_m > s_{m-1} > ... > s_1 \geq 0\end{aligned} \tag{B.13}$$

Note, there is no ordering between the sets $\{t_i\}$ and $\{s_j\}$ ($i \in \{1,2,\ldots,n\}$ and $j \in \{1,2,\ldots,m\}$).

Let denote the time-ordering of the set $\{t_1,t_2,...,t_n,s_1,s_2,...,s_m\}$ by $\{\theta_1,\ldots,\theta_{m+n}\}$. So that

$$\theta_{m+n} \geq \theta_{m+n-1} \geq \ldots \geq \theta_1 \geq 0. \tag{B.14}$$

We want to prove that projections of multi-time correlation functions satisfy quantum regression theorem [35]

$$\begin{aligned}&\langle\langle I|\, O_{\theta_{m+n}}\, \mathcal{U}_{SA}(\theta_{m+n},\theta_{m+n-1})\, O_{\theta_{m+n-1}}\, \mathcal{U}_{SA}(\theta_{m+n-1},\theta_{m+n-2})\ldots \\ &\qquad \ldots O_{\theta_1}\, \mathcal{U}_{SA}(\theta_1,0)|\rho_{SA}(0)\rangle\rangle\end{aligned} \tag{B.15}$$

where O_{θ_i} is superoperator, Eq. (2.23), corresponding to operator $\hat{B}$ or $\hat{C}$ (backward or forward branch of the contour, respectively) at real time θ_i.

We prove (B.15) by mathematical induction. First, we note that Eqs. (2.22) and (B.10) are special cases of Eq. (B.15) with $m+n=2$. Suppose that for any combination (m,n) satisfying

$m+n=k$, Eq. (B.15) holds. Now let consider $(k+1)$-time correlation function

$$\left\langle \hat{B}_1(s_1)\hat{B}_2(s_2)\dots\hat{B}_m(s_m)\hat{O}_{\theta_{k+1}}(\theta_{k+1})\hat{C}_n(t_n)\dots\hat{C}_2(t_2)\hat{C}_1(t_1)\right\rangle \tag{B.16}$$

where $\theta_{k+1} > t_n > t_{n-1} > ... > t_1 \geq 0$ and $\theta_{k+1} > s_m > s_{m-1} > ... > s_1 \geq 0$. As previously, we time-order both sets,

$$\theta_{k+1} > \theta_k \geq \theta_{k-1} \geq \ldots \geq \theta_1 \geq 0, \tag{B.17}$$

and take the derivative with respect to the latest time

$$\begin{aligned}
&\frac{d}{d\theta_{k+1}}\left\langle \hat{B}_1(s_1)\,\hat{B}_2(s_2)\dots\hat{B}_m(s_m)\,\hat{O}_{k+1}(\theta_{k+1})\,\hat{C}_n(t_n)\dots\hat{C}_2(t_2)\,\hat{C}_1(t_1)\right\rangle \\
&\equiv \frac{d}{d\theta_{k+1}}\langle\langle I|\,O_{\theta_{k+1}}\,\mathcal{U}^{aux}(\theta_{k+1},\theta_k)\,O_{\theta_k}\,\mathcal{U}^{aux}(\theta_k,\theta_{k-1})\dots\mathcal{U}^{aux}(\theta_1,0)|\rho^{aux}(0)\rangle\rangle \\
&= \mathrm{Tr}_{SA}\left\{\hat{O}_{\theta_{k+1}}\frac{d}{d\theta_{k+1}}\langle\langle I_{LR}|\,\mathcal{U}^{aux}(\theta_{k+1},\theta_k)\,O_{\theta_k}\,\mathcal{U}^{aux}(\theta_k,\theta_{k-1})\dots\mathcal{U}^{aux}(\theta_1,0)|\rho^{aux}(0)\rangle\rangle_{LR}\right\} \\
&= \mathrm{Tr}_{SA}\left\{\hat{O}_{\theta_{k+1}}\mathcal{L}_{SA}(\theta_{k+1})\,\langle\langle I_{LR}|\,\mathcal{U}^{aux}(\theta_{k+1},\theta_k)\,O_{\theta_k}\,\mathcal{U}^{aux}(\theta_k,\theta_{k-1})\dots\mathcal{U}^{aux}(\theta_1,0)|\rho^{aux}(0)\rangle\rangle_{LR}\right\}
\end{aligned} \tag{B.18}$$

where we followed the argument leading to (B.5) and (B.6) in B.1. In (B.18) $\mathcal{U}^{aux}$ is the Liouville space analog of the Hilbert space evolution operator $\hat{U}^{aux}$ defined in Eq. (2.21).

Taking into account that $\hat{O}_{\theta_1}$ is an arbitrary operator, we get

$$\begin{aligned}
&\frac{d}{d\theta_{k+1}}\langle\langle I_{LR}|\,\mathcal{U}^{aux}(\theta_{k+1},0)\dots|\rho^{aux}(0)\rangle\rangle_{LR} \\
&\qquad = \mathcal{L}_{SA}(\theta_{k+1})\,\langle\langle I_{LR}|\,\mathcal{U}^{aux}(\theta_{k+1},0)\dots|\rho^{aux}(0)\rangle\rangle_{LR}
\end{aligned} \tag{B.19}$$

where $\langle\langle I_{LR}|\,\mathcal{U}^{aux}(\theta_{k+1},0)\dots|\rho^{aux}(0)\rangle\rangle_{LR}$ is shorthand notation for the expression introduced in (B.18).

Solving (B.19) and utilizing quantum regression theorem for its initial condition, $\theta_{k+1} =$

θ_k, leads to

$$\left\langle \hat{B}_1(s_1)\hat{B}_2(s_2)\ldots\hat{B}_m(s_m)\,\hat{O}_{\theta_{k+1}}(\theta_{k+1})\,\hat{C}_n(t_n)\ldots\hat{C}_2(t_2)\hat{C}_1(t_1)\right\rangle \tag{B.20}$$
$$= \langle\langle I|\,O_{\theta_{k+1}}\,\mathcal{U}_{SA}(t_{\theta_{k+1}},t_{\theta_k})\,O_{\theta_k}\,\mathcal{U}_{SA}(t_{\theta_k},t_{\theta_{k-1}})\ldots O_{\theta_1}\,\mathcal{U}_{SA}(t_{\theta_1},0)|\rho_{SA}(0)\rangle\rangle$$

which is quantum regression theorem for $(k+1)$-time correlation function. Thus, by induction we prove Eq. (2.27).

Appendix C

Supplemental Materials for Chapter 3

C.1 Derivation of Eqs. (3.5)-(3.7)

Detailed derivation of the nonequilibrium dual fermion approach was originally introduced in Ref. [32]. For completeness here we give some details of the derivation.

We start form partition function defined on the Keldysh contour as [99]

$$Z = \int D[d^*, d] \int D[c^*, c]\, e^{iS[d^*,d,c^*,c]} \tag{C.1}$$

where

$$\begin{aligned} S[d^*, d, c^*, c] = \sum_{1,2} \Big(& d_1^* \left[G_0^{-1} \right]_{12} d_2 + c_1^* \left[g_B^{-1} \right]_{12} c_2 \\ & + d_1^* V_{12} c_2 + c_1^* V_{21} d_2 \Big) + S^{int}[d^*, d] \end{aligned} \tag{C.2}$$

is the action of an interacting system (d^* and d) coupled to non-interacting contacts (c^* and c). Here, G_0^{-1} is defined in Eq. (3.2) of the main text and g_B^{-1} is the inverse Green function for free

electrons in contacts

$$\left[g_B^{-1}\right]_{12} = \delta(\tau_1,\tau_2)\left[i\partial_{\tau_1} - \varepsilon_k\right] \tag{C.3}$$

After integrating out contacts degrees of freedom [63] the system is represented by effective action given in Eq. (3.1) of the main text.

Next we introduce *a reference system*, which is identical to the original one in all intra-system interactions but differs from it by its hybridization function. The reference system can be exactly solved, and the effective action of the original system is be related to that of the reference system via Eq. (3.4) of the main text. In our case exact solution of the reference system is obtained by solving the auxiliary Lindbald quantum master equation.

Next we consider the Hubbard-Stratonovich transformation (summation over repeated indices is assumed)

$$e^{d_1^* N_{12} M_{23}^{-1} N_{34} d_4} = \det D \int D[f^*,f] e^{-f_1^* D_{12} f_2 + f_1^* N_{12} d_2 + d_1^* N_{12} f_2}$$

with

$$N_{12} = i g_{12}^{-1} \tag{C.4}$$

$$D_{14} = i \sum_{2,3} g_{12}^{-1} \left[\tilde{\Delta}^B - \Delta^B\right]_{23}^{-1} g_{34}^{-1} \tag{C.5}$$

so that

$$\sum_{2,3} N_{12} M_{23}^{-1} N_{34} \equiv i\left[\tilde{\Delta}^B - \Delta^B\right]_{14} \tag{C.6}$$

Applying the transformation to the partition function (C.1) with the action given by Eq. (3.4) of the main text yields

$$Z = Z_f \int D[d^*,d] \int D[f^*,f] e^{iS[d^*,d,f^*,f]} \tag{C.7}$$

where

$$S[d^*,d,f^*,f] = \tilde{S}[d^*,d] \tag{C.8}$$
$$+\sum_{1,2}\left(-f_1^*\left(g^{-1}\left[\tilde{\Delta}^B-\Delta^B\right]g^{-1}\right)_{12} f_2 + f_1^* g_{12}^{-1} d_2 + d_1^* g_{12}^{-1} f_2\right)$$

$$Z_f = -i\det\left(g\left[\tilde{\Delta}^B-\Delta^B\right]g\right) \tag{C.9}$$

Thus, auxiliary quasi-particle - dual fermion (f) - was introduced.

Formal integration out of the real quasiparticle, d^* and d, in (C.7) leads to

$$Z = Z_f\tilde{Z}\int D[f^*,f]e^{i\left[\Sigma_{12}f_1^*\left(G_0^{DF}\right)^{-1}_{12}f_2+V[f^*,f]\right]} \tag{C.10}$$

where $\left(G_0^{DF}\right)^{-1}_{12}$ is defined in Eq. (3.5) of the main text, $\tilde{Z}$ is the partition function of the reference system, and $V[f^*,f]$ is unknown interaction between dual fermions.

To get the interaction $V[f^*,f]$ we expand (C.7) in $f-d$ interaction - last two terms in (C.8) - and integrate out real quasiparticles, d^* and d. Taking g to be single particle Green function of the reference system

$$g_{12} = \frac{-i}{\tilde{Z}}\int D[d^*,d]\,d_1 d_2^* e^{i\tilde{S}[d^*,d]} \tag{C.11}$$

and comparing the resulting expression to expansion of (C.10) yields expression for $V[f^*,f]$. In particular, for expansion up to fourth order in f^* and f

$$V[f^*,f] = \frac{i}{4}\sum_{1,2,3,4}\Gamma_{13;24}f_1^* f_3^* f_4 f_2 \tag{C.12}$$

Here $\Gamma_{13;24}$ is the two-particle vertex of the reference system defined in Eq. (3.11) of the main text. Finally, expansion of (C.10) with interaction given by (C.12) to lowest order and utilization of the Wick's theorem for the dual fermions yields the dual fermion self-energy in the form given in Eq. (3.6) of the main text.

The generating function $Z[\eta,\eta^*]$ satisfies:

$$\begin{aligned} S[d^*,d,f^*,f,\eta^*,\eta] &= S[d^*,d] + f^*\eta + \eta^* f - d^*\left(\tilde{\Delta}^B - \Delta^B\right) d \\ &\quad - f^*\left(g^{-1}\left[\tilde{\Delta}^B - \Delta^B\right] g^{-1}\right) f + f^* g^{-1} d + d^* g^{-1} f \\ Z[\eta,\eta^*] &= \frac{1}{Z}\int D[d^*,d,f^*,f] e^{iS[d^*,d,f^*,f,\eta^*,\eta]} \\ &= \frac{Z_f}{Z}\int D[d^*,d] e^{iS[d^*,d,\eta^*,\eta]} \end{aligned}$$

where

$$S[d^*,d,\eta^*,\eta] = S[d^*,d] + \eta^*[g\left(\tilde{\Delta}^B - \Delta^B\right)]d + d^*[\left(\tilde{\Delta}^B - \Delta^B\right) g]\eta + \eta^*[g\left(\tilde{\Delta}^B - \Delta^B\right) g]\eta \quad \text{(C.13)}$$

Hence,

$$G^{DF} \equiv -i\langle \hat{f}_1 \hat{f}_2^\dagger \rangle = i\frac{\delta^2 Z[\eta,\eta^*]}{\delta\eta_1^*\delta\eta_2} \quad \text{(C.14)}$$

$$= -g(\tilde{\Delta}^B - \Delta^B)g + g\left[(\tilde{\Delta}^B - \Delta^B)G(\tilde{\Delta}^B - \Delta^B)\right]g \quad \text{(C.15)}$$

From which we can easily get Eq.(3.7).

C.2 Green functions from QME

To evaluate dual-fermion self-energy, one has to calculate the two-particle vertex (see Eq.(3.6) of the main text). The latter depends on single- and two-particle Green functions of the reference system (see Eq.(3.11) of the main text). The Green functions are obtained by employing the quantum regression relation as proved in Chapter 1.

Evaluation of single-particle Green functions

Here we discuss details of evaluation of single-particle Green function

$$g_{12} = -i\langle T_c \hat{d}_1 \hat{d}_2^\dagger \rangle_{ref} \tag{C.16}$$

where as previously $\hat{d}_i = \hat{d}_{m_i}(\tau_i)$, and where subscript 'ref' indicates quantum mechanical and statistical average of the reference system. Evaluation of the Green function requires consideration of four projections

$$g^{\gtrless +}_{m_1 m_2}(t_1,t_2) \equiv \theta(t_1 - t_2) g^{\gtrless}_{m_1 m_2}(t_1,t_2) \tag{C.17}$$

$$g^{\gtrless -}_{m_1 m_2}(t_1,t_2) \equiv \theta(t_2 - t_1) g^{\gtrless}_{m_1 m_2}(t_1,t_2) \tag{C.18}$$

where

$$g^{>}_{m_1,m_2}(t_1,t_2) = -i\langle \hat{d}_{m_1}(t_1) \hat{d}^\dagger_{m_2}(t_2) \rangle_{ref} \tag{C.19}$$

$$g^{>}_{m_1,m_2}(t_1,t_2) = i\langle \hat{d}^\dagger_{m_2}(t_2) \hat{d}_{m_1}(t_1) \rangle_{ref}. \tag{C.20}$$

Fourier transforms of the four projections are

$$g^{>+}_{m_1 m_2}(E) = \sum_\gamma \sum_{\{S_i\},\{S_i'\}} \left[\xi^{m_1}_{S_3 S_3'}\right]^* \xi^{m_2}_{S_2 S_1} \rho^S_{S_1 S_1'} \frac{\ll S_3 S_3' | R^{(+1)}_\gamma \gg \ll L^{(+1)}_\gamma | S_2 S_1' \gg}{E - \lambda^{(+1)}_\gamma} \tag{C.21}$$

$$g^{<+}_{m_1 m_2}(E) = -\sum_\gamma \sum_{\{S_i\},\{S_i'\}} \left[\xi^{m_1}_{S_3 S_3'}\right]^* \xi^{m_2}_{S_1' S_2'} \rho^S_{S_1 S_1'} \frac{\ll S_3 S_3' | R^{(+1)}_\gamma \gg \ll L^{(+1)}_\gamma | S_1 S_2' \gg}{E - \lambda^{(+1)}_\gamma} \tag{C.22}$$

$$g^{>-}_{m_1 m_2}(E) = -\sum_\gamma \sum_{\{S_i\},\{S_i'\}} \xi^{m_2}_{S_3' S_3} \left[\xi^{m_1}_{S_2' S_1'}\right]^* \rho^S_{S_1 S_1'} \frac{\ll S_3 S_3' | R^{(-1)}_\gamma \gg \ll L^{(-1)}_\gamma | S_1 S_2' \gg}{E + \lambda^{(-1)}_\gamma} \tag{C.23}$$

$$g^{<-}_{m_1 m_2}(E) = \sum_\gamma \sum_{\{S_i\},\{S_i'\}} \xi^{m_2}_{S_3' S_3} \left[\xi^{m_1}_{S_1 S_2}\right]^* \rho^S_{S_1 S_1'} \frac{\ll S_3 S_3' | R^{(-1)}_\gamma \gg \ll L^{(-1)}_\gamma | S_2 S_1' \gg}{E + \lambda^{(-1)}_\gamma} \tag{C.24}$$

Here $\xi^m_{S_2S_1} \equiv \langle S_2|\hat{d}^\dagger_m|S_1\rangle$; $\lambda^{(\pm1)}_\gamma$, $|R^{(\pm1)}_\gamma \gg$ and $\ll L^{(\pm1)}_\gamma|$ are eigenvalue, right and left eigenvectors of the Liouvillian $\mathcal{L}^{(\pm1)}$.

Evaluation of two-particle Green functions

Here we provide details of evaluation for two-particle Green function

$$g^{(2)}_{13,24} = -\langle T_c\, \hat{d}_1\, \hat{d}_3\, \hat{d}^\dagger_4\, \hat{d}^\dagger_2\rangle \tag{C.25}$$

To connect (C.25) to Liouville QME formulation, one has to consider $2^4 = 16$ projections of the Green function on the contour and $4! = 24$ time orderings.

It is convenient to introduce Liouville space matrix elements of electron annihilation operators at time-ordered ($s = 0$ or $-$) and anti-time ordered ($s = 1$ or $+$) branches of the Keldysh contour

$$\ll S^2_- S^2_+|\hat{d}^s_m|S^1_- S^1_+ \gg = \begin{cases} \delta_{S^2_+,S^1_+}\langle S^2_-|\hat{d}_m|S^1_-\rangle & s = 0 \\ \delta_{S^2_-,S^1_-}\langle S^1_+|\hat{d}_m|S^2_+\rangle & s = 1 \end{cases} \tag{C.26}$$

Similar definitions hold for creation operators.

Explicit form of quantum regression relation for two particle Green function will depend on time ordering in (C.25). For example, for $t_4 > t_3 > t_2 > t_1$ and indicating contour projections of operators by respectively s_4, s_3, s_2, and s_1 expression for two-particle Green function in terms

of QME solution (Liouvillian eigenvalues λ_γ and eigenvectors $|R_\gamma \gg$ and $\ll L_\gamma|$) is

$$
\begin{aligned}
&-\sum_{\{\gamma_i\}}(-1)^p e^{-i\lambda_{\gamma_3}^{(-1)}(t_4-t_3)}\, e^{-i\lambda_{\gamma_2}^{(0)}(t_3-t_2)}\, e^{-i\lambda_{\gamma_3}^{(-1)}(t_2-t_1)} \times \sum_S \prod_{\{s_i=\mp\}} \sum_{\{S_{s_i}^j\}} \ll SS|d_{m_4}^{\dagger s_4}|S_-^7 S_+^7 \gg \\
&\ll S_-^7 S_+^7|R_{\gamma_3}^{(-1)} \gg \ll L_{\gamma_3}^{(-1)}|S_-^6 S_+^6 \gg \ll S_-^6 S_+^6|d_{m_3}^{s_3}|S_-^5 S_+^5 \gg \ll S_-^5 S_+^5|R_{\gamma_2}^{(0)} \gg \ll L_{\gamma_2}^{(0)}|S_-^4 S_+^4 \gg \\
&\ll S_-^4 S_+^4|d_{m_2}^{\dagger s_2}|S_-^3 S_+^3 \gg \ll S_-^3 S_+^3|R_{\gamma_1}^{(-1)} \gg \ll L_{\gamma_1}^{(-1)}|S_-^2 S_+^2 \gg \ll S_-^2 S_+^2|d_{m_1}^{s_1}|S_-^1 S_+^1 \gg \rho_{S_-^1 S_+^1}^S
\end{aligned}
\tag{C.27}
$$

where p is permutation of creation and annihilation operators ($\hat{d}$ and $\hat{d}^\dagger$) in the projection. Similar expressions can be written to other 23 time orderings.

Because time dependence is explicit in (C.27), time integrals in Eq.(3.6) of the main text can be evaluated analytically. Also, terms in second and third rows of (C.27) can be combined into groups in which matrix products may be pre-calculated only once and stored in memory. Specifically for (C.27) second and third rows of the expression can be presented as product of two matrices and two vectors

$$
v_{\gamma_3} M_{\gamma_3\gamma_2} N_{\gamma_2\gamma_1} w_{\gamma_1} \tag{C.28}
$$

where

$$
\begin{aligned}
v_{\gamma_3} &= \sum_{S,S_-^7,S_+^7} \ll SS|d_{m_4}^{\dagger s_4}|S_-^7 S_+^7 \gg \ll S_-^7 S_+^7|R_{\gamma_3}^{(-1)} \gg \qquad (C.29)\\
M_{\gamma_3\gamma_2} &= \sum_{S_-^6,S_+^6,S_-^5,S_+^5} \ll L_{\gamma_3}^{(-1)}|S_-^6 S_+^6 \gg \ll S_-^6 S_+^6|d_{m_3}^{s_3}|S_-^5 S_+^5 \gg \ll S_-^5 S_+^5|R_{\gamma_2}^{(0)} \gg \\
N_{\gamma_2\gamma_1} &= \sum_{S_-^4,S_+^4,S_-^3,S_+^3} \ll L_{\gamma_2}^{(0)}|S_-^4 S_+^4 \gg \ll S_-^4 S_+^4|d_{m_2}^{\dagger s_2}|S_-^3 S_+^3 \gg \ll S_-^3 S_+^3|R_{\gamma_1}^{(-1)} \gg \\
w_{\gamma_1} &= \sum_{S_-^2,S_+^2,S_-^1,S_+^1} \ll L_{\gamma_1}^{(-1)}|S_-^2 S_+^2 \gg \ll S_-^2 S_+^2|d_{m_1}^{s_1}|S_-^1 S_+^1 \gg \rho_{S_-^1 S_+^1}^S
\end{aligned}
$$

C.3 $\tilde{\Delta}^B$ from QME

The easiest way to obtain self-energy due to coupling to contacts when solving reference system with auxiliary QME was introduced in Ref. [8].

Utilizing the fact that the self-energy does not depend on intra-system interactions, one can first consider a non-interacting ($U = 0$) reference model. Single-particle Green function, G_0, can be evaluated from QME solution of the model following approach described above. The only contribution to self-energy in such non-interacting reference system comes from coupling to contacts (hybridization) [64]

$$G_0(E) = \left[\left(E - H_M \right) \sigma_z - \sigma_z \tilde{\Delta}^B(E) \sigma_z \right] \tag{C.30}$$

Here σ_z is the Pauli matrix, which distinguishes direction of time propagation on the branches of the Keldysh contour, H_M is the matrix in molecular subspace, and G_0 and $\tilde{\Delta}^B$ are matrices in both spatial and contour branches dimensions.

Thus, self-energy $\tilde{\Delta}^B$ can be obtained from the Green function G_0 as follows

$$\tilde{\Delta}^B(E) = (E - H_M) \sigma_z - \sigma_z G_0^{-1}(E) \sigma_z \tag{C.31}$$

$\tilde{\Delta}^B$ calculated for the non-interacting reference system can be used in the DF procedure for interacting system, Eqs. (3.5) and (3.7) of the main text, because the self-energy is the same for the reference system with and without intra-system interactions.

Appendix D

Supplemental Materials for Chapter 4

D.1 Derivation of dual boson EOMs

Here we present derivation of the expressions for the zero order GFs, G_0^{DF} and D_0^{DB}, and self-energies, Σ^{DF} and Π^{DB}, for the dual boson technique, Eq. (6) of the main text.

We consider a physical system which consists from the molecule (d) coupled to Fermi (c) and Bose (a) baths. Its partition function on the Keldysh contour is [99]

$$Z = \int_c D[\bar{d}, d, \bar{c}, c, \bar{a}, a]\, e^{iS[\bar{d}, d, \bar{c}, c, \bar{a}, a]} \tag{D.1}$$

where

$$\begin{aligned} S[\bar{d}, d, \bar{c}, c, \bar{a}, a] = \bar{d}_1 \left[G_0^{-1}\right]_{12} d_2 + S^{int}[\bar{d}, d] + \bar{c}_1 \left[g_B^{-1}\right]_{12} c_2 + \bar{a}_1 \left[d_B^{-1}\right]_{12} a_2 \\ + \bar{d}_1 V_{12} c_2 + \bar{c}_2 V_{21} d_1 + \bar{b}_1 V_{12} a_2 + \bar{a}_2 V_{21} b_1 \end{aligned} \tag{D.2}$$

is the action of an interacting system (molecule) coupled to non-interacting contacts (Fermi bath) and plasmon (Bose bath). Here, G_0^{-1} is defined in Eq. (2) of the main text and g_B^{-1} and d_B^{-1} are

the inverse GFs for free electrons in the contacts and free photons in the Bose bath

$$\begin{aligned}\left[g_B^{-1}\right]_{12} &= \delta(\tau_1,\tau_2)\left[i\partial_{\tau_1}-\varepsilon_k\right]\\ \left[d_B^{-1}\right]_{12} &= \delta(\tau_1,\tau_2)\left[i\partial_{\tau_1}-\omega_\alpha\right]\end{aligned} \tag{D.3}$$

After integrating out baths degrees of freedom [63] one gets effective action presented in Eq. (1) of the main text.

Next we introduce *an exactly solvable reference system*, which is identical to the original one in all intra-system interactions but differs from it by its hybridization function. Effective action of the original system will be related to that of the reference system via Eq. (4) of the main text. Because direct application of perturbation theory to Eq. (4) is not possible, we apply two Hubbard-Stratonovich transformations to introduce new particles, *dual fermion* (f) and *dual boson* (η), which disentangle last two terms in Eq. (4). Following Ref. [92] we get

$$\begin{aligned}e^{\bar{d}_1 N_{12} d_2} &= Z_f \int_c D[\bar{f},f]\, e^{-\bar{f}_1\alpha^f_{12}\left[N^{-1}\right]_{23}\alpha^f_{34}f_4+\bar{f}_1\alpha^f_{12}d_2+\bar{d}_1\alpha^f_{12}f_2}\\ e^{\bar{b}_1 M_{12} b_2} &= Z_b \int_c D[\bar{\eta},\eta]\, e^{-\bar{\eta}_1\alpha^b_{12}\left[M^{-1}\right]_{23}\alpha^b_{34}\eta_4+\bar{\eta}_1\alpha^b_{12}b_2+\bar{b}_1\alpha^b_{12}\eta_2}\end{aligned} \tag{D.4}$$

with

$$\begin{aligned}&\alpha^f = i\,g^{-1} \quad N = i\,\delta\Delta^B \quad Z_f = \left(\det\left[\alpha^f N^{-1}\,\alpha^f\right]\right)^{-1}\\ &\alpha^b = i\chi^{-1} \quad M = i\,\delta\Pi^B \quad Z_b = \det\left[\alpha^b M^{-1}\,\alpha^b\right]\end{aligned} \tag{D.5}$$

Applying the transformation to the partition function (C.1) with the action given by Eq. (4) of the main text yields

$$Z = Z_f Z_b \int_c D[\bar{d},d,\bar{f},f,\bar{\eta},\eta] e^{iS[\bar{d},d,\bar{f},f,\bar{\eta},\eta]} \tag{D.6}$$

where

$$
\begin{aligned}
S[\bar{d},d,\bar{f},f,\bar{\eta},\eta] &= \tilde{S}[d^*,d] \\
&- \bar{f}_1\, g^{-1}_{12}\, \left[\delta\Delta^B\right]^{-1}_{23}\, g^{-1}_{34}\, f_4 + \bar{f}_1\, g^{-1}_{12}\, d_2 + \bar{d}_1\, g^{-1}_{12}\, f_2 \\
&- \bar{\eta}_1 \chi^{-1}_{12}\, \left[\delta\Pi^B\right]^{-1}_{23}\, \chi^{-1}_{34}\, \eta_4 + \bar{\eta}_1\, \chi^{-1}_{12}\, b_2 + \bar{b}_1\, \chi^{-1}_{12}\, \eta_2
\end{aligned}
\tag{D.7}
$$

Thus, auxiliary quasi-particles - dual fermion (f) and dual boson (η) - were introduced.

Integrating out of the real quasiparticle, $\bar{d}$ and d, in (C.7) leads to

$$
Z = Z_f\, Z_b\, \tilde{Z} \int_c D[\bar{f},f,\bar{\eta},\eta] e^{iS[\bar{f},f\bar{\eta},\eta]}
\tag{D.8}
$$

with

$$
\begin{aligned}
S[\bar{f},f,\bar{\eta},\eta] &= \bar{f}_1\, \left[G^{DF}_0\right]^{-1}_{12}\, f_2 + \bar{\eta}_1\, \left[D^{DB}_0\right]^{-1}_{12}\, \eta_2 \\
&+ V[\bar{f},f,\bar{\eta},\eta]
\end{aligned}
\tag{D.9}
$$

$\left[G^{DF}_0\right]^{-1}_{12}$ and $\left[D^{DB}_0\right]^{-1}_{12}$ are defined in Eq. (6) of the main text, $\tilde{Z}$ is the partition function of the reference system, and $V[\bar{f},f,\bar{\eta},\eta]$ is unknown interaction between dual particles.

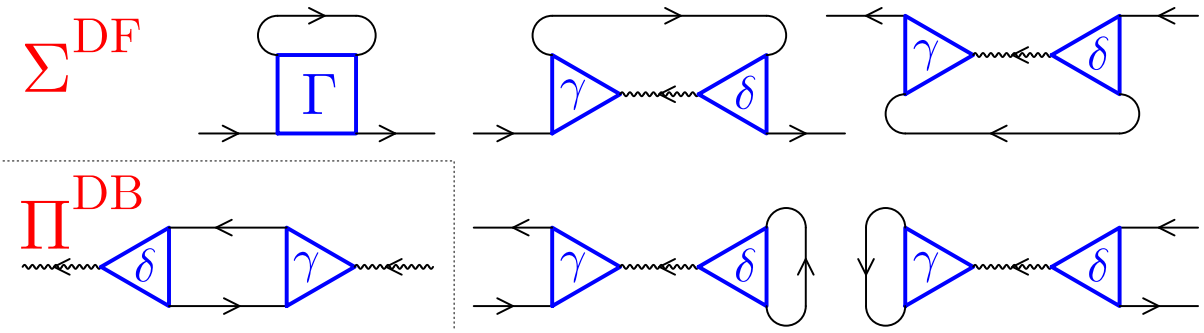

Figure D.1: Contributions to diagrams for dual fermion, Σ^{DF}, and dual boson, Π^{DB}, self-energies, Eq. (6). Directed solid and wavy lines (black) indicate dual fermion and dual boson GFs, G^{DF}_0 and D^{DB}_0, respectively. Triangle and square (blue) indicate vertices γ and Γ of the reference system.

To get the interaction $V[\bar{f},f,\bar{\eta},\eta]$ we expand (C.7) in $f-d$ and $\eta-b$ interactions and

integrate out real quasiparticles, $\bar{d}$ and d. Taking g and χ to be single electron and single molecular excitaton GFs of the reference system

$$\begin{aligned} g_{12} &= \frac{-i}{\tilde{Z}} \int_c D[\bar{d},d]\, d_1 \bar{d}_2\, e^{i\tilde{S}[\bar{d},d]} \equiv -i\langle T_c\, \hat{d}_1\, \hat{d}_2^\dagger \rangle_{ref} \\ \chi_{12} &= \frac{-i}{\tilde{Z}} \int_c D[\bar{d},d]\, \delta b_1\, \delta \bar{b}_2\, e^{i\tilde{S}[\bar{d},d]} \equiv -i\langle T_c\, \hat{b}_1\, \hat{b}_2^\dagger \rangle_{ref} \end{aligned} \tag{D.10}$$

and comparing the resulting expression to expansion of (C.10) yields expression for $V[\bar{f},f,\bar{\eta},\eta]$. In particular, for expansion up to fourth order in $\bar{f}$, f and second order in $\bar{\eta}$, η

$$\begin{aligned} V[\bar{f},f,\bar{\eta},\eta] &= \bar{\eta}_1\, \chi_{12}^{-1}\, \langle b_2 \rangle_{ref} + \langle \bar{b}_1 \rangle_{ref}\, \chi_{12}^{-1}\, \eta_2 \\ &- \frac{i}{4} \bar{f}_1\, \bar{f}_3 \Gamma_{13;24} f_2 f_4 - \bar{\eta}_1\, \gamma_{123}\, \bar{f}_2\, f_3 - \bar{f}_3\, f_2\, \delta_{321}\, \eta_1 \end{aligned} \tag{D.11}$$

Here γ_{123}, δ_{321} and $\Gamma_{13;24}$ are vertices of the reference system

$$\begin{aligned} \Gamma_{13;24} &= g_{11'}^{-1} g_{33'}^{-1} \big[-\langle T_c\, \hat{d}_{1'}\, \hat{d}_{2'}^\dagger\, \hat{d}_{3'}\, \hat{d}_{4'}^\dagger \rangle_{ref} \\ &\quad - g_{1'2'}\, g_{3'4'} + g_{1'4'}\, g_{3'2'} \big]\, g_{2'2}^{-1}\, g_{4'4}^{-1} \\ \gamma_{123} &= \chi_{11'}^{-1}\, g_{22'}^{-1}\, \langle T_c\, \delta\hat{b}_{1'}\, \hat{d}_{2'}\, \hat{d}_{3'}^\dagger \rangle_{ref}\, g_{3'3}^{-1} \\ \delta_{321} &= g_{33'}^{-1}\, \langle T_c\, \hat{d}_{3'}\, \hat{d}_{2'}^\dagger\, \delta\hat{b}_{1'}^\dagger \rangle_{ref}\, \chi_{1'1}^{-1}\, g_{2'2}^{-1} \end{aligned} \tag{D.12}$$

Here T_c is contour ordering operator, subscript ref indicates Markov Lindblad-type evolution of the reference system and $\delta\hat{b} \equiv \hat{b} - \langle \hat{b} \rangle_{ref}$. We note in passing that projections of the vertices γ_{123} and δ_{321} are related via

$$\big[\gamma_{123}^{s_1 s_2 s_3}\big]^* = -\delta_{321}^{\bar{s}_3 \bar{s}_2 \bar{s}_1} \tag{D.13}$$

where $s_{1,2,3} \in \{-,+\}$ indicate branches of the Keldysh contour and $\bar{s}$ is the branch opposite to s.

Finally, using (D.8) with interaction given by (D.11) in expansion of GFs for the dual

particles

$$
\begin{aligned}
G_{12} &\equiv -i\langle T_c\, f_1\, \bar{f}_2\rangle \\
D_{12} &\equiv -i\langle T_c\, b_1\, \bar{b}_2\rangle
\end{aligned}
\tag{D.14}
$$

up to second order and employing the Wick's theorem yields the dual particles self-energies given in Eq. (6) of the main text. Corresponding diagrams are shown in Fig. D.1.

D.2 Derivation of Eq.(4.8)

The generating function $Z[\bar{\zeta},\zeta,\bar{\xi},\xi]$ satisfies:

$$
\begin{aligned}
S[\bar{d},d,\bar{f},f,\bar{\eta},\eta,\bar{\zeta},\zeta,\bar{\xi},\xi]] &= S[d^*,d] - \bar{f}\delta\Delta^B f - \bar{b}\delta\Pi^B b + \bar{\zeta} f + \bar{f}\zeta + \bar{\xi}\eta + \bar{\eta}\xi \\
&\quad - \bar{f}_1\, g_{12}^{-1}\, \left[\delta\Delta^B\right]_{23}^{-1}\, g_{34}^{-1}\, f_4 + \bar{f}_1\, g_{12}^{-1}\, d_2 + \bar{d}_1\, g_{12}^{-1} f_2 \\
&\quad - \bar{\eta}_1 \chi_{12}^{-1}\, \left[\delta\Pi^B\right]_{23}^{-1}\, \chi_{34}^{-1}\, \eta_4 + \bar{\eta}_1\, \chi_{12}^{-1}\, b_2 + \bar{b}_1\, \chi_{12}^{-1}\, \eta_2 \\
Z[\bar{\zeta},\zeta,\bar{\xi},\xi] &= \frac{1}{Z}\int_c D[\bar{d},d,\bar{f},f,\bar{\eta},\eta] e^{iS[\bar{f},f,\bar{\eta},\eta,\bar{\zeta},\zeta,\bar{\xi},\xi]} \\
&= \frac{Z_f Z_b}{Z}\int D[\bar{d},d] e^{iS[\bar{d},d,\bar{\zeta},\zeta,\bar{\xi},\xi]}
\end{aligned}
\tag{D.15}
$$

where

$$
\begin{aligned}
S[\bar{d},d,\bar{\zeta},\zeta] = S[d^*,d] &+ \bar{\zeta}^*(g\delta\Delta^B)d + \bar{d}(\delta\Delta^B g)\zeta + \bar{\zeta}(g\delta\Delta^B g)\zeta \\
&+ \bar{\xi}^*(\chi\delta\Pi^B)d + \bar{d}(\delta\Pi^B\chi)\xi + \bar{\xi}(\chi\delta\Pi^B\chi)\xi
\end{aligned}
\tag{D.16}
$$

Hence,

$$
\begin{aligned}
G^{DF} &\equiv -i\langle \hat{f}_1 \hat{f}_2^{\dagger} \rangle = i \frac{\delta^2 Z[\bar{\zeta},\zeta,\bar{\xi},\xi]}{\delta\bar{\zeta}_1 \delta\zeta_2}|_{\bar{\zeta}=\zeta=\bar{\xi}=\xi=0} \\
&= -g\delta\Delta^B g + g(\delta\Delta^B G \delta\Delta^B)g \\
D^{DB} &\equiv -i\langle \hat{\eta}_1 \hat{\eta}_2^{\dagger} \rangle = i \frac{\delta^2 Z[\bar{\zeta},\zeta,\bar{\xi},\xi]}{\delta\bar{\xi}_1 \delta\xi_2}|_{\bar{\zeta}=\zeta=\bar{\xi}=\xi=0} \\
&= -\chi\delta\Pi^B\chi + \chi(\delta\Pi^B D \delta\Pi^B)\chi
\end{aligned}
\tag{D.17}
$$

From which we can easily get Eq.(4.8).

D.3 Fitting hybridization functions with auxiliary modes

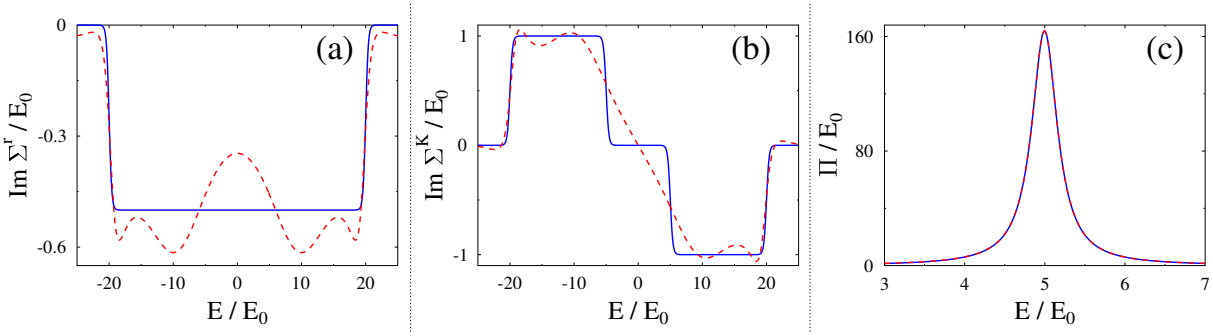

Figure D.2: Hybridization functions of the physical (solid line, blue) and auxiliary (dashed line, red) systems. Shown are (a) retarded and (b) Keldysh projections of the self-energy due to coupling to contacts and (c) hybridization function due to coupling to thermal bath. Fitting is done for parameters adopted in the first numerical example presented in the main text.

Recently, exact proof of possibility to map unitary evolution of a physical system onto Markov Lindblad-type evolution of an auxiliary system was established for systems interacting with Fermi [21, 27, 31, 101] and Bose [29, 100] baths. At the heart of the mapping is fitting of hybridization functions of the physical system with set of auxiliary modes in the auxiliary system. Here, we give details of the fitting procedure.

Explicit form for the Markov Lindblad-type QME (9) is

$$\frac{d\rho^{SA}(t)}{dt} = -i\mathcal{L}\rho^{SA}(t) \equiv -i[\hat{H}_{SA}, \rho^{SA}(t)] + \mathcal{D}\rho^{SA}(t) \tag{D.18}$$

with the Liouvillian taken as

$$\begin{aligned}
\hat{H}_{SA} &= \hat{H}_S + \sum_{n_1,n_2} \varepsilon_{m_1m_2} \hat{c}^\dagger_{n_1} \hat{c}_{n_2} \\
&+ \sum_{m,n} \left(t_{mn} \hat{d}^\dagger_m \hat{c}_n + t^*_{mn} \hat{c}^\dagger_n \hat{d}_m \right) \\
&+ \sum_{\beta_1,\beta_2} \omega_{\beta_1\beta_2} \hat{e}^\dagger_{\beta_1} \hat{e}_{\beta_2} \\
&+ \sum_{m_1,m_2,\beta} r^\beta_{m_1m_2} (\hat{b}^\dagger_{m_1m_2} + \hat{b}^\dagger_{m_1m_2})(\hat{e}_\beta + \hat{e}^\dagger_\beta) \\
\mathcal{D}\rho &= \sum_{n_1,n_2} \Big(\Gamma^{(R)}_{n_1n_2} \left(2\hat{c}_{n_2} \hat{\rho} \hat{c}^\dagger_{n_1} - \{\hat{\rho}, \hat{c}^\dagger_{n_1} \hat{c}_{n_2}\} \right) \\
&\qquad + \Gamma^{(L)}_{n_1n_2} \left(2\hat{c}^\dagger_{n_1} \hat{\rho} \hat{c}_{n_2} - \{\hat{\rho}, \hat{c}_{n_2} \hat{c}^\dagger_{n_1}\} \right) \Big) \\
&+ \sum_{\beta_1,\beta_2} \gamma^{(P)}_{\beta_1\beta_2} \left(2\hat{e}_{\beta_2} \hat{\rho} \hat{e}^\dagger_{\beta_1} - \{\hat{e}^\dagger_{\beta_1} \hat{e}_{\beta_2}, \hat{\rho}\} \right)
\end{aligned} \tag{D.19}$$

Here $\hat{c}^\dagger_n$ ($\hat{c}_n$) and $\hat{e}^\dagger_\beta$ ($\hat{e}_\beta$) create (annihilate) excitation in auxiliary Fermi mode n and Bose mode β, respectively.

Following Refs. [31, 101] we construct retarded, $\tilde{\Sigma}^r$, and Keldysh, $\tilde{\Sigma}^K$, projections of the Fermi hybridization function in the auxiliary system as

$$\begin{aligned}
\tilde{\Sigma}^r_{m_1m_2}(E) &= \sum_{n_1,n_2} t_{m_1n_1} \tilde{G}^r_{n_1n_2}(E) t^*_{m_2n_2} \\
\tilde{\Sigma}^K_{m_1m_2}(E) &= \sum_{n_1,n_2} t_{m_1n_1} \tilde{G}^K_{n_1n_2}(E) t^*_{m_2n_2}
\end{aligned} \tag{D.20}$$

where

$$\begin{aligned}\tilde{G}^r(E) &= \left(E\,I - \varepsilon + i(\Gamma^{(R)} + \Gamma^{(L)})\right)^{-1} \\ \tilde{G}^K(E) &= 2i\,\tilde{G}^r(E)\left(\Gamma^{(L)} - \Gamma^{(R)}\right)\tilde{G}^a(E)\end{aligned} \tag{D.21}$$

are retarded, $\tilde{G}^r(E)$, and Keldysh, $\tilde{G}^K(E)$ projections of the Fermi auxiliary modes Green's functions, and where $\tilde{G}^a(E) \equiv [\tilde{G}^r(E)]^\dagger$ is its advanced projection. Hybridization functions (D.20) should fit corresponding hybridization functions

$$\begin{aligned}\Sigma^r_{m_1m_2}(E) &= \sum_{k\in\{L,R\}} V_{m_1k}\,g^r_k(E)\,V_{km_2} \\ \Sigma^K_{m_1m_2}(E) &= \sum_{k\in\{L,R\}} V_{m_1k}\,g^K_k(E)\,V_{km_2}\end{aligned} \tag{D.22}$$

of the physical system. Here

$$\begin{aligned}g^r_k(E) &\equiv \left(E - \varepsilon_k + i\delta\right)^{-1} \\ g^K_k(E) &\equiv 2\pi i\,(2n_k - 1)\delta(E - \varepsilon_k)\end{aligned} \tag{D.23}$$

are the retarded and Keldysh projections of the free electron in state k in contacts, n_k is the Fermi-Dirac thermal distribution and $\delta = 0^+$

We construct Bose hybridization function in the auxiliary system following Refs. [29,100]. For the physical system-bosonic bath coupling taken in the form

$$\sum_{m_1m_2}\sum_{\alpha} V^{\alpha}_{m_1m_2}(\hat{b}_{m_1m_2} + \hat{b}^\dagger_{m_1m_2})(\hat{a}_\alpha + \hat{a}^\dagger_\alpha) \tag{D.24}$$

the effect of the bosonic environment can be fully encoded by correlation function

$$\begin{aligned}&\Pi_{m_1m_2,m_3m_4}(t-t') = \\ &\quad\sum_{\alpha} V^{\alpha}_{m_1m_2}\,\langle(\hat{a}_\alpha+\hat{a}^\dagger_\alpha)(t)\,(\hat{a}_\alpha+\hat{a}^\dagger_\alpha)(t')\rangle\,V^{\alpha}_{m_3m_4}\end{aligned} \tag{D.25}$$

Similarly, coupling to auxiliary Bose modes in (D.19) is fully described by correlation function

$$\begin{aligned}&\tilde{\Pi}_{m_1m_2,m_3m_4}(t-t') = \\ &\quad\sum_{\beta_1,\beta_2} r^{\beta_1}_{m_1m_2}\,\langle(\hat{e}_{\beta_1}+\hat{e}^\dagger_{\beta_1})(t)\,(\hat{e}_{\beta_2}+\hat{e}^\dagger_{\beta_2})(t')\rangle\,r^{\beta_2}_{m_3m_4} \\ &\quad\equiv i\sum_{\beta_1,\beta_2} r^{\beta_1}_{m_1m_2}\big(\tilde{D}^{>}_{\beta_1\beta_2}(t-t')+\tilde{D}^{<}_{\beta_2\beta_1}(t'-t)\big)\end{aligned} \tag{D.26}$$

Here $\tilde{D}^{>}$ and $\tilde{D}^{<}$ are the greater and lesser projections of Bose auxiliary mode Green's function

$$\tilde{D}_{\beta_1\beta_2}(\tau_1,\tau_2) = -i\langle T_c\,\hat{e}_{\beta_1}(\tau_1)\,\hat{e}^\dagger_{\beta_2}(\tau_2)\rangle \tag{D.27}$$

Fourier transform of the correlation function (D.26) is

$$\tilde{\Pi}_{m_1m_2,m_3m_4}(E) = i\sum_{\beta_1,\beta_2} r^{\beta_1}_{m_1m_2}\big(\tilde{D}^{>}_{\beta_1\beta_2}(E)+\tilde{D}^{<}_{\beta_2\beta_1}(-E)\big) \tag{D.28}$$

According to Ref. [29] in auxiliary system one considers Bose bath at zero temperature with eigenmodes spanning energy range from -∞ to +∞. Thus, greater and lesser projections of the Green's function (D.27) satisfy

$$\begin{aligned}&\tilde{D}^{>}(E) = -2i\tilde{D}^{r}(E)\,\gamma^{(P)}\,\tilde{D}^{a}(E) \\ &\tilde{D}^{<}(E) = 0\end{aligned} \tag{D.29}$$

where

$$\tilde{D}^r(E) = \left(E\,I - \omega + i\gamma^{(P)}\right)^{-1}$$
$$\tilde{D}^a(E) = \left[\tilde{D}^r(E)\right]^\dagger \tag{D.30}$$

are the retarded projection and advanced projections.

For the correlation function (D.25) representing physical system and for the case of thermal Bose bath with inverse temperature β

$$\Pi_{m_1m_2,m_3m_4}(E) = \left(1 + \coth\frac{\beta E}{2}\right) \tag{D.31}$$
$$\times \left(J_{m_1m_2,m_3m_4}(E)\,\theta(E) - J_{m_3m_4,m_1m_2}(-E)\,\theta(-E)\right)$$

where

$$J_{m_1m_2,m_3m_4}(E) \equiv \pi \sum_\alpha V^\alpha_{m_1m_2} V^\alpha_{m_3m_4}\,\delta(E-\omega_\alpha) \tag{D.32}$$

Following Ref. [100] we stress that although the auxiliary Bose bath is taken at zero temperature this does not restrict the temperature of Bose bath in the physical system: the information about finite temperature will be provided by parameters of the auxiliary Bose modes.

Finally note that parameters $\varepsilon_{m_1m_2}$, t_{mn}, $\omega_{\beta_1\beta_2}$, $r^\beta_{m_1m_2}$, $\Gamma^{(L)}_{n_1n_2}$, $\Gamma^{(R)}_{n_1n_2}$ and $\gamma^{(P)}_{\beta_1\beta_2}$ of the Lindblad equation (D.18)-(D.19) are used to fit hybridization functions (D.22) and (D.31) of the physical system with corresponding hybridization functions (D.20) and (D.28) of the auxiliary model employing a cost function to quantify deviation [101]. Figure D.2 shows hybridization functions for the physical model (solid lines) and their fitting with auxiliary modes (dashed lines) as utilized in simulations of the RLM and AIM with symmetric coupling to thermal bath presented in the main text. We used four Fermi and one Bose auxiliary modes to fit the corresponding hybridization functions.

Bibliography

[1] Jiang L, Hodges J S, Maze J R, Maurer P, Taylor J M, Cory D G, Hemmer P R, Walsworth R L, Yacoby A, Zibrov A S and Lukin M D, Science **326**, 267–272 (2009)

[2] Khasminskaya S, Pyatkov F, Słowik K, Ferrari S, Kahl O, Kovalyuk V, Rath P, Vetter A, Hennrich F, Kappes M M, Gol'tsman G, Korneev A, Rockstuhl C, Krupke R and Pernice W H P, Nat. Photon. **10**, 727–732 (2016)

[3] Gaita-Ariño A, Luis F, Hill S and Coronado E, Nature Chem. **11**, 301–309 (2019)

[4] P.W. Anderson, Phys. Rev. **124**, 41-53 (1961)

[5] A. Cyril, *The Kondo Problem to Heavy Fermions* (Cambridge University Press, Cambridge, UK, 1997).

[6] Aoki H, Tsuji N, Eckstein M, Kollar M, Oka T and Werner P, Rev. Mod. Phys. **86**, 779–837 (2014)

[7] Anisimov V and Izyumov Y, *Electronic Structure of Strongly Correlated Materials* (Springer, 2010)

[8] Dorda A, Nuss M, von der Linden W and Arrigoni E, Phys. Rev. B **89**, 165105 (2014)

[9] Stephan Braig and Karsten Flensberg, Phys. Rev. B **68**, 205324 (2003)

[10] Anders F B, Phys. Rev. Lett. **101**, 066804 (2008)

[11] Schmitt S and Anders F B, Phys. Rev. B **81**, 165106 (2010)

[12] Wegner F, Annalen der Physik **506**, 77–91 (1994)

[13] Kehrein S, *The Flow Equation Approach to Many-Particle Systems* (*Springer Tracts in Modern Physics* vol 217) (Springer-Verlag, 2006)

[14] Schollwöck U, Rev. Mod. Phys. **77**, 259–315 (2005)

[15] Schollwöck U, Ann. Phys. **326**, 96 – 192 (2011)

[16] Wang H and Thoss M, J. Chem. Phys. **131**, 024114 (2009)

[17] Wang H and Thoss M, Chem. Phys. **509**, 13–19 (2018)

[18] Cohen G, Gull E, Reichman D R and Millis A J, Phys. Rev. Lett. **115**, 266802 (2015)

[19] Antipov A E, Dong Q, Kleinhenz J, Cohen G and Gull E, Phys. Rev. B **95**, 085144 (2017)

[20] Ridley M, Singh V N, Gull E and Cohen G, Phys. Rev. B **97**, 115109 (2018)

[21] Arrigoni E, Knap M and von der Linden W, Phys. Rev. Lett. **110**, 086403 (2013)

[22] Chen F, Cohen G and Galperin M, Phys. Rev. Lett. **122**, 186803 (2019)

[23] Nazir A and Schaller G, The Reaction Coordinate Mapping in Quantum Thermodynamics *Thermodynamics in the Quantum Regime: Fundamental Aspects and New Directions* Fundamental Theories of Physics ed Binder F, Correa L A, Gogolin C, Anders J and Adesso G (Cham: Springer International Publishing, 2018) pp 551–577

[24] Strasberg P, Schaller G, Schmidt T L and Esposito M, Phys. Rev. B **97**, 205405 (2018)

[25] McConnell C and Nazir A, J. Chem. Phys. **151**, 054104 (2019)

[26] Schwarz F, Goldstein M, Dorda A, Arrigoni E, Weichselbaum A and von Delft J, Phys. Rev. B **94**, 155142 (2016)

[27] Dorda A, Sorantin M, Linden W v d and Arrigoni E, New J. Phys. **19**, 063005 (2017)

[28] Arrigoni E and Dorda A, *Master Equations Versus Keldysh Green's Functions for Correlated Quantum Systems Out of Equilibrium* (Cham: Springer International Publishing, 2018) pp 121–188 ISBN 978-3-319-94956-7

[29] D. Tamascelli, A. Smirne, S. F. Huelga, and M. B. Plenio, Phys. Rev. Lett. **120**, 030402 (2018).

[30] Imamoglu A, Phys. Rev. A **50**, 3650–3653 (1994)

[31] A. Dorda, M. Ganahl, H. G. Evertz, W. von der Linden, and E. Arrigoni, Phys. Rev. B **92**, 125145 (2015).

[32] Jung C, Lieder A, Brener S, Hafermann H, Baxevanis B, Chudnovskiy A, Rubtsov A, Katsnelson M and Lichtenstein A, Ann. Phys. (Berlin) **524**, 49–61 (2012)

[33] Bauer B, Carr L D, Evertz H G, Feiguin A, Freire J, Fuchs S, Gamper L, Gukelberger J, Gull E, Guertler S, Hehn A, Igarashi R, Isakov S V, Koop D, Ma P N, Mates P, Matsuo H, Parcollet O, Pawlowski G, Picon J D, Pollet L, Santos E, Scarola V W, Schollwock U, Silva C, Surer B, Todo S, Trebst S, Troyer M, Wall M L, Werner P and Wessel S, J. Stat. Mech. P05001 (2011)

[34] Dolfi M, Bauer B, Keller S, Kosenkov A, Ewart T, Kantian A, Giamarchi T and Troyer M, Computer Physics Communications **185**, 3430 – 3440 (2014)

[35] Breuer H P and Petruccione F, *The Theory of Open Quantum Systems* (Oxford University Press, 2003)

[36] A. Aviram and M. A. Ratner , Chem. Phys. Lett. **29**, 277 (1974)

[37] M. A. Reed, C. Zhou, C. J. Muller, T. P. Burgin, and J. M. Tour, Science **278**, 252 (1997).

[38] H. Haug and A.-P. Jauho, *Quantum Kinetics in Transport and Optics of Semiconductors* (Springer, Berlin Heidelberg, 2008), second, substantially revised edition ed.

[39] G. Stefanucci and R. van Leeuwen, *Nonequilibrium Many-Body Theory of Quantum Systems. A Modern Introduction.* (Cambridge University Press, 2013).

[40] A. J. White, M. A. Ochoa, and M. Galperin, Journal of Physical Chemistry C **118**, 11159 (2014).

[41] J. H. Oh, D. Ahn, and V. Bubanja, Phys. Rev. B **83**, 205302 (2011).

[42] F. Chen, M. A. Ochoa, and M. Galperin, J. Chem. Phys. **146**, 092301 (2017).

[43] K. Miwa, F. Chen, and M. Galperin, Scientific Reports **7**, 9735 (2017).

[44] W. Wang, T. Lee, I. Kretzschmar, and M. A. Reed, Nano Letters **4**, 643 (2004).

[45] T. Frederiksen, M. Paulsson, M. Brandbyge, and A.-P. Jauho, Phys. Rev. B **75**, 205413 (2007).

[46] R. Avriller and T. Frederiksen, Phys. Rev. B **86**, 155411 (2012).

[47] M. Poot, E. Osorio, K. O'Neill, J. M. Thijssen, D. Vanmaekelbergh, C. A. v. Walree, L. W. Jenneskens, and H. S. J. v. d. Zant, Nano Letters **6**, 1031 (2006).

[48] R. Chikkaraddy, B. de Nijs, F. Benz, S. J. Barrow, O. A. Scherman, E. Rosta, A. Demetriadou, P. Fox, O. Hess, and J. J. Baumberg, Nature **535**, 127 (2016).

[49] J. Repp, P. Liljeroth, and G. Meyer, Nature Physics **6**, 975 (2010).

[50] J. S. Seldenthuis, H. S. J. van der Zant, M. A. Ratner, and J. M. Thijssen, ACS Nano **2**, 1445 (2008).

[51] A. J. White, B. D. Fainberg, and M. Galperin, J. Phys. Chem. Lett. **3**, 2738 (2012).

[52] J. Park, A. N. Pasupathy, J. I. Goldsmith, C. Chang, Y. Yaish, J. R. Petta, M. Rinkoski, J. P. Sethna, H. D. Abruña, P. L. McEuen, D. C. Ralph, Nature **417**, 722 (2002).

[53] W. Liang, M. P. Shores, M. Bockrath, J. R. Long, and H. Park, Nature **417**, 725 (2002).

[54] L. H. Yu, Z. K. Keane, J. W. Ciszek, L. Cheng, J. M. Tour, T. Baruah, M. R. Pederson, and D. Natelson, Phys. Rev. Lett. **95**, 256803 (2005).

[55] E. A. Osorio, K. O'Neill, M. Wegewijs, N. Stuhr-Hansen, J. Paaske, T. Bjørnholm, and H. S. J. van der Zant, Nano Letters **7**, 3336 (2007).

[56] J. J. Parks, A. R. Champagne, T. A. Costi, W. W. Shum, A. N. Pasupathy, E. Neuscamman, S. Flores-Torres, P. S. Cornaglia, A. A. Aligia, C. A. Balseiro, G. K.-L Chan, H. D. Abruña, D. C. Ralph, Science **328**, 1370 (2010).

[57] S. Wagner, F. Kisslinger, S. Ballmann, F. Schramm, R. Chandrasekar, T. Bodenstein, O. Fuhr, D. Secker, K. Fink, M. Ruben, H. B. Weber, Nature Nanotechnology **8**, 575 (2013).

[58] D. Rakhmilevitch and O. Tal, Beilstein Journal of Nanotechnology **6**, 2417 (2015).

[59] A. N. Rubtsov, M. I. Katsnelson, and A. I. Lichtenstein, Phys. Rev. B **77**, 033101 (2008).

[60] G. Rohringer, H. Hafermann, A. Toschi, A. A. Katanin, A. E. Antipov, M. I. Katsnelson, A. I. Lichtenstein, A. N. Rubtsov, and K. Held, Rev. Mod. Phys. **90**, 025003 (2018), ISSN 0034-6861, 1539-0756,

[61] Hafermann, H., Jung, C., Brener, S., Katsnelson, M. I., Rubtsov, A. N., and Lichtenstein, A. I., EPL **85**, 27007 (2009).

[62] A. E. Antipov, J. P. F. LeBlanc, and E. Gull, Physics Procedia **68**, 43 (2015).

[63] J. W. Negele and H. Orland, *Quantum Many-Particle Systems*, vol. 68 (Addison-Wesley Publishing Company, Redwood City, California, 1988).

[64] M. Wagner, Phys. Rev. B **44**, 6104 (1991).

[65] A. L. Fetter and J. D. Walecka, *Quantum Theory of Many-Particle Systems* (McGraw-Hill Book Company, 1971).

[66] P. Coleman, *Introduction to Many-Body Physics* (Cambridge University Press, 2015).

[67] A.-P. Jauho, N. S. Wingreen, and Y. Meir, Phys. Rev. B **50**, 5528 (1994).

[68] D. M. Newns, Physical Review **178**, 1123 (1969).

[69] Y. Meir, N. S. Wingreen, and P. A. Lee, Phys. Rev. Lett. **70**, 2601 (1993).

[70] N. S. Wingreen and Y. Meir, Phys. Rev. B **49**, 11040 (1994).

[71] N. Sivan and N. S. Wingreen, Physical Review B **54**, 11622 (1996).

[72] G. Cohen, E. Gull, D. R. Reichman, and A. J. Millis, Phys. Rev. Lett. **112**, 146802 (2014).

[73] M. Leijnse and M. R. Wegewijs, Physical Review B **78**, 235424 (2008).

[74] Z. Ioffe, T. Shamai, A. Ophir, G. Noy, I. Yutsis, K. Kfir, O. Cheshnovsky, and Y. Selzer, Nature Nanotech. **3**, 727 (2008).

[75] D. R. Ward, N. J. Halas, J. W. Ciszek, J. M. Tour, Y. Wu, P. Nordlander, and D. Natelson, Nano Lett. **8**, 919 (2008).

[76] D. R. Ward, D. A. Corley, J. M. Tour, and D. Natelson, Nature Nanotech. **6**, 33 (2011).

[77] Z. Liu, S.-Y. Ding, Z.-B. Chen, X. Wang, J.-H. Tian, J. R. Anema, X.-S. Zhou, D.-Y. Wu, B.-W. Mao, X. Xu, B. Ren, Z. Q. Tian, Nat. Commun. **2**, 305 (2011).

[78] N. Chiang, N. Jiang, D. V. Chulhai, E. A. Pozzi, M. C. Hersam, L. Jensen, T. Seideman, and R. P. V. Duyne, Nano Lett. **15**, 4114 (2015).

[79] J. Lee, N. Tallarida, X. Chen, P. Liu, L. Jensen, and V. A. Apkarian, ACS Nano **11**, 11466 (2017).

[80] N. L. Schneider, J. T. Lü, M. Brandbyge, and R. Berndt, Phys. Rev. Lett. **109**, 186601 (2012).

[81] E. Ćavar, M.-C. Blüm, M. Pivetta, F. Patthey, M. Chergui, and W.-D. Schneider, Phys. Rev. Lett. **95**, 196102 (2005).

[82] C. Chen, P. Chu, C. A. Bobisch, D. L. Mills, and W. Ho, Phys. Rev. Lett. **105**, 217402 (2010).

[83] Z. C. Dong, X. L. Zhang, H. Y. Gao, Y. Luo, C. Zhang, L. G. Chen, R. Zhang, X. Tao, Y. Zhang, J. L. Yang, J. G. Hou, Nat. Photon. **4**, 50 (2010).

[84] H. Imada, K. Miwa, M. Imai-Imada, S. Kawahara, K. Kimura, and Y. Kim, Nature **538**, 364 (2016), ISSN 1476-4687.

[85] H. Imada, K. Miwa, M. Imai-Imada, S. Kawahara, K. Kimura, and Y. Kim, Phys. Rev. Lett. **119**, 013901 (2017).

[86] K. Kimura, K. Miwa, H. Imada, M. Imai-Imada, S. Kawahara, J. Takeya, M. Kawai, M. Galperin, and Y. Kim, Nature **570**, 210 (2019).

[87] M. Galperin and A. Nitzan, Phys. Chem. Chem. Phys. **14**, 9421 (2012).

[88] M. Galperin, Chem. Soc. Rev. **46**, 4000 (2017).

[89] J. Gersten and A. Nitzan, J. Chem. Phys. **73**, 3023 (1980).

[90] N. Kongsuwan, A. Demetriadou, R. Chikkaraddy, F. Benz, V. A. Turek, U. F. Keyser, J. J. Baumberg, and O. Hess, ACS Photonics **5**, 186 (2018).

[91] A. Rubtsov, M. Katsnelson, and A. Lichtenstein, Ann. Phys. **327**, 1320 (2012).

[92] E. G. C. P. van Loon, A. I. Lichtenstein, M. I. Katsnelson, O. Parcollet, and H. Hafermann, Phys. Rev. B **90**, 235135 (2014a).

[93] E. G. C. P. van Loon, H. Hafermann, A. I. Lichtenstein, A. N. Rubtsov, and M. I. Katsnelson, Phys. Rev. Lett. **113**, 246407 (2014b).

[94] E. G. C. P. van Loon, M. I. Katsnelson, and M. Lemeshko, Phys. Rev. B **92**, 081106(R) (2015).

[95] E. A. Stepanov, E. G. C. P. van Loon, A. A. Katanin, A. I. Lichtenstein, M. I. Katsnelson, and A. N. Rubtsov, Phys. Rev. B **93**, 045107 (2016a).

[96] E. G. C. P. van Loon, F. Krien, H. Hafermann, E. A. Stepanov, A. I. Lichtenstein, and M. I. Katsnelson, Phys. Rev. B **93**, 155162 (2016).

[97] E. A. Stepanov, A. Huber, E. G. C. P. van Loon, A. I. Lichtenstein, and M. I. Katsnelson, Phys. Rev. B **94**, 205110 (2016b).

[98] E. A. Stepanov, S. Brener, F. Krien, M. Harland, A. I. Lichtenstein, and M. I. Katsnelson, Phys. Rev. Lett. **121**, 037204 (2018).

[99] A. Kamenev, *Field Theory of Non-Equilibrium Systems* (Cambridge University Press, 2011).

[100] F. Mascherpa, A. Smirne, D. Tamascelli, P. F. Acebal, S. Donadi, S. F. Huelga, and M. B. Plenio, Phys. Rev. A **101**, 052108 (2020).

[101] F. Chen, E. Arrigoni, and M. Galperin, New J. Phys. **21**, 123035 (2019).

[102] L. Mühlbacher and E. Rabani, Phys. Rev. Lett. **100**, 176403 (2008).

[103] Karsten Flensberg, Phys. Rev. B **68**, 205323 (2003).

[104] V. Khlus, Sov. Phys. JETP **66**, 1243 (1987).

[105] V. Lefloch, C. Hoffmann, M. Sanquer, D. Quirion, Phys. Rev. Lett. **90**, 067002 (2003).

[106] A. Braggio, M. Governale, M. G. Pala, J. König, Solid State Commun. **151**, 155 (2011).

[107] L. Saminadayar, D. C. Glattli, Y. Jin, B. Etienne, Phys. Rev. Lett. **79**, 2526 (1997).

[108] L. S. Levitov, and G. B. Lesovik, JETP Lett. **58**, 230 (1993).

[109] L. S. Levitov, H. Lee, and G. B. Lesovik, J. Math. Phys. **37**, 4845 (1996).

[110] M. Esposito, U. Harbola, and S. Mukamel, Rev. Mod. Phys. **81**, 1665 (2009).

[111] A. A. Dzhioev, and D. S. Kosov, J. Chem. Phys. **134**, 044121 (2011).

[112] A. O. Gogolin, and A. Komnik, Phys. Rev. B **73**, 195301 (2006).

[113] G. Vidal, Phys. Rev. Lett. **93**, 040502 (2004).

[114] E.M. Stoudenmire, S.R. White, New J. Phys. **12**, 055026 (2010).

[115] S. Paeckel, T. Köhler, A. Swoboda, S.R. Manmana, S.R. Manmana, U. Schollwöck, C. Hubig, Annals of Physics **411**, 167998 (2019).

[116] Gao-Min Tang, Fuming Xu, Jian Wang, Phys. Rev. B **89**, 205310 (2014).

[117] P. Werner, T. Oka, A.J. Millis, Phys. Rev. B **79**, 035320 (2009).

[118] ITensor Library, http://itensor.org.